Cuticular Hydrocarbons in Myrmecophiles are a Mechanism of Symbiotic Entrenchment

Thesis by

Thomas Houser Naragon

In Partial Fulfillment of the Requirements for

the degree of

Doctor of Philosophy

CALIFORNIA INSTITUTE OF TECHNOLOGY

Pasadena, California

2025

(Defended May 21st, 2025)

Thomas Houser Naragon
ORCID: 0000-0002-5373-4257

anything goes
–Paul Feyerabend

ACKNOWLEDGEMENTS

Professional Mentors
Joe Parker–Took a chance on a chemist who knew nothing about bugs
Betty Hong–Level-headed about what constitutes a PhD project
Rustem Ismagilov–Always practical
Alison Draper–Taught me how science works
Michelle Kovarik–Why I became a chemist, taught me analytical techniques
Janet Morrison–Why I remained a chemist, taught me analytical techniques
Charles Kolmer–Made biology significantly more confusing

Labmates (The early years)
David–Helped me not take things too seriously
Julian–Always there to commiserate and question, worked together to establish the *Sceptobius* system
Mina–Kept the lab running, kept everyone in line
Adrian–Knew the outcome of my project before it had even started
Sheila–What meagre bioinformatics skills I picked up in grad school were because of her

Labmates (The later years)
A motley crew that made grad school less of a grind

Cohort
Lev–Brought the whimsy
John–Brought the finer things
Sharan–Brought the jazz
Albert–Introduced me to East African Geopolitics
Zander–Enabled some bad habits
Varun–Enabled some good habits
Aditi–A stabilizing force in my life. I would not have made it through grad school without her

Family–Support and perspective

Rad Bio Crew–Envisioning a different biology

ABSTRACT

The velvety tree ant, *Liometopum occidentale*, hosts three myrmecophilous rove beetles, *Sceptobius lativentris, Platyusa sonomae,* and *Liometoxenus newtonarum.* The three beetles independently evolved to mimic the nestmate recognition pheromones of *L. occidentale* with varying degrees of accuracy. The accuracy of the mimicry determines the degree of integration of the beetles into nests of their host; *P. sonomae* achieves the least accurate mimicry and is located at the nest periphery, whereas *S. lativentris* employs the most accurate mimicry and has access to the entirety of the ant nest and its resources. The accuracy of the mimicry was found to be dependent on the mechanism by which it is achieved. *P. sonomae* synthesizes the pheromone blend *de novo* and *S. lativentris* acquires the pheromones from the host ant. The approach taken by *S. lativentris* is significant, because the class of chemicals used as nestmate recognition pheromones in ants play a more primary role, forming a desiccation barrier that coats the surface of all insects. In the transition into the nests of its hosts, which occurs after the pupal developmental stage, *S. lativentris* permanently shuts off its production of these anti-desiccation compounds, opting instead to steal them from its host. This high-fidelity mimicry comes at a cost. *S. lativentris* is locked into an obligate and irreversible dependence on *L. occidentale,* dying within a day away from its host ant.

PUBLISHED CONTENT AND CONTRIBUTIONS

Naragon, Thomas H, Julian M Wagner, and Joseph Parker. “Parallel Evolutionary Paths of Rove Beetle Myrmecophiles: Replaying a Deep-Time Tape of Life.” *Current Opinion in Insect Science* 51 (June 1, 2022): 100903. https://doi.org/10.1016/j.cois.2022.100903.

T.H.N participated in conception, figure making, and writing of this review article.

Kitchen SA, Naragon TH, Brückner A. Ladinsky MS, Quinodoz SA, Badroos JM, Viliunas JW, Kishi Y, Wagner JM, Miller DR, Yousefelahiyeh M, Antoshechkin IA, Eldredge KT, Pirro S, Guttman M, Davis SR, Aardema ML, Parker J. The Genomic and Cellular Basis of Biosynthetic Innovation in Rove Beetles. *Cell* 187, 3563-3584.e26 (2024) https://doi.org/10.1016/j.cell.2024.05.012

T.H.N collected critical samples, and participated in data generation and analysis.

Naragon TH, Viliunas JW, Yousefelahiyeh M, Brückner A, Wagner JM, Ryon HM, Collinson D, Wijker RS, Sessions AL, Parker J. Symbiotic entrenchment by an ecological Catch-22. In preparation, 2025

T.H.N helped conceive of the project, collected all data, performed all analysis, generated figures, and drafted the manuscript.

TABLE OF CONTENTS

Acknowledgements iv
Abstract v
Published Content and Contributions vi
Table of Contents vii
List of Figures viii
List of Tables xii
Chapter I: Natural History 1
Liometopum occidentale 1
Myrmecophilus sp. 10
Anchomma costatum 12
Haeterius sp. 14
Pseudacteon californiensis 15
Platyusa sonomae 17
Liometoxenus newtonarum 22
Sceptobius lativentris 24
Chapter II: Phylogenomics and Convergent Mimicry 32
Generating Transcriptomes 33
Phylogenomic Tree Construction 35
Time Calibrated Species Tree Construction 37
Accuracy of CHC Mimicry 42
Chapter III: Mimicry Mechanisms 47
Isolation of *Platyusa sonomae* 48
CHC Stable Carbon Isotope Analysis in *Platyusa sonomae* 50
CHC Biosynthesis in *Platyusa sonomae* 52
The CHC Biosynthesis Pathway in *Platyusa sonomae* 57
The CHC Mimicry Mechanism in *Sceptobius lativentris* 61
Chapter IV: CHC Production During Development 68
The CHC Biosynthesis Pathway in *Sceptobius lativentris* 68
CHC Biosynthesis in *Sceptobius lativentris* 72
The Problem of Endogenous Biosynthesis and its Resolution 76
Endogenous Biosynthesis Revisited 84
Chapter V: Life History Consequences of Mimicry 87
Desiccation is a Cause of Death 87
The Catch-22 92
Appendix 95
Bibliography 132

LIST OF FIGURES

Number *Page*

1. *Liometopum occidentale* 1
2. *L. occidentale* GCMS trace 3
3. *Myrmecophilus* sp. with *L. occidentale* 10
4. *Myrmecophilus* sp. and *L. occidentale* CHC profiles 11
5. *Anchomma costatum* 12
6. *A. costatum* and *L. occidentale* CHC profiles 13
7. *Haeterius* sp. 14
8. *Haeterius* sp. and *L. occidentale* CHC profiles 15
9. *Pseudacteon californiensis* 15
10. *P. californiensis* and *L. occidentale* CHC profiles 17
11. *Platyusa sonomae* 17
12. *P. sonomae* preys on *L. occidentale* 18
13. *P. sonomae* and *L. occidentale* CHC profiles 19
14. *P. sonomae* appeasement behavior 20
15. *P. sonomae* gland morphology 21
16. *Liometoxenus newtonarum* 22
17. *L. newtonarum* and *L. occidentale* CHC profiles 23
18. *Sceptobius lativentris* 24
19. *S. lativentris* consuming a mass of *L. occidentale* eggs 26
20. *S. lativentris* adaptations for grooming *L. occidentale* 26
21. *S. lativentris* and *L. occidentale* CHC profiles 27
22. *S. lativentris* gland morphology 28
23. *S. lativentris* egg comparison 29
24. *S. lativentris* sclerotization 30
25. *S. lativentris* life cycle 31
26. Maximum likelihood species tree with myrmecophiles 37

27. Time-calibrated species tree 42
28. NMDS ordination of CHC profiles in *L. occidentale* and associates 44
29. Bray-Curtis dissimilarity of profiles in *L. occidentale* and associates. 45
30. Hierarchical clustering of profiles 46
31. *P. sonomae* isolation experiment GCMS traces 48
32. Bray-Curtis dissimilarity of isolated *P. sonomae* to food sources 49
33. ∂^{13}C measurements of *P. sonomae* and *L. occidentale* CHCs 52
34. HCR labelling of *CYP4G1* in *P. sonomae* abdomen 54
35. *CYP4G1* RNAi in adult *P. sonomae* 56
36. CHC biosynthesis pathway in *P. sonomae* 60
37. HCR labelling of CHC biosynthesis pathway in *P. sonomae* 61
38. Isolation in *S. lativentris* causes CHC loss and death 62
39. ∂^{13}C measurements of *S. lativentris* and *L. occidentale* CHCs 63
40. Behavior arena for measuring interaction 64
41. Species typical behaviors occur in the behavior arena 64
42. Time spent in contact with *L. occidentale* in the behavior arena 65
43. Deuterated hydrocarbon transfer in the behavior arena 67
44. HCR labelling of *CYP4G1* in *S. lativentris* abdomen 69
45. CHC biosynthesis pathway in *S. lativentris* 71
46. HCR labelling of CHC biosynthesis pathway in *S. lativentris* 71
47. Teneral and integrated *S. lativentris* CHC profiles 72
48. NMDS ordination of CHC profiles in *S. lativentris* life stages 73
49. Teneral and isolated *S. lativentris* CHC quantification 74
50. CHC quantification across *S. lativentris* life stages 75
51. CHC quantification across *Dalotia coriaria* life stages 76
52. Stacked plot of teneral and integrated *S. lativentris* CHCs 76
53. NMDS ordination of adulterated *S. lativentris* CHC profiles 78
54. *CYP4G1* HCR signal in teneral *S. lativentris* 79
55. Oenocyte cell segmentation 80
56. Quantification of HCR signal in individual oenocytes across time 81

57. qPCR of CHC biosynthesis gene expression over time 83
58. NMDS ordination of *P.sonomae* modified *S. lativentris* 86
59. *CYP4G1* RNAi and *L. occidentale* CHC coating in *D. coriaria* 89
60. Desiccation plots for *S. lativentris* and *D. coriaria* 92
61. A model of obligate myrmecophily 93
62. *P. sonomae* CHC biosynthesis enzyme expression heatmap..... 102
63. *S. lativentris* CHC biosynthesis enzyme expression heatmap 103
64. *FAS1* gene tree 104
65. *FAS2* gene tree 105
66. *FAS3* gene tree 106
67. *elo1* and *elo11* gene tree..... 107
68. *elo2* and *elo5* gene tree 108
69. *elo3* gene tree 109
70. *elo4* gene tree 110
71. *elo6* gene tree 111
72. *elo7* gene tree 112
73. *elo8* gene tree 113
74. *elo9* gene tree 114
75. *elo10* gene tree 115
76. *elo12* gene tree 116
77. *desat1* gene tree..... 117
78. *desat2* gene tree..... 118
79. *desat3* gene tree..... 119
80. *desat4* gene tree..... 120
81. *desat5* gene tree..... 121
82. *FAR1* gene tree..... 122
83. *FAR2* gene tree..... 123
84. *FAR3* gene tree..... 124
85. *FAR4* gene tree..... 125
86. *FAR5* gene tree..... 126

87. *FAR6* gene tree 127
88. *FAR7* gene tree 128
89. *FAR8* gene tree 129
90. *CPR* gene tree 130
91. *CYP4G* gene tree 131

LIST OF TABLES

Number *Page*

1. Genomes used for phylgenomics 95
2. *L. occidentale* CHCs 97
3. CHC biosynthesis enzymes in *D. coriaria* 98
4. CHC biosynthesis enzymes in *P. sonomae* 99
5. CHC biosynthesis enzymes in *S. lativentris* 101

Chapter 1

NATURAL HISTORY

Liometopum occidentale

Figure 1. A *Liometopum occidentale* worker. Photo by David Miller.

The ant species *Liometopum occidentale* (Emery, 1895) is a dolichoderine ant native to the southwestern United States[1–3]. It is one of three Nearctic *Liometopum* species along with *L. luctuosum* and *L. apiculatum*[1,4,5]. As its name would suggest, *L. occidentale* is the westernmost of the three Nearctic *Liometopum* species and is found throughout California and as far north as Oregon[2]. While we have observed sympatry of *L. occidentale* with *L. luctuosum*, *L. occidentale* typically occupies lower elevations than *L. luctuosum*[2]. Our observations have primarily occurred in the Angeles National Forest and San Bernardino National Forest in California, though I have explored nests in the vicinity of Palo Alto, California and Cupertino, California. Previous references to *L. occidentale* were unclear on the nesting sites of the ant[4,6], however the affinity of the species to deciduous tree species, particularly oak, had been noted[2,3]. I have personally found *L. occidentale* nests within holes in the trunks of trees, primarily coast live oak (*Quercus agrifolia*), though the ants can also be found in California bay laurel (*Umbellularia californica*) and jacaranda (*Jacaranda mimisifolia*). In all trees,

the presence of the winged reproductive caste of the ant, as well as a high density of workers, carton nest material[7], and presence of ant brood (eggs, larvae, and pupae) were indicative of the presence of nests. A probable nest was also found in a pine tree of unknown species, as well as a decaying wooden post, from which the entire colony was extracted and transported back to the laboratory for further observation. Nuptial mating flights are thought to occur during late spring[1], and mated queens will form colonies in the laboratory if given sufficient food, humidity, shelter, and a proper range of temperatures.

The size of *L. occidentale* colonies has been previously estimated at roughly 60,000 workers[1], though personal observations would suggest that at their largest extent, they are one to two orders of magnitude more populated. One study suggested that *L. occidentale* may form supercolonies[6], which extend over more than 1km from end to end. Supercoloniality is epitomized in the Argentine ant, *Linepithema humile,* which, in the regions of the globe where the species is introduced, forms large polydomous (multiple nest sites) and polygynous (multiple queens) colonies that spread over thousands of kilometers[7–9]. These sprawling assemblages of individuals exhibit no aggression towards other workers from any point in the same supercolony, despite potentially many hundreds of kilometers of separation[10], yet will fight to the death when confronted by individuals from other *Linepithema* supercolonies within the same geographic region, such as the well-studied warzones in San Diego[11]. While I have not made observations across the entire range of the species, nor at the sites listed in the cited paper, all of my work within the Angeles National Forest would suggest that the *L. occidentale* colonies I observed were not part of a supercolony. *L. occidentale* nests were located in canyons with active streams for at least part of the year. Nest trees were typically separated by roughly 50 meters, and interactions between ants from adjacent nests, carried out both in the field as well as in the laboratory, resulted in aggression, and often death of one of the interacting ants. This

would suggest that the ants were able to identify individuals from other nest trees as foreign, and that these different nests constituted distinct colonies. In nature, *L. occidentale* are known to prey on other arthropods, consume seeds, and collect honeydew produced by various hemipteran insects[2,12]. In captivity, we feed *Liometopum* sugar water, frozen crickets, and frozen *Drosophila*, though the ants are opportunistic in their feeding habits and will consume left out candy, garbage, and—to our horror—pet lizards if given the opportunity.

L. occidentale are very aggressive[2,4], growing very active and releasing an alarm pheromone when disturbed. Headspace sampling of disturbed *L. occidentale* in a vial with a solid phase microextraction fiber (65µm PDMS/DVB, Supelco) combined with gas-chromatography mass-spectrometry (GCMS, Shimadzu QP2020) analysis of the volatiles emitted pointed to 6-methyl-5-hepten-2-one (sulcatone) as the primary component of the alarm pheromone. Sulcatone is known to act as an alarm pheromone in other ant species[13,14], and exposure of *L. occidentale* to synthetic sulcatone elicits an increase in activity. Extracting the surface and exocrine glands of *L. occidentale* by immersion in hexane and analysis via GCMS revealed, in addition to sulcatone, a second set of excocrine compounds called iridoids (Figure 2). Iridoids are a common class of monoterpene found in insects[15], which are known to function as trail pheromones in other ant species[16,17]. Recent work determined that the *L. occidentale* iridoids are used as trail pheromones[18].

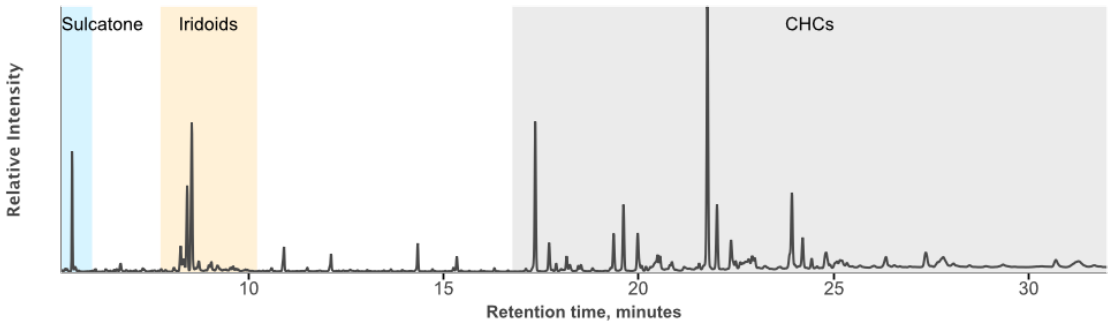

Figure 2. A GCMS Trace of *Liometopum occidentale* exocrine gland and surface chemistry.

A third set of compounds present on the surface of *L. occidentale* are cuticular hydrocarbons (CHCs, Appendix Table 2). CHCs are a class of compound present on the cuticle of all insects[19,20], where they act as a desiccation barrier[21,22]. Insects, due to their small size, have a high surface area to volume ratio, and are thus particularly prone to desiccation[23]. While water loss does occur through respiratory transpiration, water loss via cuticular transpiration is the primary water-efflux route[24,25]. CHCs are typically composed of mixtures of very-long-chain straight and methyl branched alkanes and alkenes, with a typical chain length between twenty-one to thirty-five carbons long[26,27]. Insect CHC profiles can contain hundreds of different hydrocarbons[21], and often these compounds will appear in species typical ratios[27]. Throughout this thesis, CHCs will be referred to using a standard notation. All n-alkanes will be listed as CX, where X is the length of the carbon chain. Methyl-branched alkanes will be listed as YmeCX, where Y is the position of the methyl branch, and X is the length of the carbon chain. If multiple methyl-branched positional isomers coelute, the peak will be listed as Y;ZmeCX, where Y and Z correspond to the methyl branch positions in the different structural-isomers. Alkenes and alkadienes will be listed as CX:Y, where X is the length of the carbon chain and Y is the number of double bonds in the molecule. In cases where the double bond position is known, the molecule will be listed as CX:YnZ, where Z corresponds to the double bond position.

The composition of the CHC profile is important as the physicochemical properties of the CHC layer are critical to its function: CHCs must be liquid enough that they can flow to spread across the cuticle from their point of deposition, but also must be solid enough that they form an effective desiccation barrier[21]. Studies have found that above a certain critical temperature, water permeability of the CHC layer rapidly increases in insects and that the critical temperature roughly corresponds to the point at which all CHCs are melted[28,29]. n-Alkanes typically have the highest melting point, as their straight structure allows for high surface contact and thus greater van der Waals forces. Methyl branched hydrocarbons have a lower melting point, as the methyl group hinders tight packing. Methyl branches

closer to the center of the molecule cause lower melting points than methyl branches closer to the ends of the molecule[22]. The presence of a double bond further reduces the melting point of the CHC[22]. It has been found that since CHC profiles are a blend of different hydrocarbons, they typically will have wide melting curves, suggesting that in their native state the CHCs likely exist as a solid-liquid mixture[21].

Maintenance of water balance is a crucial homeostatic function in insects[23], and thus CHCs are likely under strong selective pressures. CHC profiles have been found to be minimally constrained by phylogeny[30], with the profile composition likely being driven more by geography and local climatic conditions[31]. However, desiccation resistance is only one of the functions played by CHCs. They are also known to function in foot-pad adhesion in insects[32], in sexual recognition in insects[33,34], and—most critically for this project—as nestmate recognition pheromones in eusocial insects[35–38]. CHCs will often times either be homogenous within an ant colony, creating a gestalt odor shared by all colony members, or vary between different ant castes and roles within a colony, specifying both colony membership as well as task within the colony[39]. The selective pressures on the variable functions that CHCs play are not guaranteed to be aligned[21,40], and thus may contribute to reproductive isolation and speciation.

The role of CHCs as a mechanism for determining colony membership in ants is critical to their success and cohesion. Ants are dominant species in the various ecosystems in which they are found, consuming up to 50% of food resources in some environments[41], and their nests have been described as "homeostatic fortresses"[42]. Ants often form subterranean nests, or nests within the trunks of trees, which create environments buffered from environmental extremes[42]. The division of labor in colonies, which can grow to massive sizes[43], allows ants to accumulate food resources[44]. Additionally the nature of multigenerational living results in the presence of large numbers of nutrient rich ant eggs, larvae,

and pupae (collectively referred to as brood) within the colony[45,46]. These resources, both food and protection from the environment, are attractive to other local arthropods, but are largely inaccessible, due to the stringent recognition systems of their owners. The most abundant arthropods in the vicinity of most ant nests are other ant species, and ants are known to prey on other ant species[47,48]; in some army ant species, prey items are dominated by the brood of sympatric ants[47]. Other ants enter heterospecific ant colonies and commit regicide, replacing the original queen with their own regent[49]. The workers in the afflicted colony end up unwittingly working for this usurper. Thus ants, in addition to maintaining the functions of their colony, must defend against intruders taking advantage of their labor and resources. The exclusion of non-nestmates is made easier by the fact that all insects produce hydrocarbons, and most of them, barring extreme chance, will produce a profile distinct from any ant colony that they encounter, especially since social insects typically have more complex CHC profiles[50].

And yet, symbionts of ants (called myrmecophiles) are extremely abundant[51]. The ubiquity of ants and their ecological dominance make them a force that all arthropods in the shared ecosystem have to contend with[47,52]. Many organisms choose avoidance[52], but others have settled on symbiosis of some form or another. Symbionts can be as simple as kleptoparasites[53], stealing food from ants, or as integrated as some army ant myrmecophiles, which have evolved myrmecoid morphologies[54]. One group of insects particularly rich in myrmecophiles are rove beetles (Staphylinidae)[39], particularly in the subfamily Aleocharinae. It is likely that some combination of their species richness[51], global distribution[55], predation on small arthropods, and defensive glandular chemistry[56] placed them in a position to interact with ants, as ants rose to global dominance[57]. A key hurdle for any myrmecophile is the CHC recognition system of the host ant. In some cases where a resource is procured for the ants, the CHC mismatch is unimportant. Aphids provide nutrient rich honeydew to ants and in return receive protection from predators by the ants, despite the clear mismatch in CHC profile[58]. In other

cases heterospecific ants have been known to live together in relative harmony[59]. But in cases where the benefit of the myrmecophile to the ant is minimal or entirely nonexistent, recognition as foreign, and death at the hands of ants is a very real concern. Many myrmecophiles take a brute force approach, becoming exceptionally well armored[60], such that recognition and ant aggression can be weathered with minimal bodily harm. Some myrmecophiles instead take a behavioral approach and have become skilled at evasive maneuvers to avoid ant attacks[61]. Other myrmecophiles use various chemicals, such as alarm pheromones of the host, to modulate ant behavior prior to, or upon recognition[13]. One of the surest ways to avoid detection, though, is CHC mimicry[61–64].

First described in a beetle symbiont of termites[65], CHC mimicry of various eusocial organisms has been documented over the last fifty years[64,66–68]. It is a phenomenon that occurs across a diverse range of arthropods[51,62,69] and this ubiquity across insect lineages hints either at the ease with which mimicry can evolve, or the potentially large fitness benefit accrued by the mimicking myrmecophile. CHC mimicry can be achieved via a number of different mechanisms[70]. Mimetic CHCs can be produced endogenously, referred to as innate chemical mimicry[70], via modifications to the currently existing CHC biosynthesis pathway of the organism. CHCs can also be acquired from the host ant, in a mechanism referred to as acquired chemical mimicry[70] or chemical camouflage by some authors[71,72]. These two approaches to CHC mimicry suggest radically different evolutionary histories.

The evolution of innate CHC mimicry requires retooling a complex biochemical pathway[73]. The pathway contains five primary enzyme families, four of which are composed of multiple gene copies[26,74]. Knockdowns of many of these enzymes in *Drosophila melanogaster* modified the relative ratios of the different chain lengths and classes of the hydrocarbons, in some cases removing one class of hydrocarbons or a single hydrocarbon species, while simultaneously increasing the amount of another in the profile[26,73]. CHC biosynthesis can be thought of as various precursor and

intermediate compounds moving through a network of different enzymes, which create a combinatorial set of possible CHC pathways to generate the full array of hydrocarbons in a profile. Loss of any one enzyme often causes the inputs and intermediates to be shunted into other arms of the pathway. For example, knockdown of desatF, an enzyme expressed in female *Drosophila melanogaster* that introduces double bonds into hydrocarbons, resulted in a decrease in alkadiene production and a concomitant increase in monoenes present in the CHC profile[75,76]. Thus, innate CHC mimicry, while it maintains the integrity of the CHC layer regardless of the presence of the host ant, is likely to fail to exactly match the CHC ratios of the host profile[77]. Because many ant species exhibit some variation in CHC profile from worker to worker, often times separating along caste or task lines[39], the size of the CHC target that innate CHC mimics have to hit may be somewhat increased. CHC profile recognition is a complex and incompletely understood phenomenon, with different mechanisms likely existing in different species[78,79], but there is evidence to suggest that not all CHCs in a given profile are used for recognition[80]. Thus, imperfect mimicry may still go unnoticed, and though it may not fully eliminate occasional ant recognition and aggression[81] it is better than no mimicry at all[63].

The evolution of acquired mimicry, on the other hand, requires changes to behavior and morphology, such that the myrmecophile can efficiently transfer hydrocarbons from the host to its own body. Grooming behavior has been described in numerous army ant symbionts[82,83] and was shown to likely result in acquired CHC mimicry[64]. Isotopically labelled hydrocarbons added to the surface of host ants have been used to measure, more definitively, the transfer of hydrocarbons onto the silverfish *Malayatelura ponerophila*[62,69]. The mechanism that likely facilitates this CHC transfer involves the silverfish rubbing its body against its host ant. All of these transfer mechanisms require the evolution of novel behavioral programs in the myrmecophile[51], though it is possible that some of these behaviors are modifications of already present self-grooming present in insects[84]. One additional

sticking point for acquired mimicry is that, since CHCs are required for desiccation resistance, most insects will produce an endogenous CHC profile, which if not suppressed, will adulterate the acquired CHC profile[85], reducing the accuracy of the mimicry. Suppression of endogenous CHC production is a potentially dangerous strategy, though, as the loss CHC self-sufficiency may make the myrmecophile dependent on the host for maintaining a key homeostatic trait. One likely manifestation of this phenomenon appears in the most integrated symbionts of army ants, which die within days or even hours of removal from their host ant[82], as CHCs are lost to the environment through foot-pad adhesion[32] and general contact between the insect and the environment[85].

CHC mimicry is not the sole solution to avoiding host ant recognition. Some insects are able to avoid ant detection purely through their diminutive size[81], or through reduced CHC production[61], called chemical insignificance, or through a mechanism called chemical crypsis[70,86], where the organism blends into the background by matching background cues. These solutions to the problem of ant recognition, similar to mimicry, still require major behavioral and morphological changes. Diminutive size is likely less accessible to certain clades as different insect orders have been found to have distinct, unimodal size distributions[87], pointing to potential optima for different insect body plans. Chemical insignificance, because it requires a reduced CHC profile, places the myrmecophile at an increased risk of desiccation. Additional adaptations[36] that reduce water loss to the environment would be needed. This approach may only be feasible in humid climates where desiccation risk is reduced. Chemical crypsis, while not tuned to the CHC profile of the ant, still requires either the innate or acquired mimicry of background cues, with all of the attendant difficulties previously mentioned for host CHC mimicry.

L. occidentale hosts a number of myrmecophilous species. A non-exhaustive list includes a cricket in the genus *Myrmecophilus*, the phorid fly *Pseudacteon californensis,* the tenebrionid beetle

Anchomma costatum, a histerid beetle in the genus *Haeterius*, and the three rove beetles *Sceptobius lativentris*, *Platyusa sonomae*, and *Liometoxenus newtonarum*. Many more species of arthropods including mites, booklice, and springtails are consistently found in or around *L. occidentale* colonies and will not be further discussed. The other Nearctic *Liometopum* species, *L. luctuosum* and *L. apiculatum* have been found to host myrmecophiles as well, including the beetles *Sceptobius schmitti*[88,89], *S. dispar*[88,89], *Dinardilla mexicanum*[88,89], *D. liometopi*[88,89], *Liometoxenus jacobsoni*[90], and we have additionally found *Platyusa sonomae* and an unknown species of *Pella* in colonies of *L. luctuosum.*

***Myrmecophilus* sp.**

Figure 3. A *Myrmecophilus* sp. with two *L. occidentale* workers.

The cricket genus *Myrmecophilus* is composed of myrmecophiles associated with many different ant species[91–93]. Some of these crickets are host specific[94,95], whereas others associate with a variety of ant hosts[91,94]. An unknown species of *Myrmecophilus* found in the leaf litter surrounding *L. occidentale* nests interacts with the ant when observed in a laboratory setting (Figure 3). While the ants typically ignore the cricket, occasional aggression was observed and crickets were found with missing limbs. The crickets can be found in large numbers in *L. occidentale* nests, though there is

likely some undetermined seasonality to their abundance within the nests. Other *Myrmecophilus* species have been documented engaging in trophallaxis (mouth to mouth feeding) and strigilation (consuming material off the surface) with their host ant, though this behavior was always carried out cautiously as the host ants were also hostile towards the crickets[96]. Extraction and GCMS profiling of CHCs in the *L. occidentale* associated *Myrmecophilus* species revealed that, for the incomplete profile measured, the cricket mimics *L. occidentale* CHCs (Figure 4). Additional measurements of the full CHC profile are needed to verify that all components of the profile are mimicked. Other *Myrmecophilus* species have been shown to mimic ant CHCs, changing their profile depending on the species they are with and exhibiting depleted CHC levels when removed from their host[97], which suggests that the cricket employs an acquired mimicry approach. Additional experiments of this nature would be required in the *L. occidentale* associated *Myrmecophilus* sp. to determine the mimicry mechanism used.

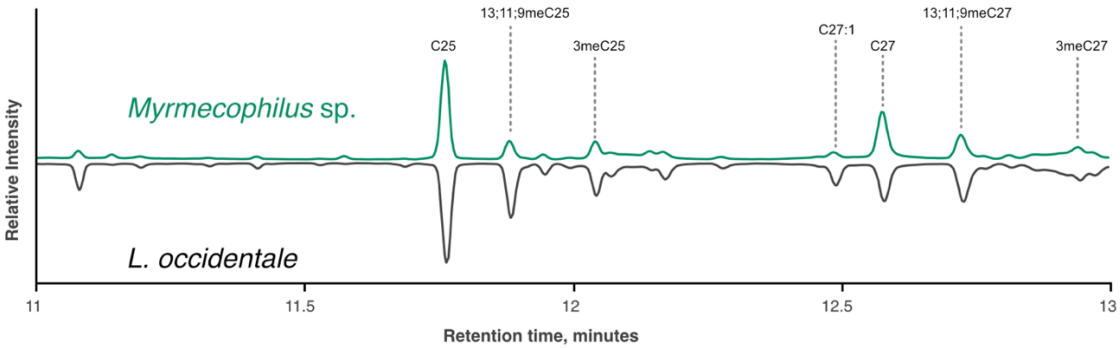

Figure 4. A Partial *Myrmecophilus* sp. GCMS profile compared to *L. occidentale*, with a few key CHCs labelled.

Anchomma costatum

Figure 5. *Anchomma costatum.*

Anchomma costatum (LeConte, 1858, Figure 5) is a tenebrionid beetle[98] distributed throughout California[99–101], which can be recovered from leaf litter surrounding *L. occidentale* nests and within the refuse piles of the nests. The beetle is regularly found in large numbers at all *L. occidentale* nests and has previously been recorded in association with ants[99], including *Pheidole hyatti*[102]. Interactions between the beetle and *L. occidentale* are minimal as the beetle freezes whenever the ant is present and *L. occidentale* workers appear to not detect *A. costatum* when they come into contact with the beetle. Pooled measurements of CHCs from multiple *A. costatum* suggest that the beetle mimics the CHC profile of *L. occidentale* (Figure 6). It is important to note, though, that chemical resemblance can function in many different ways[70]. Because the beetle is typically found in refuse piles of the ant and has not been observed actively interacting with *L. occidentale*, it is possible that the chemical resemblance functions to avoid interacting with the host entirely, instead of facilitating social interactions with the host; the beetle may be engaging in chemical crypsis, matching the chemical profile of some other component of *L. occidentale* nests, such as the nest wall, in order to blend into the background of the nest. I have not made measurements of *L. occidentale* nests myself, but in other

ant species, it has been found that some ant CHCs are deposited on the walls of the nest[103]. The ratios of these nest-wall hydrocarbons were slightly different from the cuticular hydrocarbons of the ant, exhibiting a relative enrichment in linear alkanes relative to the rest of the profile. Similarly, the CHC profile of on *A. costatum* is slightly enriched in linear alkanes (C25, C27, and C29) compared to the CHC profile of *L. occidentale* (Figure 6). Because *A. costatum* is found with other ant species, it would be reasonable to assume that the beetle also mimics the CHCs or background chemicals in those contexts as well. Unless the CHC biosynthesis machinery of the beetle is extremely plastic, these CHCs are likely obtained from the host or the environment of the host, and the CHC mimicry or crypsis is acquired instead of innate. The offset in n-alkane amount relative to the *L. occidentale* profile could also result from low-level endogenous CHC production by the beetle. Isolation of *A. costatum* from *L. occidentale* workers and nest material for a short period of time could help determine if the *A. costatum* CHC profile is acquired, and if the endogenous profile is composed primarily of linear alkanes.

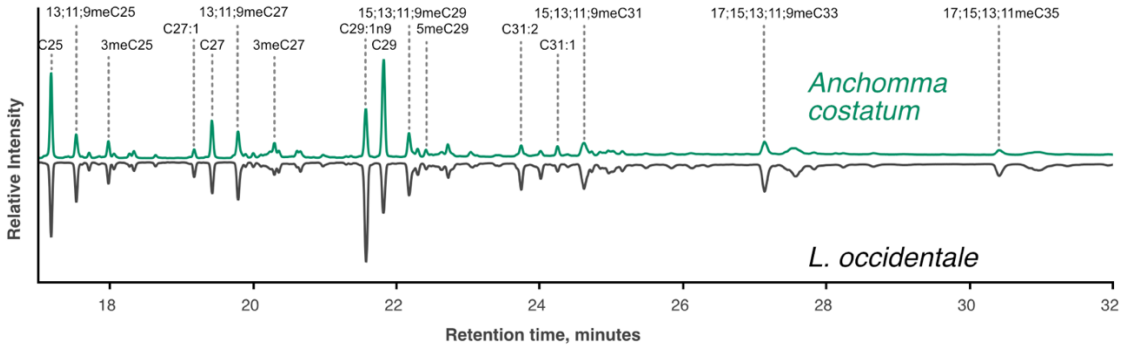

Figure 6. An *Anchomma costatum* GCMS profile compared to *L. occidentale*, with a few key CHCs labelled.

***Haeterius* sp.**

Figure 7. *Haeterius* sp. Photo by Julian Wagner.

One of the largest radiations of myrmecophiles, Haeteriinae[51], sits within the beetle family Histeridae, also called clown beetles. Numbering more than 300 species, the subfamily has likely been populated by myrmecophiles for the last 100 million years[104], placing the origins of myrmecophily close to the origins of ants as eusocial organisms. Members of the tribe are known to interact with ants in highly specialized ways, such as trophallaxis and host grooming[105], and some haeteriines mimic the CHCs of their ant hosts[77,81], with one of the species being found to produce its mimetic profile endogenously[77]. The *Haeterius* sp. found with *L. occidentale* (Figure 7) is quite rare, with only a handful of specimens being found over the course of eight years of fieldwork. Extraction and GCMS analysis of the CHC profile of the *Haeterius* species revealed that the beetle mimics the profile of *L. occidentale*, though notably the beetles profile is enriched in some n-alkanes relative to *L. occidentale* (Figure 8).

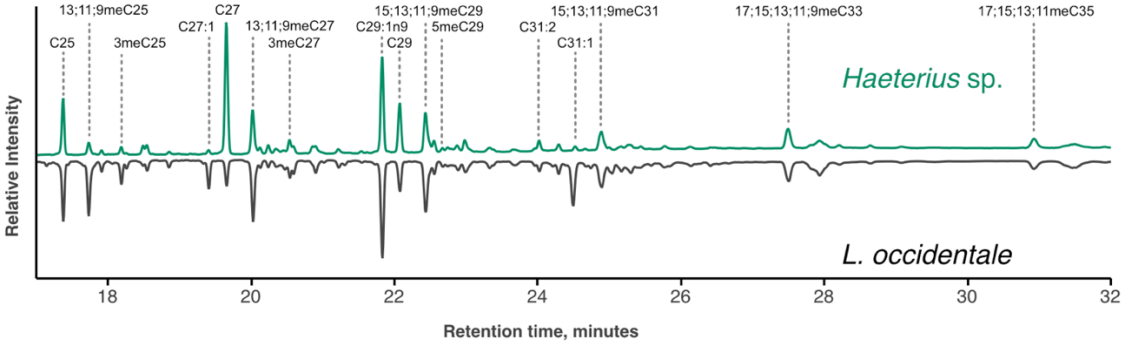

Figure 8. *Haeterius* sp. GCMS trace, compared to *L. occidentale.* Major CHC compounds are labelled.

Pseudacteon californiensis

Figure 9. A Female *Pseudacteon californiensis.*

Pseudacteon californiensis (Disney, 1984, Figure 9) belongs to the family Phoridae, colloquially referred to as scuttle flies, which contains numerous parasitoids[106]—species whose larvae develop inside another organism. Not all phorids are parasitoids[106], and of those that are, some are specialists[107] while others are generalists[106]. Some of the most well-known phorids are found within the genus *Pseudacteon* and parasitize *Solenopsis*[107,108]. Female *Pseudacteon* hover over their *Solenopsis* target prior to quickly diving towards the ant and using their sharp ovipositor (Figure 9) to inject eggs into

the ant gaster. The eggs then hatch and the larvae develop inside the ant, eventually leading to the death of the ant and the emergence of an adult fly from within the ant[108]. The presence of phorids has been found to change ant behavior, due to defensive strategies employed by the ants, which can reduce ant foraging[109] and decrease ant competitiveness with other ant species[110]. In *Solenopsis,* defensive behavior was typically initiated after initial oviposition events[111,112], though the ant additionally utilized close range visual cues to identify the phorids[108,111]. Little work has been done on *P. californiens*is beyond its initial species description[113], associating the phorid with *L. occidentale*, and a masters thesis[114] on the effects of the phorid on *L. occidentale* foraging behavior, which found that foraging behavior decreased following phorid attacks. *P. californiensis* (Figure 9) were collected by aspirating flies directly while they were hovering at the entrance to a *L. occidentale* nest. The prevalence of *P. californiensis* around *L. occidentale* nests is unknown. GCMS analysis of *P. californiensis* CHCs revealed that the phorid shares a number of common CHCs with *Liometopum* (Figure 10). As is clear from the GCMS traces, the relative ratios of these compounds do not match those of the ant. Additionally, *P. californiensis* has a number of 2-methyl hydrocarbons (2meC25, 2meC26, and 2meC27) that dominate its profile, which are not present on the host ant. While it is unclear if this profile is mimetic, the presence of alkenes and alkadienes (C29:2, C29:1n9, and C31:2) which match those of *L. occidentale* would suggest that it might play some role in reducing detection by the ant. Not all phorid species oviposit as quickly as the *Pseudacteon* species that parasitize *Solenopsis*[115], in some cases landing on the ant and positioning themselves prior to oviposition. The oviposition behavior of *P. californiensis* may fall into this slower category, with the fly landing on the ant prior to oviposition[113] instead of engaging in the faster, aerial oviposition of *Solenopsis* parasitoids[108]. During this slower maneuver, reduced detection by *L. occidentale* workers through partial CHC mimicry would improve the survival chances of the phorid. Alternatively the shared CHCs could act as a mechanism to reduce identification of *P. californiensis* by *L. occidentale* after

the adult parasitoid emerges from the dead ant and makes its way out of the ant nest, similar to other parasitoid species emerging from their ant prey[116].

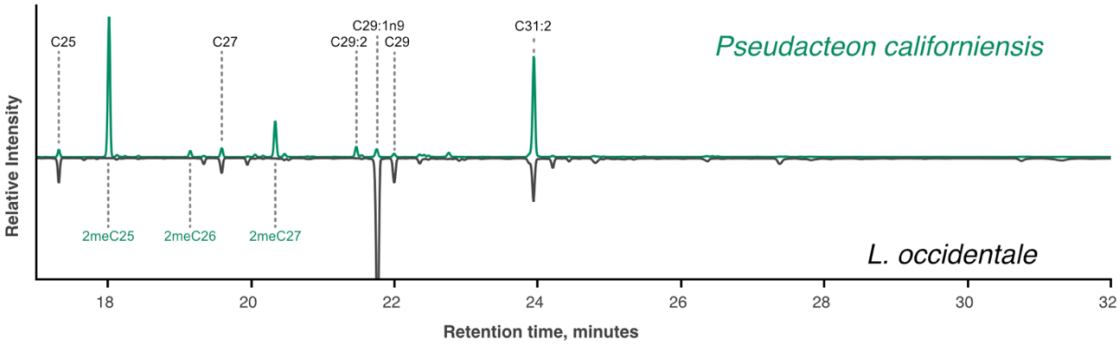

Figure 10. A *Pseudacteon californensis* GCMS trace, compared to *L. occidentale.*

Platyusa sonomae

Figure 11. *Platyusa sonomae.* Photo by David miller.

The beetle *Platyusa sonomae* Casey, 1885 is an aleocharine rove beetle within the tribe *Lomechusini*[117], that associates with nests of *Liometopum occidentale*. Individuals have also been collected from *Liometopum luctuosum* nests in areas where they are sympatric with *L. occidentale*. Prior studies of *Platyusa* have consisted either of systematics work[117,118] or collecting records[119], which also found the beetle associated with *Liometopum* species. *P. sonomae* can be found in *L. occidentale* nests year-round, though the greatest numbers are obtained during the spring, summer, and fall. Occasionally, hundreds of beetles would be found at a single nest in an afternoon. The conditions that lead to these large aggregations are unknown. Most collecting of *P. sonomae* occurred in the Angeles National Forest, though a single individual was found in a *L. occidentale* nest on the

Stanford campus in Palo Alto. Collecting records of the beetle span the state of California[119]. The beetle is often found at the periphery of *L. occidentale* nests, in leaf litter at the base of the nest tree, in or adjacent to bivouacs at neighboring trees, or moving along the edge of foraging trails. Similar to closely related beetles in the tribe Lomechusini, the beetle hunts its host ant, often times while moving along foraging trails[120]. In these better studied beetle systems, the beetles prey on ants by mounting the ants from behind and biting through the neck or the petiole[120]. Similarly, *Platyusa* maintained in the lab will engage in ant predation if they have enough of an appetite and are presented with a live ant (Fig 12).

Figure 12. *Platyusa sonomae* preying on *Liometopum occidentale*. Similar to other lomechusines, the beetle bites through the ant's petiole, separating the gaster from the rest of the body.

GCMS analysis of the CHCs in *P. sonomae* shows that the beetle mimics the CHC profile of *L. occidentale* (Figure 13). The ratios of the CHCs in the profile are somewhat divergent from the host ant, and *P. sonomae* produces a few additional alkenes and alkadienes that are either not present in the profile of *L. occidentale* or present in very low quantities. The beetle evades detection by ants much more than free-living beetles, but because *P. sonomae* CHC mimicry is imperfect, occasionally the beetle is recognized as a foreigner and attacked. To avoid this aggression escalating, *Platyusa*

makes use of a gland at the tip of its abdomen, from which an unknown substance is released which calms down *L. occidentale* (Fig 14, appeasement behavior). This gland has been described in a number of other members of the same tribe, Lomechusini[120–122], though identifying the contents of the gland has remained elusive across these systems. The imperfect CHC mimicry of the beetle precludes it from more intimate associations with ants seen in other myrmecophiles. The beetle is relegated to the periphery of nests and has never been observed inside of the nest trees themselves.

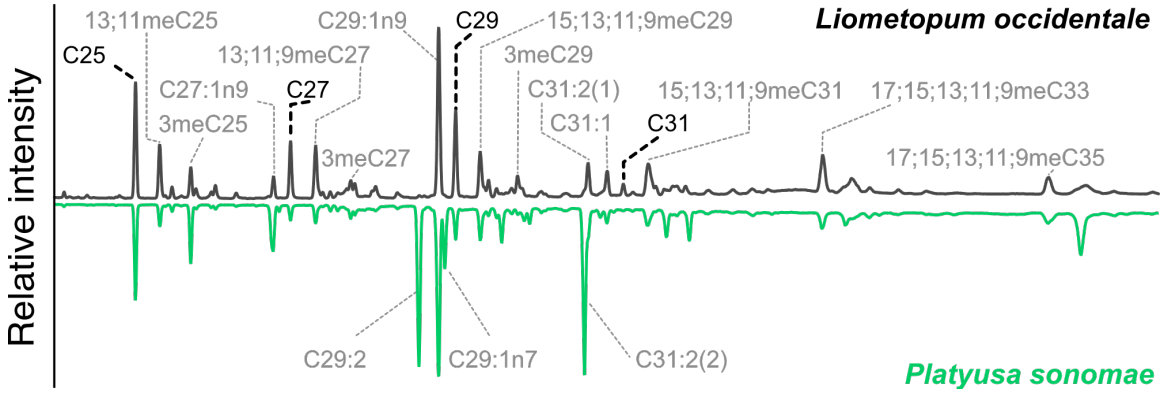

Figure 13. *P sonomae* GCMS trace compared to *L. occidentale*. Major hydrocarbons common to both species are labelled above and compounds specific to the profile of *P. sonomae* are labelled below.

P. sonomae also possesses a defensive gland in its abdomen (Figure 15), composed of D1 gland cells[123] which produce a noxious mixture of benzoquinones, which dissolve into an alkane and ester solvent produced by the walls of the gland reservoir, similar to other members of the higher aleocharinae subfamily[56,124,125]. This gland is thought to be one of the adaptations in aleocharine rove beetles that has contributed to their species richness and success at forming symbiotic relationships with eusocial organisms[124–126]. Whereas free-living aleocharine rove beetles use their defensive gland liberally when confronted with predatory arthropods[56], *P. sonomae* forgoes the use of its defensive gland in favor of its appeasement gland when interacting with *L. occidentale*, even while being actively bitten by the host ant. The appeasement behavior in the beetle appears to be highly targeted,

as aggressive interactions between other species of ants, such as *Linepithema humile* or *Pogonomyrmex*, and *P. sonomae* result in defensive gland deployment by the beetle.

Figure 14. *P. sonomae* appeasement behavior of *L. luctuosum.* The ant approaches the beetle with flared mandibles, a sign of aggression, as *P. sonomae* presents the tip of its abdomen, and appeasement gland, to the ant.

An additional unexplored peculiarity in *P. sonomae* is that the defensive gland contains a small amount of the compound sulcatone, which is the alarm pheromone of *L. occidentale.* As previously discussed, sulcatone is an alarm pheromone in a number of other ant species[13,14], and some associated myrmecophiles of these ants, which are closely related to *P. sonomae*, also possess sulcatone in their defensive glands[13]. In these other myrmecophiles, it has been suggested that the undecane and quinones in the gland cause ants to become more aggressive but the presence of sulcatone in the gland acts to disperse the host ant, counteracting the behavioral changes induced by the main gland components. In *P. sonomae*, this may also be the case; in a scenario where the beetle uses its defensive gland in the vicinity of *L. occidentale*, the additional presence of sulcatone in the mixture could prevent an overwhelming number of *L. occidentale* from being attracted to the beetle, which could otherwise be fatal.

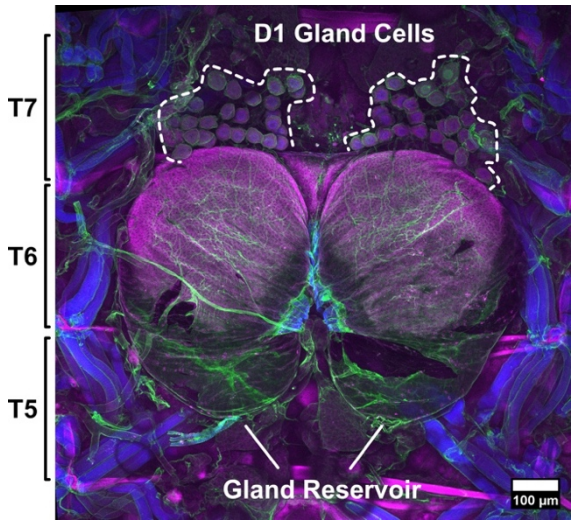

Figure 15 *Platyusa Gland Morphology*. Green – wheat germ agglutinin (WGA, cell membranes), Blue – phalloidin (muscle), Magenta – engrailed and autofluorescence (Reservoir nuclei and general structures).

In the laboratory, *Platyusa* were maintained on a damp bed of packed coconut husk fiber and were fed either a diet of frozen *L. occidentale* or frozen *Drosophila melanogaster*. Beetles could be maintained for multiple months on either food source, suggesting that the beetle is able to survive in the absence of *L. occidentale* ants, at least in an artificial lab environment. Occasionally, *P. sonomae* would lay eggs in the substrate of their containers, and these eggs would hatch and develop to adulthood. *P. sonomae* eggs are quite large, roughly 2 mm in diameter, compared to adults which are 5-6 mm in length. Larvae would pass through three instars prior to pupation, with the second and third instars exhibiting progressively greater degrees of sclerotization. Pupation occurred in the substrate, and occurred within cocoons which incorporated the surrounding substrate. Eggs and larvae were also recovered from our field sites, in the soil and leaf litter surrounding *L. occidentale* nests. This would suggest that the entire life cycle of *P. sonomae* occurs within the vicinity of the nest.

Liometoxenus newtonarum

Figure 16. *Liometoxenus newtonarum.* Photo by David Miller.

The beetle *Liometoxenus newtonarum* Kistner, Jacobson, and Jensen, 2002 is an aleocharine rove beetle in the tribe Oxypodini[90]. Due to the recent description of the genus, little is known about the beetle, with its status as a true myrmecophile only recently being confirmed[119]. Within the genus, *L. newtonarum* is found in nests of *L. occidentale* and *L. jacobsoni* is found in nests of *L. luctuosum*[90]. *L. newtonarum* has been collected from *L. occidentale* nests between Monterrey, CA and San Diego, CA[90,119]. The beetle is highly seasonal in its association with *L. occidentale*, being found in nests of the ant between February and May at field sites in the Angeles National Forest. The beetle has been collected in pitfall traps at the base of *L. occidentale* nest trees, moving within foraging trails of the host ant, in leaf litter at the base of nest trees, and from the surface of nest trees, including from nest openings. To the best of my knowledge, the beetle has access to the full extent of the host nest.

In lab, *L. newtonarum* can be maintained with *L. occidentale* collected from the same nest for multiple weeks, so long as the ants are well fed. The beetle can also be maintained for a few weeks in the absence of ants on a diet of frozen *Drosophila melanogaster.* The beetle has been observed preying on *L. occidentale* workers, biting through the neck to decapitate the ant. How large of a portion of the diet of the beetle is made up by *L. occidentale* workers is unknown, though it likely is not the exclusive food source of the beetle, as *L. newtonarum* is absent from *L. occidentale* nests for more than half the

year. Because the beetle spends time inside the nest proper, it is possible that *L. newtonarum* may also consume brood as well, but this has yet to be verified.

Nothing is known about the life cycle of *L. newtonarum*. Immature life stages of the beetle have never been found at *L. occidentale* nest sites and the beetle has never laid eggs in the laboratory. It is possible that reproduction occurs during the portion of the year when *L. newtonarum* is not associated with *L. occidentale*, or that eggs of the beetle are laid inside the ants brood galleries, similar to other myrmecophiles[127].

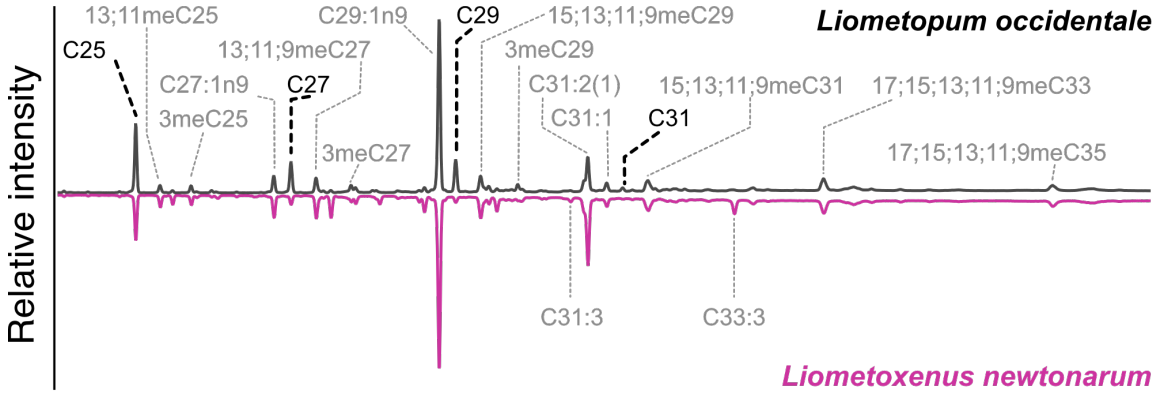

Figure 17. *L. newtonarum* GCMS trace compared to *L. occidentale*. Major hydrocarbons common to both species are labelled above and compounds specific to the profile of *L. newtonarum* are labelled below.

L. occidentale aggression towards *L. newtonarum* from the same colony has never been observed in the field or in lab settings. GCMS analysis of the CHCs in *L. newtonarum* shows that the beetle mimics the CHC profile of *L. occidentale* (Figure 17). The ratios of the various CHCs in the profile differ slightly between the ant and the beetle, and there are a few additional trienes present on *L. newtonarum* that are absent from *L. occidentale*. In addition to CHC mimicry, *L. newtonarum* also possesses a defensive gland in its abdomen, similar to other higher Aleocharinae[124]. Unlike many of the other members of the subfamily, the defensive gland of *L. newtonarum* is dominated by long chain aliphatic esters and aromatic esters, with low levels of benzoquinones and geranial also present[125]. It

is unclear if the gland is still used in defensive contexts, or if it has taken on some new role in modulating *L. occidentale* behavior. In observations of *L. newtonarum* interacting with the host ant in a laboratory setting, the beetle appeared to deploy its gland in the vicinity of *L. occidentale*, which resulted in inhibited locomotion and aggression in the ant. Follow-up experiments would be required to verify that gland components are responsible for the apparent shift in host-ant behavior.

Sceptobius lativentris

Figure 18. *Sceptobius lativentris.* Photo by David Miller.

Sceptobius lativentris Fenyes, 1909 is an aleocharine rove beetle that lives exclusively in nests of *Liometopum occidentale*. The genus *Sceptobius* contains three species, all of which live with different *Liometopum* species[89]. It has been suggested that the ancestor of the three beetle species lived with the ancestor of the three *Liometopum* species, and that the *Sceptobius* clade cospeciated with its host ant[128]. The beetle can be collected from *L. occidentale* nests year-round, with the greatest numbers being found during the spring. In some rare instances, more than a hundred beetles could be recovered from a single *L. occidentale* nest in the course of an afternoon. The beetle can be found running within foraging trails of the host ant, distributed with ants in leaf litter around the base of nest trees, in host bivouacs located in leaf litter around trees near to the nest tree, and also moving in and around nest openings. During the mid-spring through fall, beetles were more often obtained by sifting leaf litter, whereas during the colder part of the fall through to the early spring, beetles were more often found directly on nest-trees. When ant activity was reduced during colder months, blowing into nest

entrances would cause *L. occidentale* to exit the nest, and *S. lativentris* would exit with the host. I collected *Sceptobius* primarily in the Angeles National Forest, though the beetle can be found in *L. occidentale* nests throughout California[89].

S. lativentris is an obligate symbiont of *L. occidentale*; the beetle dies within a day or two if isolated from the host ant, similar to many highly integrated army ant myrmecophiles[82,83]. Beetles brought back from the field require a constant *L. occidentale* presence in their containers to survive, though once that requirement has been satisfied, the beetle can survive for multiple months in an artificial environment so long as areas of higher humidity and sugar water are provided for the ants. The diet of *S. lativentris* is still somewhat enigmatic. The beetle may engage in trophallaxis with *L. occidentale*[88] and we recorded the beetle consuming the eggs of *L. occidentale* on one occasion (Figure 19), but we do not know if host eggs constitute the major part of the beetle's diet or are merely consumed opportunistically. Unlike *P. sonomae* and *L. newtonarum*, *S. lativentris* has never been recorded killing or consuming adult *L. occidentale* workers. While beetles can be maintained in lab with workers collected from the field, we found that the introduction of *Sceptobius* to young, artificially reared *L. occidentale* colonies in lab resulted in colony death within a month. The mechanism underlying this phenomenon is unclear, but work in other ant species has found that collective colony behavior stabilizes as colonies mature[129]. While this young colony death phenomenon may be due to increased metabolic load on the colony caused by the symbiont, there could be some less direct effect resulting from the social instability of the juvenile colony. In contrast, a number of mature *L. occidentale* nests at our field sites have been stably populated with *S. lativentris* for at least seven years. More work is required to understand these dynamics but it appears that the stability of the ant-beetle symbiosis is, in part, dependent on the age of the ant colony.

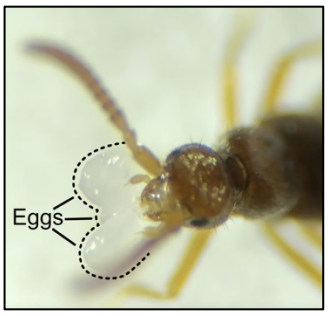

Figure 19. *S. lativentris* consuming a mass of *L. occidentale* eggs. The eggs are held and manipulated by the front legs.

When in the presence of *L. occidentale*, *S. lativentris* carries out a highly stereotyped behavior where it climbs onto the host ant, latches onto the antennae with its mandibles and groom the worker with its front legs (Figure 20), carrying out this behavior for hours at a time[18,130]. Analysis of the front legs of *Sceptobius* revealed that the tarsi are covered in dense hairs, especially compared to free-living relatives (Figure 20). These setae are potentially involved in transferring compounds from the surface of the ant to the beetle's own body. In other beetle species, this grooming behavior has been suggested as a mechanism for stealing hydrocarbons from the host ant[51].

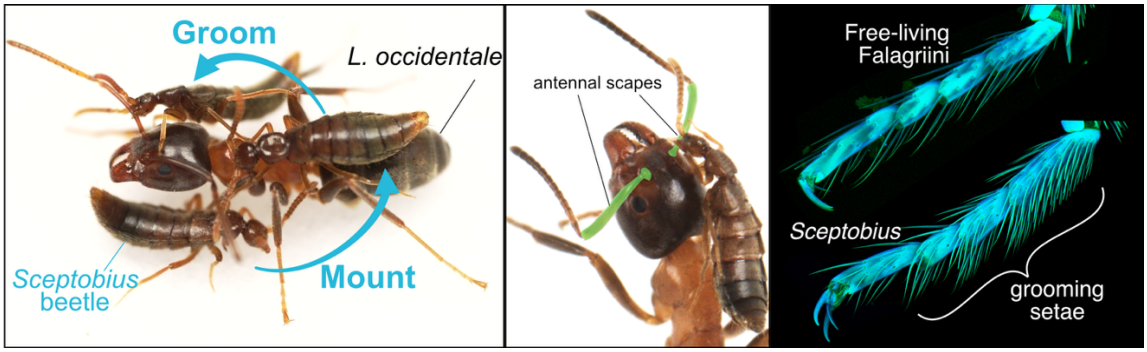

Figure 20. *S. lativentris* mounts and grooms Liometopum, typically grasping the antennal scapes to stabilize itself while running its legs over the surface of the ant and its own body. The front tarsi of *S. lativentris*, compared to a closely related free-living beetle, are much more densely coated in hairs (setae).

GCMS measurements of *Sceptobius lativentris* CHCs show that the beetle achieves near perfect CHC mimicry, possessing the same hydrocarbons as the ant, in the same ratios, with no detectible adulterating compounds (Figure 21). The fidelity of the mimicry allows *S. lativentris* full access to

the *L. occidentale* nest, where the beetle experiences no aggression from the host ant. The accuracy of the CHC mimicry and the grooming behavior in *S. lativentris* together hint that the beetle may take an acquired mimicry approach, stealing the hydrocarbons directly off of the hosts that they are mimicking.

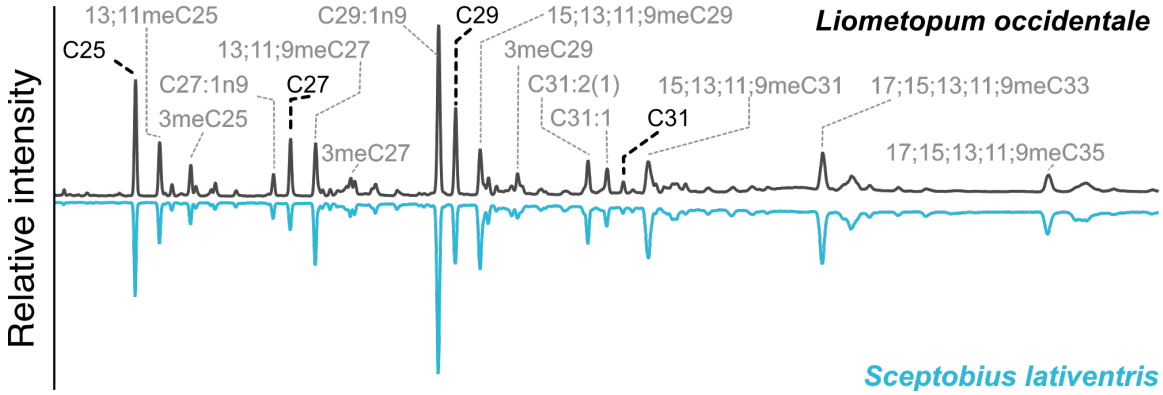

Figure 21. *S. lativentris* GCMS trace compared to *L. occidentale*. Major hydrocarbons common to both species are labelled above.

As a result of *S. lativentris* spending all of its time in ant nests, where it encounters neither aggression from the ant nor aggression from other predatory arthropods, due to the protection of the ant host, the beetle has secondarily lost the defensive abdominal gland, present in almost all aleocharine rove beetles (Figure 22). Whereas the defensive gland is typically located between the 6th and 7th abdominal segments, in *S. lativentris*, a novel gland is present between the 7th and 8th abdominal segments. It is unknown whether this novel gland has any function, or if it is merely a vestigial structure remaining after the loss of the defensive gland. When interacting with *L. occidentale*, the beetle occasionally flexes its abdomen in a manner reminiscent of defensive gland usage in other aleocharines, which may indicate that there is some low concentration compound in the novel gland which modulates ant behavior.

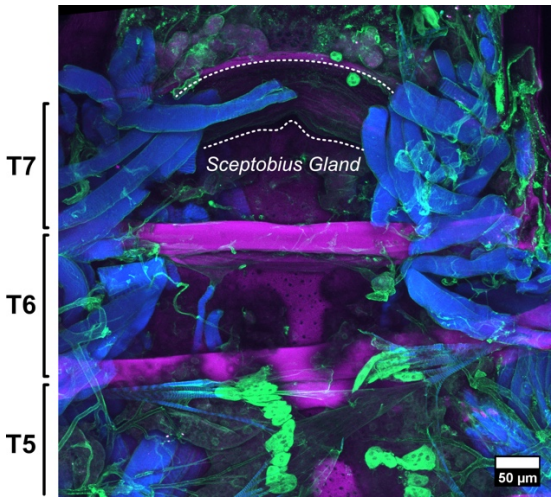

Figure 22 *Sceptobius Gland Morphology*. Green – wheat germ agglutinin (WGA, cell membranes), Blue – phalloidin (muscle), Magenta – engrailed and autofluorescence (General structures).

S. lativentris collected from the field and maintained in the laboratory would occasionally lay eggs when transferred to small petri dishes with a damp piece of filter, but these eggs were never viable. The eggs were quite large, more than 1mm along the long axis, compared to the approximately 3mm length of adult beetles (Figure 23). Large eggs that fill the abdomen of female beetle have also been documented in obligate army ant myrmecophiles[131]. Viable *S. lativentris* eggs as well as larvae could be collected in soil at the base of *Liometopum* nest-trees in periods shortly after rain, when the soil was slightly damp. At some nest sites with large, ground-level entrances, *Sceptobius* eggs and larvae could be collected from soil within the opening itself. Eggs and larvae were once recovered from decaying plant matter in the crook of a tree, which also hosted a *Liometopum* bivouac, roughly 15 meters from the main nest.

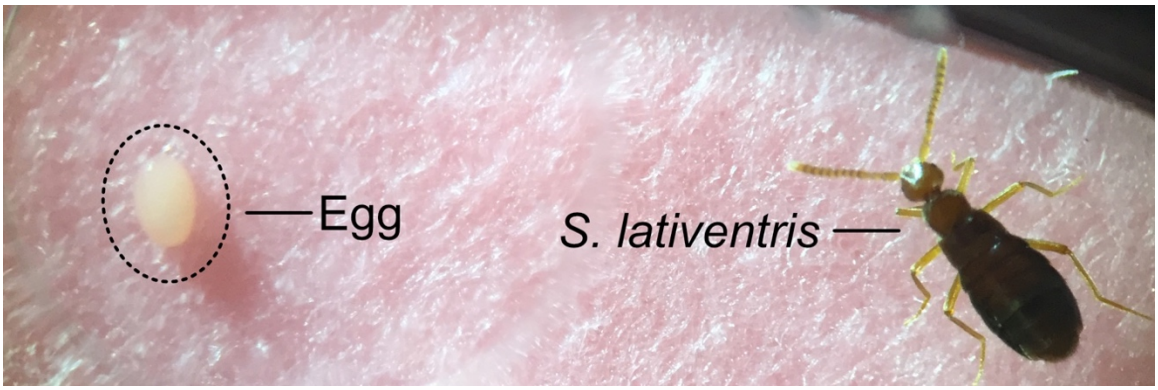

Figure 23. *Sceptobius lativentris* next to a freshly laid egg. This egg is small compared to viable *S. lativentris* eggs collected from the field.

Soil suspected to contain eggs and larvae was transported back to the laboratory, where eggs and larvae were located under a dissecting microscope. Eggs were stored on slightly damp filter paper in petri dishes and observed daily for the presence of freshly hatched larvae. Larvae were transferred to fresh petri dishes with damp filter paper. Attempts to identify a food source for *S. lativentris* larvae were unsuccessful, though it was found that the larvae do not require feeding to successfully pupate. After passing through two instars, late second instar larvae were transferred to a small container filled with the soil from which the larvae were originally collected. This was found to result in better survival chances for the beetles during pupation. The pupa box was checked twice daily for the presence of freshly eclosed, teneral beetles, which were either used immediately in experiments, or placed into small petri dishes with damp filter paper and ~5 *L. occidentale*. Eggs took, at most, 7 days to hatch, larvae took roughly 7 days to pupate, split evenly between the instars, and pupae took 12-13 days to eclose. The large sizes of *S. lativentris* eggs and the ability of the immature stages to reach adulthood in the absence of food might be an adaptation to reduce the duration of the immature stages, during which the beetle is outside of the nest away from the protection of the host ant and exposed to the arid conditions of southern California. Abbreviated development exists in another highly integrated symbiont, the aleocharine rove beetle *Corotoca melantho.* The beetle mimics the CHCs of its termite host, *Constrictotermes cyphergaster*[132] and lives inside of nests of the termite. *Corotoca*

species are viviparous[133] and exit the nest to deposit their larvae on the backs of foraging termites[134], which eventually results in the larvae falling off into the soil surrounding the termite nest, where the larvae then burrow into the soil. It is possible that the loss of traits and gain of various adaptations that accompany obligate myrmecophily and life in ant nests[51] causes the immature forms of myrmecophiles, which are external to the nest, to be less adapted to the surrounding environment. Thus early developmental processes of the immature stages become extended within the gravid female, which is protected inside of the nest. Conversely, for many myrmecophilous lycaenid butterflies, which spend their immature stages inside the nest and their mature stage outside the nest, the immature stages take longer to develop than closely related, free-living species[135].

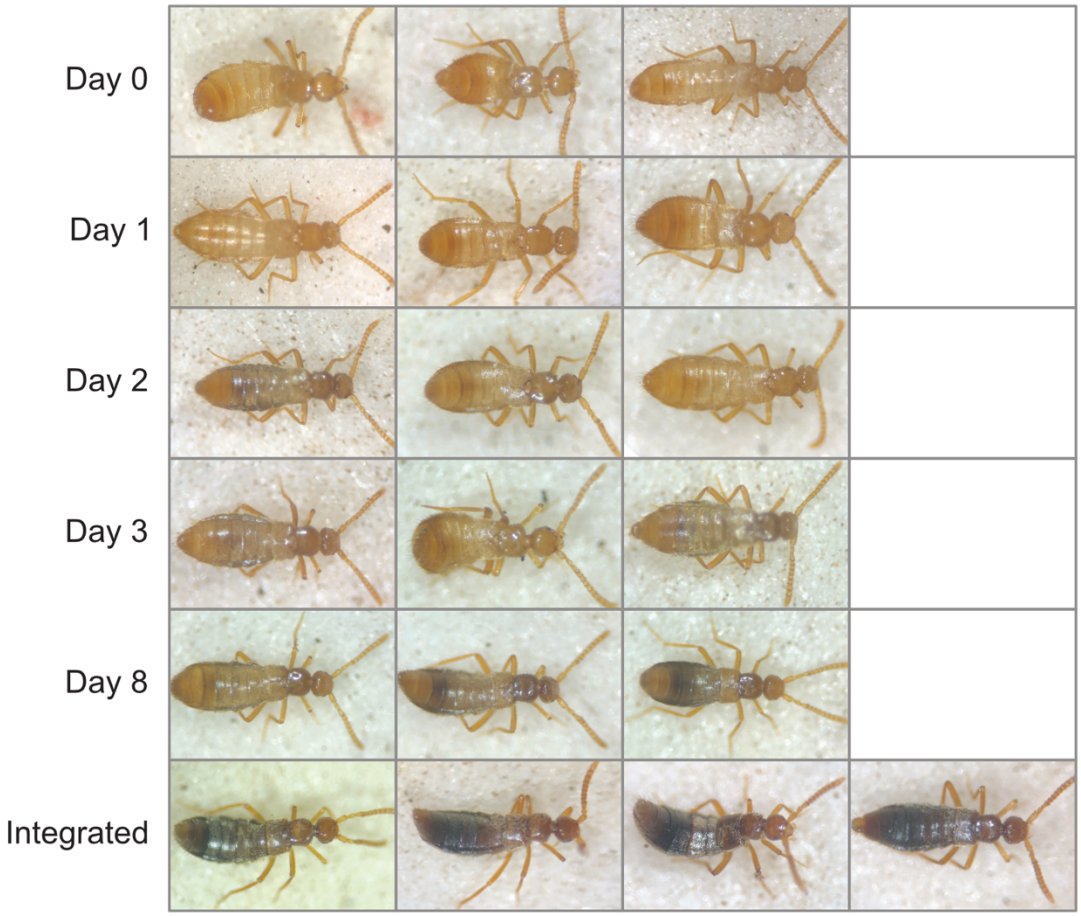

Figure 24. *Sceptobius* ecloses minimally sclerotized and further sclerotizes throughout the following week.

Once they have eclosed, the young teneral beetles likely make their way back into the nest. In the field, teneral beetles have been observed moving within foraging trails at night, and these may have been beetles making their way into the nest for the first time. The freshly eclosed teneral beetles exhibit minimal sclerotization (the hardening of the insect cuticle via polymerization with proteins and chitin, which typically results in a darkening of the cuticle), and were also found to die in the absence of ants. Teneral beetles, provided immediately with ants, exhibited an impressive cuticle tanning, which occurred throughout the first two weeks after eclosing (Figure 24). The full life cycle of *S. lativentris* is shown in Figure 25. To summarize, adult beetles, which live in the nests of *L. occidentale*, leave the nest and lay their eggs in the soil surrounding the nest. The larvae hatch and undergo two molts, without eating, prior to pupating, also in the soil surrounding the nest. Teneral beetles eventually eclose, making their way back into the nest and sclerotizing in the process.

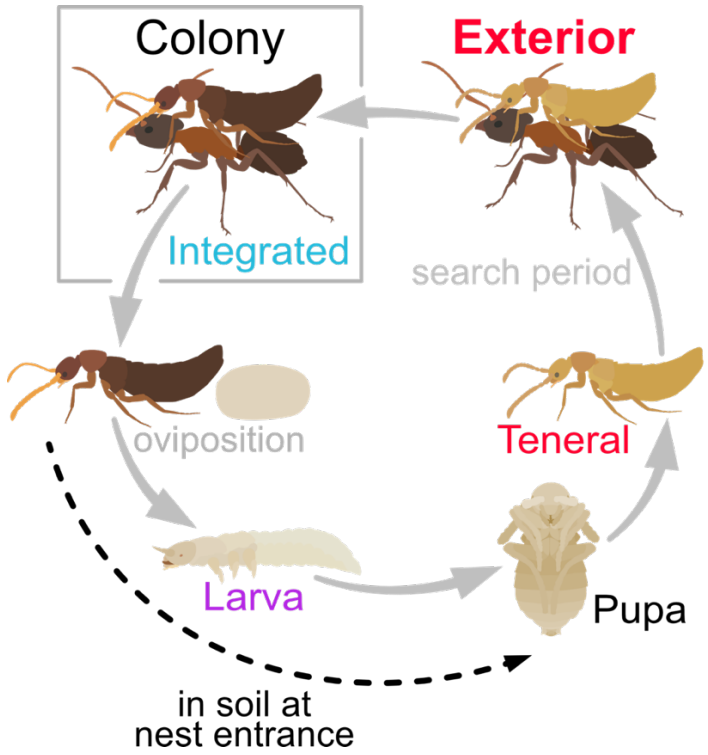

Figure 25. The full life cycle of *S. lativentris.*

C h a p t e r 2

PHYLOGENOMICS AND CONVERGENT MIMICRY

Knowing that the three rove beetles mimic the CHC profiles of *L. occidentale* with varying degrees of accuracy and engage in distinct behaviors that allow them to interact with the host ant, we wanted to verify that the three beetles had convergently evolved symbioses with *L. occidentale*. Obviously, the placement of the three beetles in three distinct aleocharine tribes would suggest that they evolved myrmecophily independently of each other, but a phylogenomic approach, in combination with fossil calibration points to generate a time calibrated species tree would verify that no mistakes had been made in the taxonomic placement of the beetles and would additionally place bounds on when the three symbioses formed. In order to generate a species tree, transcriptomes or mRNA predictions from the genome were needed for the three species, as well as many other beetle species from within Aleocharinae and outgroup species from across the rest of the Coleoptera. Free-living beetle species from sister taxa to the three myrmecophiles were included in the tree in order to demonstrate that the three myrmecophiles emerged from within independent, free-living groups. Within Lomechusini, the free-living beetle *Drusilla canaliculata*[136] was chosen as a partner to *P. sonomae.* Within the Oxypodini, the free-living beetle *Oxypoda opaca*[125] was paired with *L. newtonarum*. Because the entire Sceptobiini tribe is myrmecophilous[89], a free-living *Falagria* species[125] and the free-living *Lissagria laeviuscula*[125] from the sister tribe Falagriini[55] were used as comparison points for *S. lativentris*. Genomes and corresponding mRNA predictions for the *Oxypoda*, *Falagria*, and *Lissagria* species had previously been generated[125], but for *D. canaliculata,* a *de novo* transcriptome was generated and used instead.

How accurately the three myrmecophile populations are able to mimic the CHC profile of their host

has some bearing on their ability to integrate into ant nests, and can begin to provide insights into whether or not the organisms are generalists or specialists[64]. Comparison of the CHC profiles of *L. occidentale* to free-living beetles could provide insights into where in CHC chemical space the ant sits relative to other organisms. Does the ant sit in a populated region within chemical space, or is its profile distinct, and unlikely to be randomly matched by some free-living organism? Many individuals of the three myrmecophiles, as well as *L. occidentale* were collected from multiple ant nests in order to quantify the accuracy of CHC mimicry for the three species. Free-living aleocharine beetles were also collected and their CHC profiles were analyzed in order to provide a free-living, non-mimetic CHC profile baseline against which the mimetic myrmecophile profiles and the *L. occidentale* profile could be compared. Various methods of data clustering and visualization were employed to verify the mimetic accuracy regardless of analysis type.

Generating Transcriptomes

De novo transcriptomes were generated for *S. lativentris, P. sonomae,* and *D. canaliculata*. A genome and mRNA predictions had previously been generated for *L. newtonarum*[125], and thus the generation of a transcriptome for the beetle was unnecessary. Both *S. lativentris* and *P. sonomae* were collected from *L. occidentale* nests near Chaney Trail in the Angeles National Forest in 2018 and 2019, and *Drusilla canaliculata* were collected and provided by Joe Parker. *S. lativentris* were maintained in the laboratory with *L. occidentale*, and *P. sonomae* and *D. canaliculata* were maintained on a diet of frozen *L. occidentale* until they were used for RNA extraction. With help from Julian Wagner, approximately 120 *S. lativentris* were dissected, separating the 6th and 7th abdominal segments from the 8th abdominal segments, flash freezing each sample as it was dissected. The choice of tissues to dissect was originally selected for a differential expression analysis project that was later abandoned, but the RNAseq reads were still useful for transcriptome assembly. The legs and antennae from the 120 *S. lativentris* above were also dissected and flash frozen, separating the samples by the sex of the

dissected beetle. To this pool, an additional 20 male and female *S. lativentris* were dissected into pools of legs, antennae, and the rest of the body, separated by sex. These flash frozen samples were stored at -80˚C until further processing. With help from David Miller, one male and one female each of *P. sonomae* and *D. canaliculata* were dissected, separating each species and sex into heads and bodies. From these various dissected samples, both freshly dissected and flash frozen, total RNA was extracted using a ZYMO *Quick-RNA* Tissue/Insect extraction kit (ZYMO Research, CA). The RNA quantity was assessed for each sample using a Nanodrop (Thermo Fisher, CA) and then samples were sent to a third party (Omega bioservices), which performed the RNA sequencing (RNAseq) library preps and sequencing. For *S. lativentris,* 150bp libraries were prepared and sequenced, paired end, to a read depth of 100 million reads, and for *P. sonomae* and *D. canaliculata*, 100bp libraries were prepared and sequenced, paired-end, to a read depth of 100 million reads. Reads were initially assembled into *de novo* transcriptomes using Trinity v2.8.6[137]. At this stage, it was found that due to an error with the library prep, there was cross contamination of the RNAseq reads for *S. lativentris*, *P. sonomae*, and *D. canaliculata*. The *S. lativentris* libraries had been cross-contaminated with *Dalotia coriaria* reads (libraries for both species had been prepared at the same time by Omega bioservices) and the *P. sonomae* libraries and *D. canaliculata* libraries were cross-contaminated (these two libraries had also been prepared at the same time by Omega bioservices).

In order to not waste the RNAseq data, the RNAseq reads for *S. lativentris*, *P. sonomae*, and *D. canaliculata* were filtered to remove the contamination. Draft genomes had been prepared for *S. lativentris*, *P. sonomae*, and *D. canaliculata*, and a reference genome had been prepared for *D. coriaria* by Sheila Kitchen, and these genomes were combined to generate a *S. lativentris*/*D. coriaria* concatenated genome and a *P. sonomae*/*D. canaliculata* concatenated genome. Reads for each of the three contaminated transcriptomes were then mapped onto their corresponding concatenated genomes using BOWTIE2 v2.3.4.1[138]. For each organism, the reads were filtered, only collecting those that

mapped to the correct portion of the concatenated genome. The contaminating reads, mapping to their respective species' portion of the concatenated genome, were thus filtered out at this step.

The filtered read quality was assessed with fastQC v0.11.8[139] and then reads were filtered further using rCorrector v.1.0.4[140] to identify and correct random sequencing errors followed by a script[141] to filter out uncorrectable reads flagged by rCorrector. Reads were then processed with TrimGalore v0.6.0[142] to remove any remaining adaptors. All reads were combined for each species and fed to TRINITY v.2.12.0[137] for *de novo* transcriptome assembly with Jaccard clipping. The assembled transcriptomes were assessed for completeness via gVolante[143] using BUSCO v5[144] with the Arthropoda orthologue set. BUSCO scores for *P. sonomae*, *D. canaliculata*, and *S. lativentris* were 99.9%, 99.9%, and 100% respectively for the 1,013 core genes analyzed. Open reading frames were identified for the *de novo* transcriptomes using transdecoder v5.5.0[137] and then CDHIT v4.8.1[145] was used to remove duplicate sequences using a 98% sequence identity threshold.

Phylogenomic Tree Construction

In order to generate a species tree, an approach was taken in which approximately single copy orthologous sequences were identified from across the different transcriptomes and gene predictions, alignments were generated for each set of orthologs, and all the ortholog alignments were concatenated, generating a supermatrix where each species was represented by a single concatenated supergene[146,147]. A tree could then be calculated from the supergene alignment, or supermatrix, using a maximum likelihood approach.

The three filtered transcriptomes were combined with gene predictions from 27 genomes which had previously been collated or assembled[125] (Appendix, Table 1) including *Drosophila melanogaster* as an outgroup and various free-living beetles spanning the beetle suborder Polyphaga. Protein coding

sequences from the 30 species were processed with Orthofinder v2.5.2[148,149] to find orthologous sequences, which were grouped into orthogroups. The generated amino acid sequence alignments from each orthogroup were filtered for alignments containing at least one sequence for 80% of the species used. These alignments were trimmed using trimal v1.4.1[150] and then maximum likelihood gene trees were generated for each of the alignments using iqtree v1.6.8[151,152] with 1,000 bootstraps, restricting the program to the WAG,LG, JTT, and Dayhoff substitution models. Some of these gene trees contained multiple gene copies for individual species, due to recent gene duplications or the inclusion of analogous gene families into the same orthogroup. In order to generate strictly orthologous, single copy gene trees, trees were processed with PhyloTreePruner v1.2.4[153] with a minimum taxa cutoff of 80% and a bootstrap support cutoff of 0.7. The resulting pruned alignments were concatenated using FASconCAT v1.04[154], generating a supermatrix containing 750,163 amino acid sites with 2,063 gene partitions. In order to improve the quality of the final species tree, MARE v0.1.2[155] was used to identify a subset of the supermatrix with high data coverage and high phylogenetic signal, resulting in a reduced supermatrix containing 374,139 amino acid sites with 1,039 gene partitions. When generating a maximum likelihood tree from large alignments, improvements in phylogenetic inference can be gained by allowing for different models of evolution for different subsets of the alignment[156], such as the different gene alignments within the supermatrix. Intuitively, this makes sense, as selection pressures can vary drastically across gene families[157]. Partitionfinder v.2.1.1[156,158] was used with raxml[159] to identify a an optimal partitioning scheme and corresponding set of molecular evolution models for the gene partitions. A maximum likelihood species tree was generated from the supermatrix and partition scheme using iqtree v1.6.8[151,152] with 1,000 bootstrap replicates (Figure 26). The positions of the three myrmecophiles appear within the expected clades, with the exception of *S. lativentris*, which appears within the tribe Falagriini instead of sister to it. This topology may represent the true placement of the genus *Sceptobius* within the tribe

Falagriini, but more careful systematics work would be required to unequivocally determine this relationship. All nodes within the tree have strong bootstrap support.

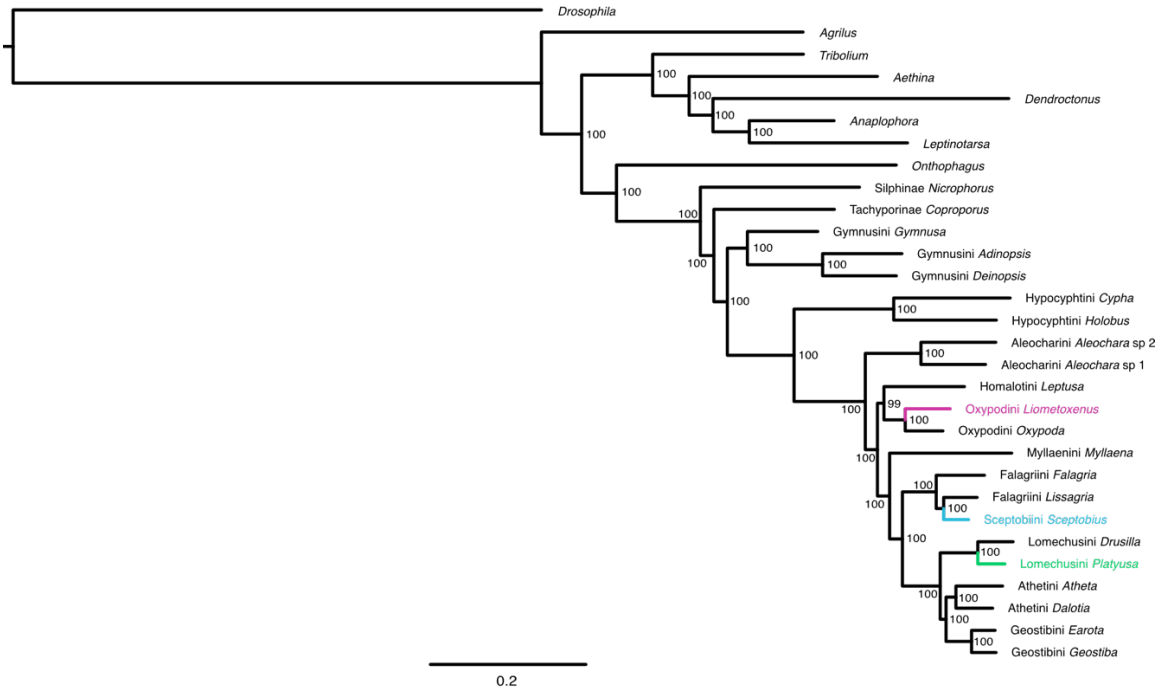

Figure 26. Species tree generated using a maximum likelihood approach for the species listed in Table 1. Numbers on nodes represent bootstrap support. Italicized names correspond to generic names whereas roman names, where given, correspond to tribes, or, in the case of Silphinae and Tachyporinae, subfamilies.

Time Calibrated Species Tree Construction

More than half a century ago, the idea of the molecular clock was proposed[160], positing that mutations in the same sequence in two different organisms should accumulate at a certain rate and thus sequence divergence between the two species should be proportional to absolute time since the species diverged. With time it became clear that substitution rates are not fixed across different taxa and that rates within a phylogenetic tree could vary between branches[161], due to differences in effective population size, generation time, and species typical mutation rates[162]. As a result, most methods for estimating divergence times allow for mutation-rate heterogeneity across the tree. Because substitution rates can vary so drastically, it is impossible to determine absolute divergence times

purely from sequence data alone. Independent sources of chronological information are required. One method for converting relative time to absolute time estimates utilizes external fossil calibration points[163]. Fossil specimens with a known placement within the phylogeny and a constrained age based on stratigraphic or radiometric dating information can be used to place lower age bounds on specific nodes within the phylogeny[164]. Because rates can vary across branches it is typically recommended that multiple calibration points spanning the phylogeny be used[165].

In order to constrain divergence times on the species tree (Figure 26), twelve fossil calibrations were selected to place bounds on specific nodes within the tree. For all fossils, the youngest age interpretation of the fossil was used, following best practices[166]. The following fossils were chosen, with corresponding nodes labelled in Figure 27.

A. MRCA of Diptera and Coleoptera

The outgroup for the species tree, *Drosophila melanogaster,* is a member of the order Diptera, whereas the other 29 species fall within Coleoptera. In order to place an upper bound on the age of the root of the tree, the median age estimate for the most recent common ancestor (MRCA) of holometabolous insects was used (345 mega annum, Ma)[167]. A lower bound was chosen for this node using the beetle fossil *Coleopsis archaica* (293.8 Ma)[168], which is a stem group beetle—it has a greater affinity to Coleoptera than to any other extant insect orders, yet cannot be placed within any modern beetle family.

B. MRCA of Buprestoidea and all other beetles in this study

Agrilus planipennis, a member of the Buprestoidea, is the earliest branching beetle within the phylogeny. Using the stem group Buprestid fossil, *Ancestrimorpha volgensis* (164.7 Ma)[169,170], a lower bound was placed on the MRCA of *A. planipennis* and the remaining beetles.

C. MRCA of Curculionoidea and Chrysomeloidea

A lower bound was placed on the MRCA of Curculionoidea (*Dendroctonus ponderosae*) and Chrysomeloidea (*Anaplophora glabripennis* and *Leptinotarsa decemlineata*) using two fossil samples, an *Archaeorrhynchus* sp. and an *Eobelus* sp. (157.3 Ma)[171,172].

D. MRCA of Chyrsomeloidea

A lower bound was placed on the MRCA of Chrysomeloidea using the beetle fossil *Creoprionus liutiaogouensis* (122.5 Ma)[172,173].

E. MRCA of Staphylinidae

The earliest diverging member of the Staphylinidae in the species tree is *Nicrophorus vespiloides*, from the subfamily Silphinae. The position of Silphinae within Coleoptera has historically been contentious[174], but recent work points to its position within Staphylinidae instead of sister to Staphylinidae[175]. Thus a lower bound was placed on the node at which *Nicropherus vespiloides* diverges from the rest of Staphylinidae using undescribed Silphid fossils[176] from the Daohugou Biota[177] (152 Ma).

F. MRCA of Aleocharinae and Tachyporinae

A lower bound was placed on the MRCA of Tachyporinae (*Coproporus ventriculus*) and Aleocharinae (includes the tribes: Gymnusini, Hypocyphtini, Aleocharini, Homalotini, Oxypodini, Myllaenini, Fallagriini, Sceptobiini, Lomechusini, Athetini, and Geostibini) using the Tachyporine beetle fossil *Protachinus minor*[178] from the Tralbrager fish beds[179] (147.28 Ma).

G. MRCA of Gymnusini

Recently the former tribe Deinopsini (*Adinopsis* and *Deinopsis* in the species tree) was synonymized under Gymnusini[180], and that convention is followed in this work. A lower bound was placed on the MRCA of Gymnusini using the crown Gymnusine beetle fossil *Cretodeinopsis aenigmatica*[181] from Burmese amber[182] (98.17 Ma).

H. MRCA of *Adinopsis* and *Deinopsis*

A lower bound was placed on the MRCA of *Adinopsis* and *Deinopsis* using the beetle fossil *Adinopsis groehni*[183] from Baltic amber[184] (43.1 Ma). It should be noted that there is some contention surrounding the age of Baltic amber formations[185]. In maintaining consistency with other dating analyses of the Aleocharinae[54,125], I have settled on the above date.

I. MRCA of Hypocyphtini

A lower bund was placed on the MRCA of the tribe Hypocyphtini using the beetle fossil *Baltioligota electrica*[186] from Baltic amber (43.1 Ma).

J. Aleocharini Stem

A lower bound was placed on the stem of Aleocharini based on the beetle fossil *Aleochara baltica*[187] from Baltic amber (43.1 Ma).

K. MRCA of Oxypodini and Homalotini

A lower bound was placed on the MRCA of Homalotini and Oxypodini using the beetle fossil *Phymatura electrica*[187] from Baltic amber (43.1 Ma).

L. MRCA of Athetini and Geostibini

The position of *Dalotia coriaria* within the tribe Athetini has been a source of debate over the past century[188], with the beetle being placed in the tribe Athetini either within a monotypic genus, or within the genus *Atheta.* This presents a problem, as the use of the fossil beetle *Atheta jantarica*[186] from Baltic amber (43.1 Ma), which is a stem-group *Atheta,* could be used to calibrate the MRCA of *Dalotia coriaria* and *Atheta pasadenae* if the two genera are distinct, but would have to be moved one node up in the tree if the *Dalotia coriaria* is a member of *Atheta*. The conservative approach, which I take, is to move the calibration point one node up, to the MRCA of Athetini and Geostibini.

MCMCtree and codeml, from PAML v4.9[189], were used to estimate divergence times, using the previously generated maximum likelihood species tree (Figure 26), the associated supermatrix, and the fossil calibration points listed above. Branch lengths were initially approximated in codeml by maximum likelihood (ML) using the WAG empirical rate matrix[190] with gamma rates among sites, approximated with four rate categories. The gradient and Hessian of the likelihood function at the ML branch length estimates were then used to run MCMCtree with the approximate method. The relevant model parameters were clock = 2, cleandata = 0, BDParas = 1 1 0.1, rgene_gamma = 2 20 1, sigma2_gamma = 1 10 1, and finetune = 1: .1 .1 .1 .1 .01 .05. All fossil calibration points were modelled as truncated Cauchy distributions[191], defined with default MCMCtree parameters, with the exception of the tree root, which was defined as a uniform distribution between the upper and lower bound with tails on either sides of the bounds[192]. After a burn in of 20,000 iterations, 200,000 samples were collected, sampling every 100 iterations. Divergence time estimates were compared between multiple runs to verify that the MCMC chains had converged to a stable posterior distribution. The resulting tree demonstrates that the three myrmecophile lineages share a free-living most recent common ancestor ~89 million year ago, prior to the rise of ants to ecological dominance[193], with each species emerging from within free-living clades at most 50 million years ago.

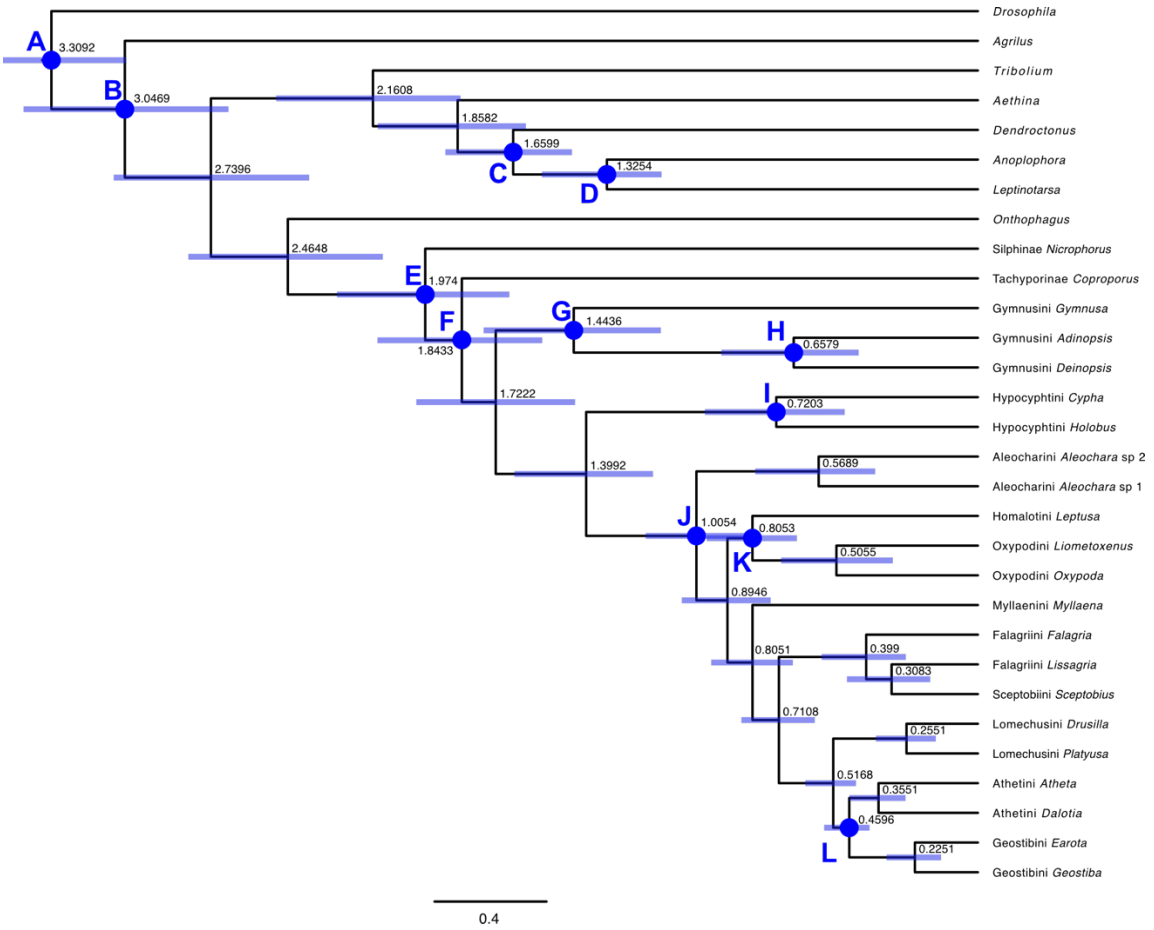

Figure 27. Time-calibrated species tree. Median node ages are listed for all nodes with 95% confidence intervals shown with blue bars. Values are listed in units of 100Ma. Blue dots represent fossil calibration points.

Accuracy of CHC Mimicry

Over the course of multiple collecting seasons and across numerous ant colonies from multiple field sites within the Angeles National Forest, *L. occidentale* and their associated *S. lativentris*, *P. sonomae*, and *L. newtonarum* were collected. Free-living beetles were accumulated from various sites over the course of a number of years. Julian Wagner collected a *Falagria* species (Falagriini) from central California, in the vicinity of Livermore. Joseph Parker collected *Drusilla canaliculata* (Lomechusini). *Dalotia coriaria* (Athetini) were collected from a population of the species maintained in the Parker lab. An *Oligota* species (Hypocyphtini) and an *Acrotona* species (Athetini)

were collected from the leaf litter surrounding *L. occidentale* nests in the Angeles National Forest. All beetles were transported to the laboratory live prior to analysis of CHCs. Whole beetles were extracted in 70 microliters, or 10 microliters for *Oligota*, of hexane for 20 minutes and crude extracts (2μL) were run on a Shimadzu QP2020 GCMS equipped with Helium as a carrier gas and a Phenomenex ZB-5MS fused silica capillary column (30m x 0.25mm ID, df=0.25μm). The injection port was operated at 310˚C in splitless mode, with a column flow rate of 2.15 mL/min. The column was held at 40˚C for 1 minute, ramped at 20˚C/min to 250˚C, ramped at 5˚C/min up to 320˚C, and then held at 320˚C for 7.5 minutes. The transfer line was held at 320˚C and the ion source temperature was held at 230˚C. Electron ionization was carried out at an ion source voltage of 70eV, and MS scans were collected between 40 m/z and 650 m/z at a scan rate of 2 scans per second. Identification of individual CHC compounds was determined based on the retention index, calculated relative to a linear alkane standard[194], diagnostic ions in the mass spectra[195] (Appendix Table 2), and comparison to previously described *L. occidentale* and *Drosophila melanogaster* GCMS data[26,196]. Peaks were manually integrated in LabSolutions Postrun Analysis (Shimadzu). Alkene double bond position was previously identified for a number of *L. occidentale* compounds[196].

CHC measurements were converted to percent composition for each spectrum, because the relative ratios of the various compounds are more important in recognition than the absolute abundance of any individual compound[197,198]. Differences in CHC profile were determined with the Bray-Curtis (BC) dissimilarity metric, as the great variety of CHCs found within the different species resulted in an abundance of zero values in the data matrix, which can result in unintuitive results if using Euclidean distances instead[199]. Pairwise BC dissimilarity was calculated across all samples and then non-metric multidimension scaling (NMDS) ordination was performed using the metaMDS function from the vegan R package[200], which is a standard approach in compositional data analysis[201]. BC dissimilarity was also calculated between all ant/myrmecophile samples and the average CHC profile

of the colony from which they were collected. The BC dissimilarity of all free-living beetle profiles was calculated relative to the overall average ant profile. The R function hclust was additionally used to perform hierarchical clustering of the pairwise BC dissimilarity matrix and also the pairwise Jaccard dissimilarity matrix of the binarized CHC data.

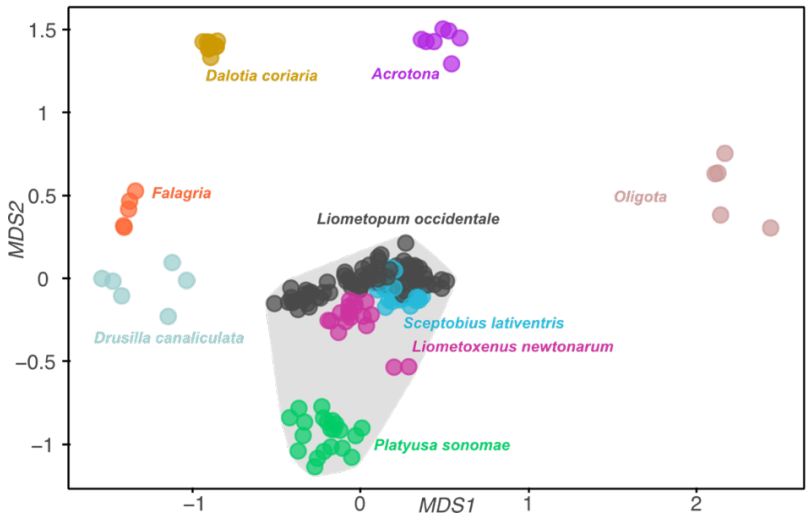

Figure 28. NMDS ordination of CHC profiles for *L. occidentale*, myrmecophiles, and free-living beetles, 2D stress: 0.1361. A convex hull is drawn around the myrmecophiles and the host ant.

NMDS ordination of pair-wise BC dissimilarities (Figure 28), revealed that the *S. lativentris* CHC profiles cluster within the *L. occidentale* CHC space, *L. newtonarum* CHCs differ slightly from *L. occidentale* CHCs, and *P. sonomae* CHCs are the most distinct of the three myrmecophiles, due to imperfect matching of the host CHC ratios, as well as the presence of beetle specific compounds not found on the host. The profiles of all three beetles are more similar to the profile of the ant, on average, than other free-living beetles, though the profile of *Drusilla canaliculata* is also quite similar to the profile of *L. occidentale*. It should be noted that *D. canaliculata*, while primarily free-living[51] is occasionally found with different species of ants[202,203] and is known to prey on a variety of species of ants. While not a myrmecophile associated with any species or clade of ants, the profile of the beetle may still possess generally ant-like CHCs in the vicinity of the chemical space of the various species

that the beetle preys on. It should also be noted that the three myrmecophiles are more similar to the host ant than they are to any of their more closely related beetle relatives.

Next, the CHC profiles of the myrmecophiles were compared to ants from the colony from which they were collected, and the free-living beetle CHC profiles were compared to the average *L. occidentale* profile (Figure 29). This revealed that on a colony-by-colony basis, the beetles are more similar to *L. occidentale* than any of the free-living beetles, and more importantly, that the *Sceptobius* CHC profile falls within the range of variation seen within *L. occidentale* nests.

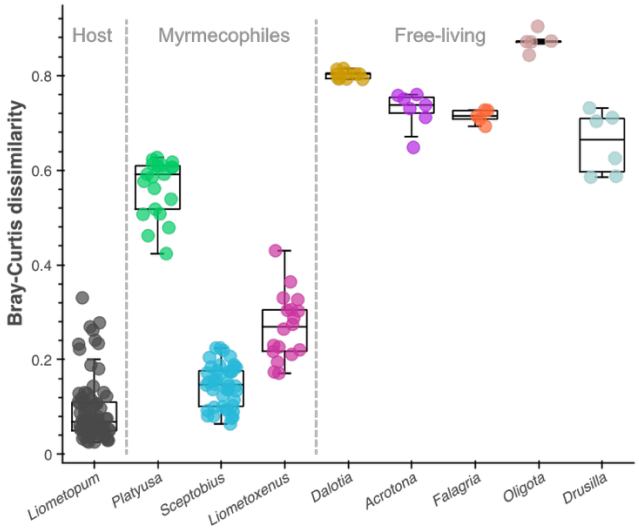

Figure 29. Bray-Curtis dissimilarity of each individual beetle calculated relative to the average *L. occidentale* colony CHC profile from which it was collected. Free-living profiles were compared to the overall average *L. occidentale* profile.

Hierarchical clustering was performed on the pairwise BC dissimilarities as an additional means of assaying CHC mimicry (Figure 30). As expected, all myrmeophiles clustered more closely with the host ant than any of the free-living species, with *P. sonomae* exhibiting the greatest difference compared to the ant of all of the myremcophiles. We also measured the Jaccard distance for all of the samples, which is similar to the Bray-Curtis dissimilarity, but instead treats CHCs as either present or absent, and calculates the intersection of the CHCs compounds between individuals over the union

of CHC compounds between the same individuals. Hierarchical clustering of the Jaccard index also recapitulated the ant-centric clustering of the myrmecophiles (Figure 30).

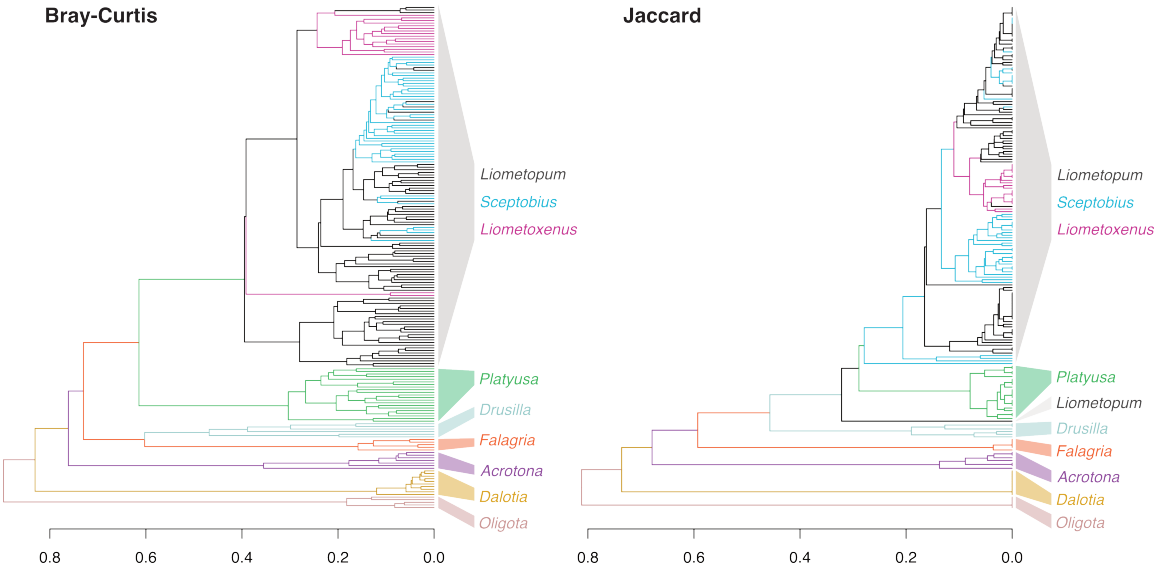

Figure 30. Hierarchical clustering of CHC dissimilarity data, using either Bray-Curtis dissimilarity, or Jaccard index.

Thus the three myrmecophiles appear to have independently evolved symbiotic lifestyles with the host *L. occidentale*, which formed within the past fifty million years. A key component of this evolved lifestyle includes mimicry of the CHC profile of their host ant, which the three beetles achieved to a greater or lesser extent. This degree of accuracy in CHC mimicry is in agreement with the degree of integration of the three beetles into their host colonies, described above in the natural history observations.

Chapter 3

MIMICRY MECHANISMS

After determining that the mimicry of the myrmecophiles is robust within their populations, we next sought to determine the mechanisms by which the beetles achieve CHC mimicry. As previously described, two primary mechanisms exist for chemical mimicry, innate mimicry and acquired mimicry. In innate mimicry, the mimetic profile is produced endogenously by the myrmecophile, whereas in acquired mimicry, CHCs are transferred from the host to the myrmecophile[70]. In addition to their bearing on the possible accuracy of CHC mimicry and resulting response from ants, the two different CHC mimicry approaches have potentially critical life history consequences, due to the dual role of CHCs in preventing desiccation. Thus, understanding how the mimicry is achieved by the beetles can help to explain other, potentially unintuitive, aspects of the biology of the beetles.

Due to a number of factors, *P. sonomae* and *S. lativentris* were chosen as the focal species to understand the mechanisms underlying the mimicry. *S. lativentris* is the most integrated into nests of *L. occidentale* of the three beetle species, exhibits the most accurate CHC profile mimicry, and experiences no aggression from the host ant. *P. sonomae* is the least integrated into the host nests, exhibits the least accurate CHC profile mimicry, and experiences some aggression from the host ant. *L. newtonarum*, having an intermediated degree of integration into *L. occidentale* colonies, and exhibiting an intermediate degree of CHC mimicry accuracy, was assumed to use a mimicry approach intermediate between *P. sonomae* and *S. lativentris.* On a more practical note, *L. newtonarum* exhibits much stronger seasonality than the other two beetles and thus is impossible to collect for experiments throughout the majority of the year.

A number of techniques were used to identify the specific mimicry mechanisms. Because *P. sonomae* is able to survive in the absence of *L. occidentale,* an isolation experiment followed by GCMS analysis was performed in *P. sonomae* to determine if the CHC profile would shift in the absence of the host ant. Next, compound specific stable carbon isotope measurements were made of CHCs on *L. occidentale* and *P. sonomae* to verify the results of the isolation experiments. Enzymes associated with CHC biosynthesis were identified in *P. sonomae*, and their role in CHC biosynthesis was verified. Stable isotope measurements were performed in *S. lativentris,* and then behavioral and chemical transfer assays were performed.

Isolation of *Platyusa sonomae*

Wild caught *P. sonomae* were housed in containers free from live *L. occidentale* and fed either a diet of frozen *L. occidentale* or frozen *D. melanogaster* over the course of a month. After the feeding period, individuals were extracted in hexane and CHC profiles were analyzed via GCMS (Figure 31), as described above. No major decrease in the amount of CHCs was seen, nor were differences in the presence of the species typical CHCs observed, though slight shifts in the overall ratios of the hydrocarbons occurred. CHCs should turn over on shorter timescales than duration of the feeding experiment[85], and thus the CHC profile of *P. sonomae* appears to be endogenously produced.

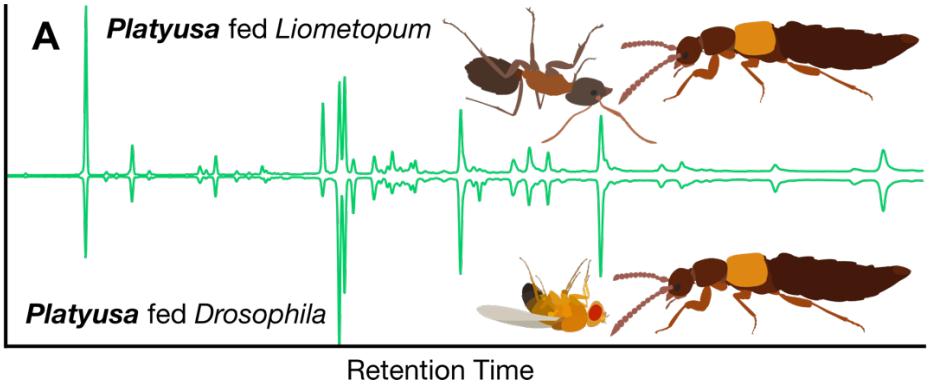

Figure 31. Representative GCMS traces of *P. sonomae* fed *L. occidentale*, top, compared to *P. sonomae* fed *D. melanogaster*, bottom.

CHC profiles of the isolated and control *P. sonomae* were analyzed quantitatively to determine if the slight shifts seen in the treatment group were the result of the beetle profile becoming more similar to that of the *D. melanogaster*, which they were consuming, and less similar to *L. occidentale*. GCMS measurements were made for a number of *D. melanogaster* and *L. occidentale*, taken from the same populations that were used for feeding *P. sonomae*. Next the Bray-Curtis dissimilarity between each *P. sonomae* and both the average *D. melanogaster* CHC profile as well as the average *L. occidentale* profile was calculated (Figure 32). These were compared to the BC dissimilarity of each *D. melanogaster* or *L. occidentale* relative to their species average profile. The *P. sonomae* CHC profiles were very distinct from the *D. melanogaster* CHC profile, with BC dissimilarity values above 0.8, and there did not appear to be any difference between the treatment and the control groups, demonstrating that the CHCs of *P. sonomae* were not becoming more similar to the *D. melanogaster* they were eating. All *P. sonomae* had CHC profiles much more similar to *L. occidentale,* with BC dissimilarity values between 0.4-0.7, in the same range as the profiles measured from freshly caught *P. sonomae* in Figure 29. There appeared to be a slight decrease in the accuracy of the mimicry in the *Drosophila* fed treatment, and thus it is possible that the beetle is able to modify its CHC profile when in the presence of ants, but this line of inquiry was not explored further.

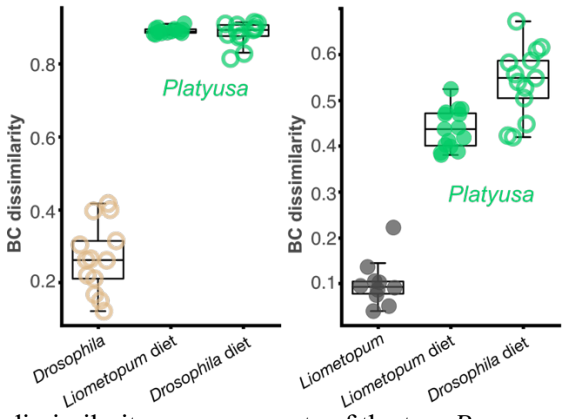

Figure 32. Bray-Curtis dissimilarity measurements of the two *P sonomae* treatment group CHC profiles, green, compared to either the average *D. melanogaster* or average *L. occidentale* CHC profile. The Bray-Curtis dissimilarity of each *D. melanogaster* and *L. occidentale* sample was also calculated relative to its species mean CHC profile.

CHC Stable Carbon Isotope Analysis in *Platyusa sonomae*

As a second, independent confirmation of *P. sonomae*'*s* innate CHC mimicry, we turned to compound specific stable isotope measurements. Stable heavy isotopes of many elements prevalent in living organisms are present in the environment at low levels and are incorporated into the biomolecules that those organisms produce[204]. Due to a number of different factors, different isotopes can fractionate within different classes of biomolecules[205], across different trophic levels[206], or modes of photosynthesis[207], making them a useful tool for tracking the flow of resources within food webs, identifying the trophic positions of organisms, or identifying biomarkers of various organisms in geochemical studies[208]. Within insects, stable isotopes have primarily been measured in bulk for entire organisms[209,210], averaging over the various tissues and biomolecules within each organism. It is possible, though, to measure isotope ratios for individual molecules by incorporating a gas-chromatographic step into the analysis, allowing for chromatographic separation of complex mixtures prior to determining isotope ratios[211]. For example, hydrogen and carbon isotope ratios can be measured in individual hydrocarbons extracted from insect cuticles and plants[208]. This opens up the possibility to measure isotope ratios in the same molecule produced in two different organisms. If the two biosynthetic pathways for the molecule fractionate a given isotope to different degrees, or if the inputs to the pathway differ in their starting isotope ratio, then the resulting molecule will have a different isotope ratio, depending on which organism it came from. While it cannot be ruled out that CHC biosynthesis in two different organisms could produce hydrocarbons with identical isotope ratios by chance, measurements of CHCs in a number of insect orders found varying isotope ratios between the different species[208] and consumers can sometimes be enriched in ^{13}C relative to their diet[212]. In the case of CHC mimicry, innate mimicry in the myrmecophile should result in hydrocarbons with a potentially distinct isotope ratio from the host ant, whereas acquired mimicry, with no endogenous production, should result in identical isotope ratios relative to the host ant.

Due to the high concentrations required for accurate measurement, ants and beetles were pooled with conspecifics from the same nest/collecting trip for stable isotope measurements. Between 28-50 ants and 20 Platyusa were pooled for each extraction. Insects were extracted in 1mL of hexane, which was then evaporated under a stream of nitrogen to a volume of roughly 100 microliters. Samples were then analyzed by gas chromatography separation followed by combustion in an oven to CO_2, followed by simultaneous mass spectrometric measurement of $^{12}C^{16}O_2$ and $^{13}C^{16}O_2$ on a Thermo Trace GC_{ultra} (Thermo Fisher, CA) interfaced to a Thermo-Scientific $Delta_{+}$XP GC-combustion-IRMS (Thermo Fisher, CA) equipped with a ZB-5MS column (30m x 0.25 mm ID, df=1µm, Phenomenex). Samples were injected in splitless mode into a PTV injection port with He as the carrier gas. The column was initially held at a temperature of 80˚C for 1 minute, followed by a 20˚C/min ramp up to 250˚C and then a 3˚C/min ramp up to 320˚C, which was held for 12 minutes. Stable carbon isotope measurements are typically reported in delta notation ($\partial^{13}C$), which corresponds to the $^{13}C/^{12}C$ ratio of the sample minus the $^{13}C/^{12}C$ ratio of a standard reference material (Vienna Pee Dee Belemnite or VPDB) divided by the ratio of the reference material and then multiplied by 1,000 to get the value into parts per thousand, or permille (‰). A CO_2 reference gas ($\partial^{13}C$ = -32.4‰) was co-injected during each sample run, generating four reference peaks against which sample $\partial^{13}C$ was calculated relative to VPDB. An external standard containing ethyl icosanoate (from the 'F8 mix' of Arndt Schimmelmann, Indiana University), which has a known $\partial^{13}C$ value of -26.1‰, was run every eight samples. The difference between the measured value and true value of the ethyl icosanoate standards bounding each set of eight runs was used to correct the $\partial^{13}C$ values of the intervening samples. Samples were measured in triplicate and arithmetic means are reported. Peaks were identified by comparison to GCMS measurements and the stereotypical elution order of the CHCs of the three organisms.

One of the challenges of compound specific stable isotope analysis arises due to the slight difference in retention time for isotopologs. Peaks being measured need to be well separated, as each shoulder of a peak will be enriched in either the heavier or lighter isotopolog[211]. The CHC profiles of *L. occidentale* and *P. sonomae* (Figure 13) possess a large number of peaks which are difficult to separate well; thus, in combination with the necessity for large sample concentrations, the number of hydrocarbons in the profile suitable for stable carbon isotope analysis is small relative to the total number of peaks present in the CHC profiles of the ants and beetles. In *P. sonomae* we were able to obtain good measurements for three of the alkanes in the profile (Figure 33), which showed that the CHCs in *P. sonomae* have a very different ∂^{13}C value from *L. occidentale*, confirming that *P. sonomae* produces an endogenous mimetic CHC profile.

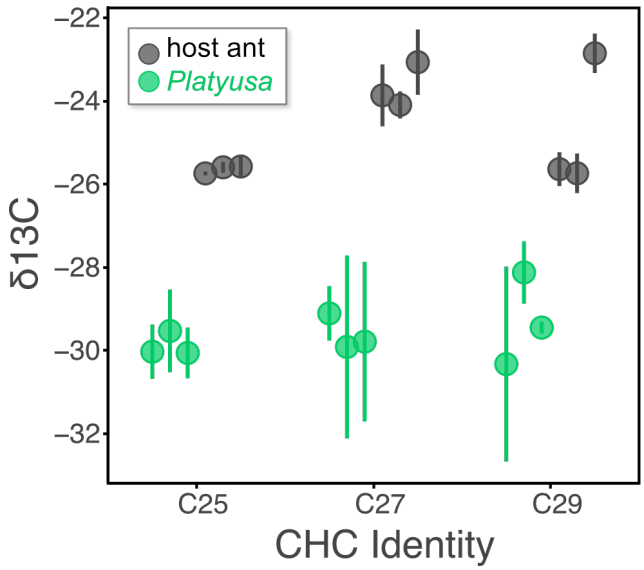

Figure 33. Stable carbon isotope measurements of selected CHCs from *P. sonomae* and *L. occidentale*. Bars represent standard deviation of triplicate measurements.

CHC Biosynthesis in *Platyusa sonomae*

Having confirmed that *P. sonomae* produces an endogenous profile, we next sought to demonstrate that the beetle possess the cells and the enzymes to produce CHCs. CHCs are produced in oenocytes, which are specialized cells located in the abdomen of insects[213]. In order to locate oenocytes in *P.*

sonomae we used Hybridization Chain Reaction Fluorescence in situ Hybridization[214] (HCR-FISH or just HCR) to label mRNA transcripts for one of the enzymes in the CHC biosynthesis pathway, which would be localized within oenocytes. I will discuss the rest of the pathway later in this chapter, but the final enzyme in the pathway is a single copy cytochrome P450[215] which performs an oxidative decarbonylation to produce the final alkanes or alkenes[216]. This enzyme had already been found and characterized via knockdown in the closely related aleocharine beetle *Dalotia coriaria*[56], and a BLAST search against the *P. sonomae* transcriptome recovered a single obvious target, called CYP4G1.

HCR probes were designed to target *CYP4G1*. Probe sets, HCR hairpins, as well as amplification buffer, hybridization buffer, and wash buffer were purchased from Molecular Instruments (Beckman Institute at Caltech; www.moleculartechnologies.org). *P. sonomae* were dissected in DEPC treated PBS with a small amount of DEPC PBST (0.1% Tween) added. Beetles were CO_2 anesthetized and then transferred to a dissecting dish and the head was removed with dissecting scissors. Grasping the thorax and abdominal segments 9 and 10 with forceps, the abdominal tip, gut, and genitalia were removed through the tip of the abdomen. The abdomen was then either separated along the sagittal plane or separated ventrally and dorsally with dissecting scissors. Samples were placed in ice-cold DEPC-PBST until fixing. Abdominal segments were fixed in 4% PFA in DEPC-PBST for 25 minutes at room temperature and subsequently rinsed three times with fresh DEPC-PBST. Samples were then dehydrated by washing with a DEPC-PBST/methanol series, finishing with a 100% methanol wash. At this step, samples were either stored at -20˚C or rehydrated using a methanol/DEPC-PBST series. Samples were rinsed two additional times for 5 minutes each at room temperature and then washed with a 0.01% Proteinase K solution in DEPC-PBST for 5 minutes at room temperature. Samples were then rinsed twice with fresh DEPC-PBST and post-fixed with a 4% PFA in DEPC-PBST solution for 25 minutes at room temperature. Samples were rinsed again with DEPC-PBST and then incubated

with hybridization buffer at 37˚C for 30 min. The probe solution was then preheated during this period, combining 2 microliters of both even and odd HCR probes with 100 µL of hybridization buffer at 37˚C. The hybridization buffer was removed from the sample and replaced with probe solution. Samples were incubated overnight at 37˚C. No-probe control samples were incubated overnight at 37˚C in hybridization buffer in the absence of the probes. The following day, samples were washed with preheated wash buffer, 2 x 5 minutes and 2 x 30 minutes, both at 37˚C. During the last wash, hairpins were snap cooled (90 seconds at 95˚C and then 30 min room temp in the dark). Samples were incubated with amplification buffer for 10 min, after which the old amplification buffer was replaced with 100 µL of fresh amplification buffer and the hairpins. Amplification occurred overnight in the dark at room temp and Alexa 488 fluorophores were used. Samples were then washed with SSCT (saline sodium citrate with tween) twice for 5 minutes in the dark. Samples were incubated for 2 hours at room temperature with Hoechst 33342 (1:2000, Thermo Fisher, CA) to mark nuclei, and then washed four more times with SSCT, twice for 5 min and twice for 30 mins. Samples were mounted in ProLong Gold Antifade Mountant (Thermo Fisher, CA), and imaged using a Zeiss LSM 880 with Airyscan fast at 10x and 40x.

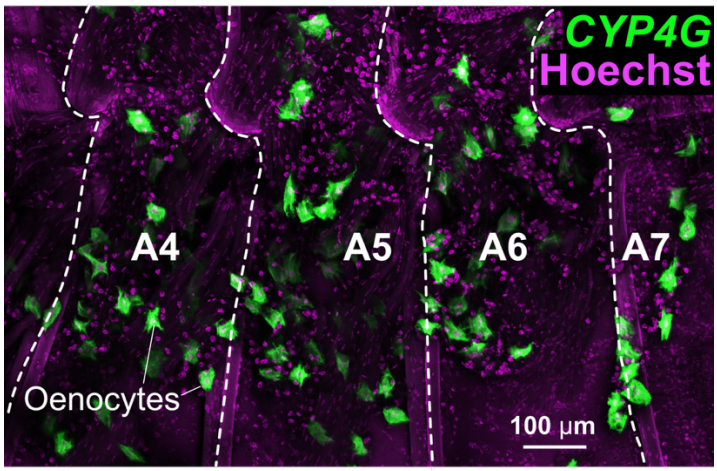

Figure 34. *CYP4G1* HCR probes (green) label oenocytes in the abdomen of *P. sonomae* (magenta, Hoechst, nuclei). The dashed lines delineate different abdominal (A) segments.

A large population of cells in the abdomen was targeted by the *CYP4G1* HCR probes (Figure 34), and their morphology and distribution looked similar to that of oenocytes in *Dalotia coriaria*[56]. This confirmed that *P. sonomae* possesses oenocytes. In order to verify that CYP4G1 is involved in CHC production in *P. sonomae,* we then performed RNA interference (RNAi) to silence expression of *CYP4G1*. RNAi is a technique that takes advantage of an endogenous regulatory mechanism in eukaryotic cells which leads to the targeted degradation of specific mRNAs[217]. By injecting double stranded RNA (dsRNA) constructs in which one of the strands is complementary to a transcript of interest, the endogenous silencing machinery selectively degrades the targeted transcript, preventing the transcription of the specific mRNA target[218]. It was found in the beetle *Tribolium castaneum* that direct injection of dsRNA into the body cavity of larvae can induce systemic knockdown across a range of tissues[219]. Subsequent work found that injections into adult *T. castaneum* also results in systemic knock down[220]. The technique functions similarly in the aleocharine rove beetle, *D. coriaria*[56,125,221].

First, Double-stranded RNA constructs were prepared as previously described[56]. Double stranded constructs targeting enhanced green fluorescent protein (*EGFP*) were used in control injections, as the sequence is not present in the genome of *P. sonomae*. Target sequences were cloned into a pCR2.1 TOPO vector (Thermo Fisher, CA) with primers containing T7 linkers. The following primers were used:

Pson *CYP4G1*:
F: 5’-TAATACGACTCACTATAGGGTCTTAGGATGTACCCACCAGTG-3'
R: 5’-TAATACGACTCACTATAGGGTGTCGCAATGCACTCGGTAT-3'

EGFP:
F: 5’- TAATACGACTCACTATAGGGTCTTCTTCAAGGACGACGGCAACTAC -3'
R: 5’- TAATACGACTCACTATAGGGTTACTTGTACAGCTCGTCCATGCCGA -3'

A MEGAscript T7 Transcription kit (Thermo Fisher, CA) was used to synthesize dsRNA, which was subsequently cleaned using a MEGAclear Transcription cleanup kit (Thermo Fisher, CA), and quantified via NanoDrop (Thermo Fisher, CA). Target dsRNA and control dsRNA, targeting green fluorescent protein (GFP), were diluted in DEPC-treated PBS and green food dye to a concentration of ~2mg/mL. Constructs were microinjected into wild caught adult *P. sonoame*. Beetles were maintained in Rubbermaid containers with a bed of packed damp coconut husk fiber and a diet of fruit flies. Beetles were sacrificed at 10 days and extracted in 100 microliters of hexane with a 10ng/microliter octadecane internal standard and analyzed via the GCMS method previously described. Total CHCs were compared between *CYP4G1*-KD and *GFP* conditions using a Welch's t-test in R.

In spite of possible perdurance of CYP4G1 enzymes transcribed prior to the knockdown and the turnover rate of CHCs on the insect cuticle, we were able to measure a significant decrease in the total CHCs in *CYP4G1*-targeted *P. sonomae* (Figure 35), establishing that CYP4G1 is involved in CHC biosynthesis in the beetle.

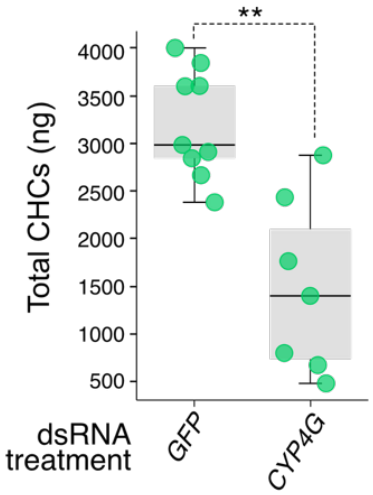

Figure 35. CYP4G-RNAi in adult *P. sonomae* leads to a statistically significant decrease in total CHCs, compared to EGFP-RNAi control beetles (p=0.0017).

The CHC Biosynthesis Pathway in *Platyusa sonomae*

We next sought to delineate the full CHC biosynthesis pathway in *P. sonomae*. Oenocytes are distributed in the abdominal fat body of the beetle (Figure 34), and not in the thorax, so we extracted and sequenced mRNA from the abdominal fat body and first thoracic segment of a number of *P. sonomae* and then performed differential expression analysis to find highly upregulated genes in the abdominal samples, some of which should correspond to CHC biosynthesis enzymes.

The abdominal fat body and entire crushed pronotum were dissected from individual *Platyusa,* in ice-cold DEPC PBS, flash frozen in a dry ice/ethanol bath, and stored at -80˚C until processing. Library preparation was carried out using the NEBNext Single Cell/Low Input RNA Library Prep Kit for Illumina, using NEBNext Multiplex Oligos (New England Biolab, MA) following the manufacturers protocol (NEB #E6420). The number of PCR cycles during cDNA amplification was 14 for the *Platyusa* samples. Final library amplification was either 8 or 12 cycles for all libraries, depending on the intermediate library concentration at this step. The quality of all libraries was assessed by running samples on a Qubit High Sensitivity dsDNA kit (Thermo Fisher, CA) and Agilent Bioanalyzer High Sensitivity DNA assay (Agilent, CA). The libraries were sequenced, either 50bp for *Platyusa*, single end to a read depth of 20-25 million reads on Illumina HiSeq2500 (Illumina, CA) at the Millard and Muriel Jacobs Genetics and Genomics Laboratory at Caltech.

SMART-seq reads were pseudoaligned to the *P. sonomae* transcriptomes using kallisto v0.46.2[222], with 100 bootstraps, single end flag, and an average fragment length of between 339-450bp with a standard deviation of 27-41bp. Next, sleuth v0.30.0[223] was run, using a full model of condition (pronotum or fat body) plus animal (paired samples were collected from each beetle) and a reduced model of animal. A likelihood ratio test was run using the two models to identify differentially

expressed transcripts, which were then filtered by the sign of the average transcripts per million (TPM) for the transcript in the abdominal fat body minus the average TPM for the transcript in the pronotum.

The CHC biosynthesis pathway, borrowing from the fatty acid biosynthesis pathway[224], involves the production and elongation of fatty acyl-CoAs from acetyl-CoA and propionyl-CoA precursors[225–227], which are potentially desaturated[225] and eventually converted to an aldehyde, which is decarbonylated[228], generating the final alkane or alkene product. While many more enzymes are involved in the pathway[229], we focused on six major classes of enzyme: fatty acid synthases (*FAS*), elongases (*elo*), desaturases (*desat*), fatty acyl-CoA reductases (*FAR*), cytochrome P450 4G (*CYP4G*), and the NADPH cytochrome P450 reductase (CPR). Fatty acid synthases create long chain fatty acids by adding malonyl-CoA or methylmalonyl-CoA units onto a growing acyl-CoA primer[230]. Elongases, in combination with three other enzymes[229], then further elongate the fatty acids to generate very long chain fatty acids[231]. Desaturases introduce double bonds into the growing fatty acid chain. The role of fatty acyl-CoA reductases is not fully resolved; initially, they were proposed to convert very long chain fatty acyl-CoAs to very long chain aldehydes[228,232], but more recent work would suggest that they instead produce an alcohol instead[233,234]. And yet, work on the alkane biosynthesis pathway in aleocharine rove beetle defensive glands, which parallels portions of the oenocyte pathway, found an aldehyde intermediate produced by the activity of a fatty acyl-CoA reductase[125]. Regardless of the product of fatty acyl-CoA reductase activity, the terminal enzyme in the CHC biosynthesis pathway, CYP4G[235], is able to convert both long chain aldehydes and alcohols to hydrocarbons[234,236–238]. The activity of the oenocyte CYP4G is dependent on an NADPH-cytochrome P450 reductase[239]. It should be noted that CPR activity is not exclusive to CYP4Gs, but partners with many different cytochrome P450s[240].

The *P. sonomae* transcriptome was annotated, so that differentially expressed transcripts could be readily connected to putative functions. The beetles transcriptome was searched against the NCBI nr (February 2019) and UniProt (February 2019) databases, taking the top five hits and using an e-value cutoff of 1e-05. The top hit for each transcript ID, sorted by highest bitscore, lowest evalue, and highest percent identify, was determined for both the NCBI nr and Uniprot results. The differentially expressed smartseq transcripts were then filtered by the NCBI nr and Uniprot annotations, selecting those transcripts annotated as elongation of very long chain fatty acids, fatty acyl-CoA reductase, fatty acid synthase, acyl-CoA desaturase, stearoyl-CoA desaturase, cytochrome P450 4G1/4G15, or NADPH-cytochrome P450 reductase. The orthogroups containing these potential CHC pathway enzymes were identified.

The enzyme list generated via differential expression analysis was supplemented with a homology based approach, drawing from cuticular hydrocarbon biosynthesis literature in *Drosophila melanogaster*[241,242] and the closely related rove beetle, *Dalotia coriaria*[56]. Orthogroups containing known *Dalotia* and *Drosophila* CHC biosynthesis enzymes as well as the differentially expressed *Platyusa* enzymes were analyzed by aligning the sequences in each orthogroup using mafft v7.453[243] and then generating phylogenetic trees using fasttree v2.1.10[244]. The resulting gene trees (Appendix, Figures 65-91) were manually curated, pruning analogous branches, removing short sequences that appeared to be fragmented, removing or splitting long sequences that appeared to be mis-predicted chimeras of adjacent genes in the genome, removing identical or nearly identical sequences, and in some cases replacing misassembled transcripts with gene predictions from the corresponding draft genomes. All *Platyusa* sequences in each gene tree were assumed to be potential CHC biosynthesis enzymes. A curated transcriptome for *Platyusa* was generated by replacing or removing those

sequences modified or removed in the process of generating the gene trees. The smartseq reads were then remapped, in a similar fashion as described above, to the curated transcriptome and differential expression analysis was performed. A total of 30/36 putative CHC biosynthesis genes were differentially expressed, including at least one member of every major gene family (Figure 62 in the appendix). The full gene list can be found in Table 4 in the appendix. The orthologous CHC biosynthesis genes in *Dalotia coriaria* are listed in Table 3 in the appendix. The final gene count for each gene family in the *P. sonomae* CHC biosynthesis pathway is listed in Figure 36.

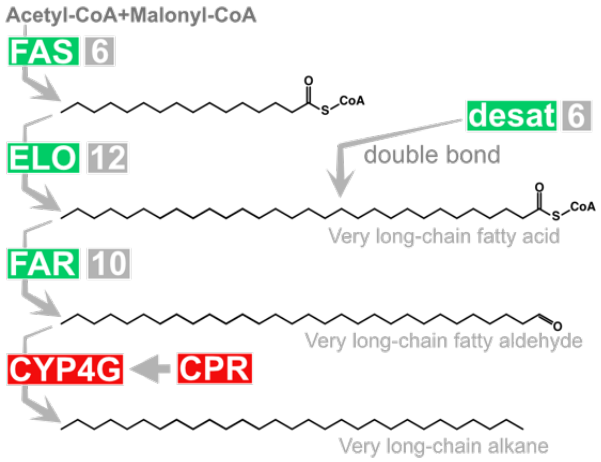

Figure 36. CHC biosynthesis enzymes in *P. sonomae*. Gene counts for each enzyme class are listed in grey boxes. Both CYP4G and CPR are single copy genes. FAS-Fatty acid synthase, ELO–elongase, FAR–fatty acyl CoA reductase, desat–desaturase, CYP4G–Cytochrome P450 4G, CPR–NADPH cytochrome P450 reductase.

Additional HCR probe sets were designed to target the other major CHC biosynthesis enzyme families in *P. sonomae* to verify that they are all expressed in oenocytes. Within the desaturases, *Desat1* was chosen because it is homologous to *Drosophila desatF*, *desat1*, *desat2*[76]. Within the elongase family, *ELO4* was chosen due to its known expression in *Dalotia* oenocytes (called elo-708 by Brückner et al.[56]). Within the FAS and FAR families, *FAS3* and *FAR4* were chosen due to their differential expression in the abdomen as well as minimal expression in the pronotum control tissue (Figure 62, Pson heatmap, in the appendix). The corresponding transcript IDs for the HCR targets are

listed in Table 4 in the appendix. Following the same HCR protocol described above, the new HCR probes were used to label oenocytes in the abdomen of *Platyusa* (Figure 37). The imaging microscope could only image four channels at a time, so two separate rounds of HCR were performed, one round targeting *CYP4G*, *ELO4*, and *Desat1*, and a second round targeting *CYP4G, FAS3,* and *FAR4.* The HCR labelling in Figure 37 clearly demonstrates that all of the transcripts are expressed in oenocytes.

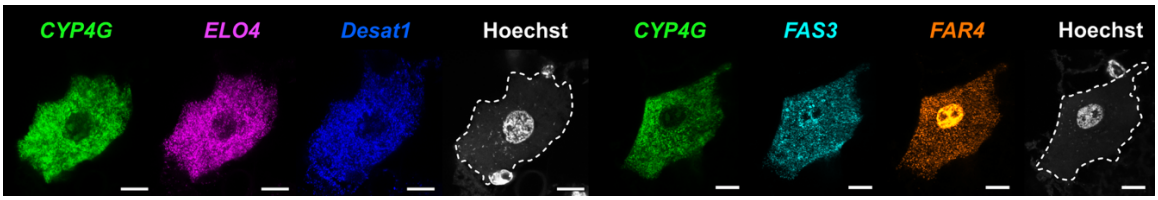

Figure 37. HCR probes targeting the major CHC biosynthesis enzyme families label oenocytes in the abdomen of *P. sonomae* (Hoechst, white, nuclei). Scale bars represent 10µm.

The CHC Mimicry Mechanism in *Sceptobius lativentris*

We next sought to determine the CHC mimicry mechanism in *Sceptobius lativentris*. We measured the survival time of two cohorts of single-housed *S. lativentris*, one isolated from *L. occidentale* and the other maintained with 12 *L. occidentale* per beetle. All beetles were maintained in small containers, roughly two inches per side, filled with damp coconut fiber in an incubator maintained at 24˚C and 90-95% relative humidity. Containers were checked twice daily for beetle death. The isolated cohort died within three days (Figure 38). We then measured the CHC content of *S. lativentris* just prior to or immediately following death, between 48-72 hours isolated (Figure 38). We found that the total hydrocarbons decrease to very low levels within this period, suggesting that the beetle acquires most, if not all, of its hydrocarbons from *L. occidentale.*

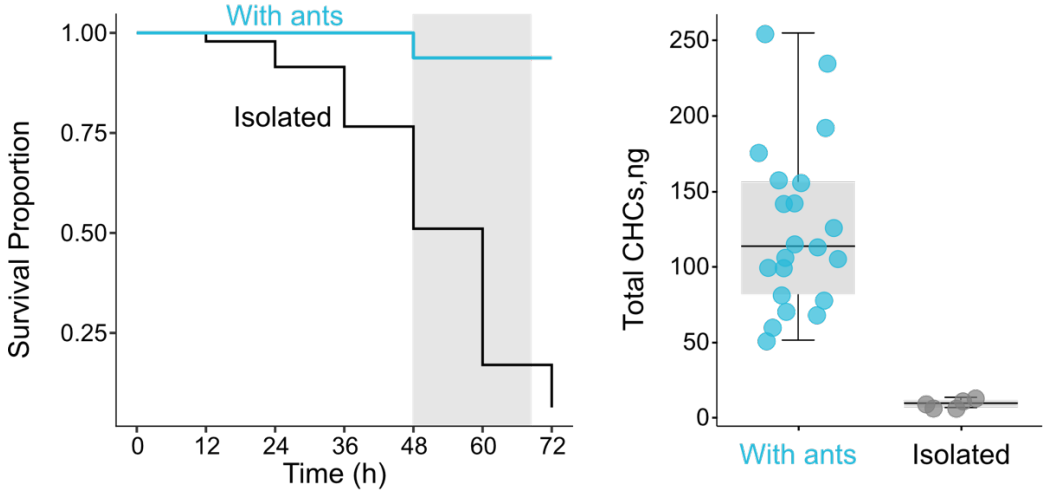

Figure 38. Isolation of *S. lativentris* from *L. occidentale* results in death within three days. *S. lativentris* CHC amounts measured in beetles isolated from *L. occidentale* for 48-72 hours are significantly reduced.

We next performed compound specific stable carbon isotope measurements of *S. lativentris* CHCs. Measurements were performed, as described above, extracting CHCs from 9-64 *S. lativentris* for each pooled measurement (Figure 39). Compared to the stable isotope measurements in *P. sonomae*, Figure 33, there was much greater overlap in the $\partial^{13}C$ values measured in *S. lativentris* compared to *L. occidentale*. It cannot be ruled out that *S. lativentris* produces hydrocarbons *de novo* and they happen to match the $\partial^{13}C$ value of the host by chance, but the congruence of the measured values across all five compounds would make this highly unlikely. There is a slight negative offset of the alkanes in *S. lativentris* compared to the *L. occidentale*, which could be due to fractionation occurring in the CHC transfer process or possibly due to very low levels of endogenous alkane production in the beetle shifting the measured $\partial^{13}C$ values.

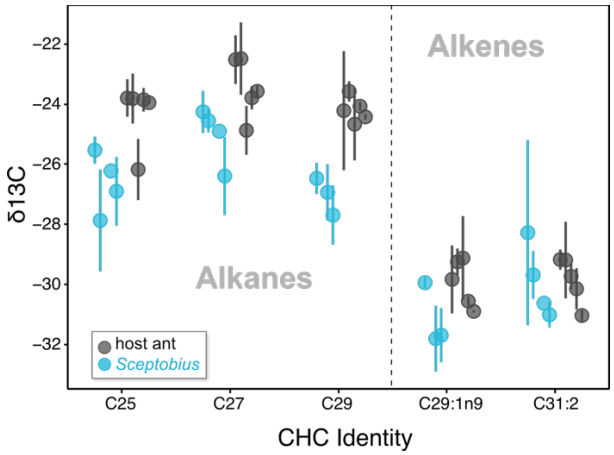

Figure 39. Stable carbon isotope measurements of selected CHCs from *S. lativentris* and *L. occidentale*. Bars represent standard deviation of triplicate measurements.

Behavioral interactions between *S. lativentris*, *P. sonomae,* and the free-living beetle *D. coriaria* with *L. occidentale* were recorded and compared to verify that *S. lativentris* behavior could explain the proposed CHC transfer. *S. lativentris* grooming behavior is already well established[130] but it is unknown how the time devoted to grooming by *S. lativentris* compares to the time that another *L. occidentale* myrmecophile or a free-living beetle spends with the ant. After initial trials found that simple 2cm diameter circular behavioral wells resulted in fast and ubiquitous discovery and killing of *D. coriaria* by *L. occidentale*, a behavioral arena was designed which contained a central well, surrounded by three additional chambers, which would give the beetles the opportunity to hide from the ant (Figure 40). The multi-well behavior arena was constructed from 1/8th inch infrared transparent acrylic and was backlit with infrared LED panel. To ensure that runs were conducted in complete darkness, the arena was placed inside of an incubator in a dark room. Small, ~5 mm diameter, pieces of damp filter paper were added to each well to increase humidity within wells. Individual *S. lativentris, D. coriaria,* and *P. sonomae* were cold anesthetized, and then loaded into arena wells, along with one cold anesthetized *L. occidentale*. Beetles were recorded at 1 hz for 24 hours using a FLIR camera (BFS-U3-51S5M-C: 5.0 MP) with a Pentax 12mm 1:1.2 TV lens (Ricoh, FL-HC1212B-VG).

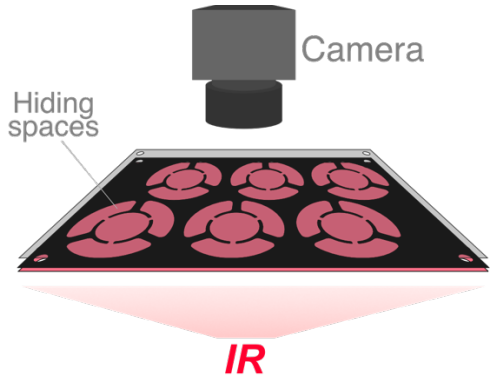

Figure 40. Behavior arenas designed to measure interaction time between different beetles and *L. occidentale*. The arena was illuminated in IR and interactions were recorded with an IR camera.

An initial survey of the video recordings found that the beetles engaged in species-typical interactions with the host ant. *P. sonomae* engaged in appeasement behavior of *L. occidentale* and *S. lativentris* could be seen grooming *L. occidentale* (Figure 41). These results reassured us that the behaviors we were measuring in the arenas approximated naturalistic interactions between the beetles and the ant. In that vein, some *Platyusa* were not fed sufficiently before their behavioral runs and ate their paired ant.

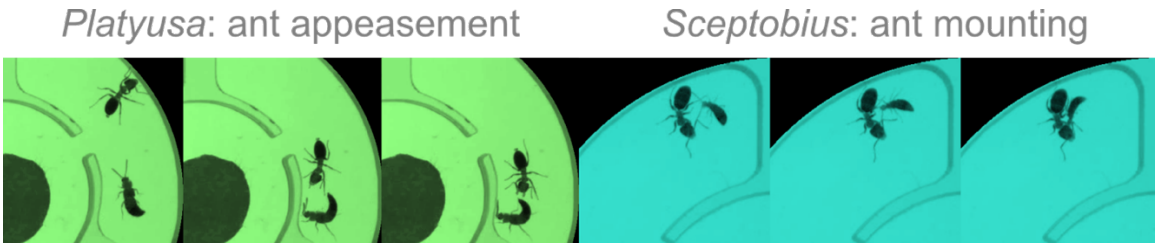

Figure 41. Species specific behaviors are recapitulated within the interaction arena.

Videos were cropped down to individual wells and analyzed with Deeplabcut v2.0.6.2[245,246]. Distinct network models, using a default ResNet50 network, were trained for each beetle, consisting of two labels for the head and abdominal tip of both *L. occidentale* and *P. sonomae*, and one label for the head of *S. lativentris* and *D. coriaria*. The networks were trained on ~500 labeled frames for the *P. sonomae* model, ~150 frames for the *S. lativentris* model, and ~50 frames for the *D. coriaria* model.

All of the models were trained over multiple iterations and the *D. coriaria* model used the training weights from the final *S. lativentris* model as its initial weights. The training and test errors were 1.27 and 0.92 pixels for the *P. sonomae* model, 1.03 and 2.79 pixels for the *S. lativentris* model, and 2.13 and 3.55 pixels for the *D. coriaria* model. The three networks were used to analyze all of the videos of their respective beetles.

Position data was filtered for frames in which the ant prediction is likely accurate by calculating the length of each ant, and then choosing an upper threshold that excludes outliers for all ants collected in a given behavioral run. Then an ellipse was drawn around the ant for each labelled video frame, such that the sum of the distances between any point on the ellipse and the head and abdominal tip of the ant summed to 1.4 times the ant length in that frame. If the beetle's head, or head or tail for *P. sonomae*, fell within the ellipse for that frame, the beetle was considered to be touching the ant. The percent of frames in which the beetle was touching the ant was then calculated for each well. Differences in the touching percent between the three beetles were compared using an ANOVA with a Tukey *post hoc* test in R. Compared to both *P. sonomae* and *D. coriaria, S. lativentris* spent significantly more time in contact with *L. occidentale* during the 24 hour trial (Figure 42), verifying the underlying ant affinity that allows *S. lativentris* to acquire CHCs from the host.

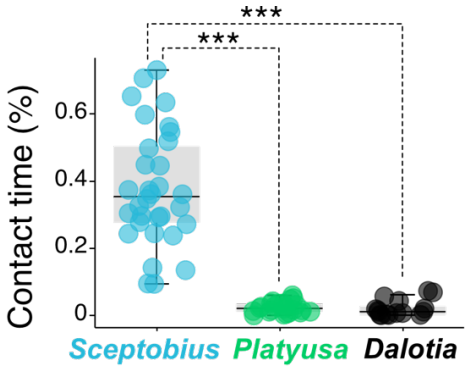

Figure 42. The percentage of time in which *S. lativentris*, *P. sonomae*, and *D. coriaria* were in contact with *L. occidentale* during a 24 hour period. Asterisks denote p<0.0001 in Tukey *post hoc* test.

The interaction behavioral trials above were simultaneously used to measure the physical transfer of hydrocarbons from *L. occidentale* to the three beetle species. The CHC profile of *L. occidentale* was supplemented with deuterated, even chain length hydrocarbons. A few hundred micrograms of fully deuterated tetracosane and triacontane (triacontane-d_{62} and tetracosane-d_{50}, 98 atom % D, Sigma-Aldrich, MO) were added to a 5 mL glass vial along with 1 mL of hexane to fully dissolve the hydrocarbons. The hexane was then evaporated off under a steady stream of nitrogen gas, leaving a thin film of the two deuterated hydrocarbons on the inner wall of the vial. *Liometopum* were added to the vial and then shaken for ~1 minute to transfer the labeled hydrocarbons to the surface of the ants, similar to transfer experiments performed in other systems[62,69]. Uncoated control ants were prepared in a similar fashion, using a vial treated only with hexane. After the 24 hour interaction period, the arena was removed and ants and beetles were extracted in 70 microliters of hexane containing 25ng/microliter of octadecane as an internal standard. Samples were run on a Shimadzu QP2020 GCMS equipped with helium as a carrier gas and a Phenomenex ZB-5MS fused silica capillary column (30m x 0.25 mm ID, df=0.25µm). The injection port was operated at 310˚C in splitless mode, with a column flow rate of 2.15 mL/min. The column oven was held at 40˚C for 1 minute, followed by a 40˚C/min ramp up to 250˚C, a 20˚C/min ramp up to 320˚C, and then a 5 minute hold at 320˚C. The transfer line was held at 320˚C and the ion source temperature was held at 230˚C. The MS was operated at an ion source voltage of 70eV and scans were collected in selected ion monitoring mode (SIM), monitoring m/z 66, 85, 98, 254, 389, and 485 at 3.33 scans per second. Videos were reviewed and only samples in which the beetle survived were used.

The C18, triacontane-d_{62}, and tetracosane-d_{50} peaks were manually integrated (sum of the selected ion counts), and the absolute amounts of the deuterated hydrocarbons were calculated by taking the ratio of the area of each peak to the C18 internal standard peak area, and multiplying by the total mass of internal standard in the extraction. The average background signal was calculated for the control

ants and beetles and subtracted from the corresponding treatment groups. The background-corrected deuterated hydrocarbon mass on each beetle was then divided by the corresponding measurement from the paired ant to calculate the ratio of deuterated hydrocarbon transferred in each interaction well. Due to greater background signal in the GCMS data as well as minimal initial transfer onto the ants because of its higher melting point, the triacontane-d_{62} data were less robust than the tetracosane-d_{50} data. Differences in the transfer ratio for both tetracosane-d_{50} and triacontane-d_{62} between the three beetles were compared using an ANOVA test with a Tukey *post hoc* test in R. During the 24-hour period *S. lativentris* obtained significantly more deuterated hydrocarbon from the host ant than the other two beetles (Figure 43), verifying that the beetle is able to acquire CHCs from the ant.

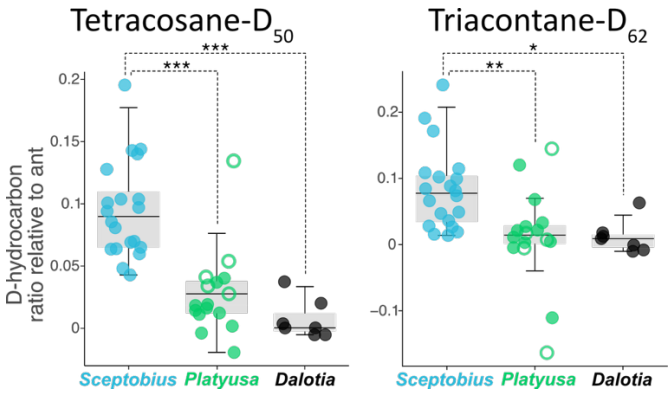

Figure 43. Baseline corrected tetracosane-d_{50} and triacontane-d_{62} levels on *S. lativentris*, *P. sonomae*, and *D. coriaria* compared to their paired ant. Open circles for *P. sonomae* represent beetles which ate their paired ant. * – $p<0.05$; ** – $p<0.005$; *** – $p<0.0001$ in Tukey *post hoc* tests. Negative values are the result of the background subtraction process.

Chapter 4

CHC PRODUCTION DURING DEVELOPMENT

S. lativentris appeared to not produce hydrocarbons, opting instead to obtain them from the host ant. In order to understand this extreme phenotype, we set out to verify if *S. lativentris* still possesses the cells and biosynthetic machinery to produce CHCs. Because the beetle only spends a portion of its lifecycle inside nests of the host ant, the complete loss of the ability to produce CHCs would present a challenge to its juvenile stages. We found the *S. lativentris* not only possesses oenocytes, but also possesses the full suite of CHC biosynthesis enzymes. This led us to look for CHC production in the earlier pre-myrmecophilous life stages of the beetle. In larvae, pupae, and teneral beetles we found measurable, albeit low, levels of CHC production. Tracking expression of key CHC transcripts across the spatiotemporal transition of the beetle into the ant nest revealed that CHC biosynthesis appears to turn off at this critical juncture in the beetle's life-cycle. We then performed experiments to probe the hypothetical consequences of the beetle failing to shut off its endogenous CHC biosynthesis, prior to entering the *L. occidentale* nest.

The CHC Biosynthesis Pathway in *Sceptobius lativentris*

In order to determine a causal mechanism for integrated *S. lativentris* lacking *de novo* CHC production, we first looked for the presence of oenocytes in the beetle. Identifying if *S. lativentris* possesses oenocytes was carried out in a similar fashion to *P. sonomae.* The CHC biosynthesis gene tree curation for *P. sonomae* included *S. lativentris* sequences, so locating the orthologous *CYP4G1* sequence in *S. lativentris* was trivial (Figure 91, CYP tree in the appendix). HCR probes were designed to target *CYP4G1* transcripts in the beetle, and the HCR labelling protocol described above was followed. Similar to *P. sonomae,* a population of cells in the abdomen was targeted by the *CYP4G1* HCR probes (Figure 44), though unlike *P. sonomae*, the signal was much closer to the

background, making the initial locating of cells more difficult. This confirmed that *S. lativentris* possesses oenocytes.

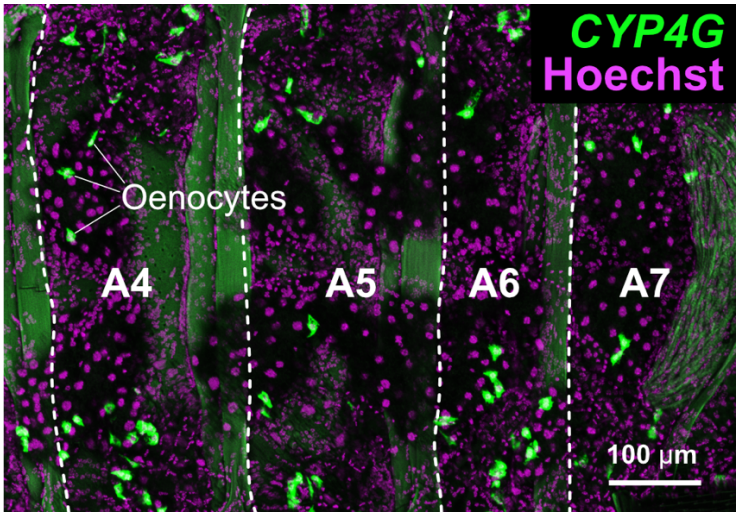

Figure 44. *CYP4G1* HCR probes (green) label oenocytes in the abdomen of *S. lativentris* (magenta, Hoechst, nuclei). The dashed lines delineate different abdominal (A) segments.

We next sought to determine if *S. lativentris* possesses a complete CHC biosynthesis pathway. We could have simply looked for *S. lativentris* orthologs to all of the genes identified in *P. sonomae*, but instead we decided to be more thorough and performed RNA sequencing and differential expression analysis, similar to *P. sonomae.* The 5th-7th abdominal segments, with gut removed, and the entire crushed pronotum were dissected from *S. lativentris* in ice-cold DEPC PBS, flash frozen in a dry ice/ethanol bath, and stored at -80˚C until processing. Library preparation was carried out using the NEBNext Single Cell/Low Input RNA Library Prep Kit for Illumina, using NEBNext Multiplex Oligos (New England Biolab, MA) following the manufacturers protocol (NEB #E6420). The number of PCR cycles during cDNA amplification was 9 for the *S. lativentris* samples. Final library amplification was either 8 or 12 cycles for all libraries, depending on the intermediate library concentration at this step. The quality of all libraries was assessed by running samples on a Qubit High Sensitivity dsDNA kit (Thermo Fisher, CA) and Agilent Bioanalyzer High Sensitivity DNA assay (Agilent, CA). The libraries were sequenced, 100 bp, single end to a read depth of 20-25 million

reads on Illumina HiSeq2500 (Illumina, CA) at the Millard and Muriel Jacobs Genetics and Genomics Laboratory at Caltech.

SMART-seq reads were pseudoaligned to transcriptomes of *Sceptobius* using kallisto v0.46.2[222], with 100 bootstraps, single end flag, and an average fragment length of between 339-450bp with a standard deviation of 27-41bp. Two paired *Sceptobius* samples from the same animal were removed at this step, due to the small percentage of reads that pseudoaligned (<4% vs 20-40% for all other samples). Next, sleuth v0.30.0[247] was run, using a full model of condition (pronotum or fat body) plus animal (paired samples were collected from each beetle) and a reduced model of animal. A likelihood ratio test was run using the two models to identify differentially expressed transcripts, which were then filtered by the sign of the average transcripts per million (TPM) for the transcript in the abdominal fat body minus the average TPM for the transcript in the pronotum.

All transcripts in the *Sceptobius* transcriptome were annotated using the same protocol as *P. sonomae* and the differentially expressed transcripts list was similarly filtered. To this differentially expressed list, orthologs to all *P. sonomae* sequences were also included. In total 40 putative CHC related genes were found in *S. lativentris*, 15 of which were differentially expressed (Figure 63 in the appendix, heatmap). The full gene list can be found in Table 5 in the appendix. Notably, neither the *CYP4G1*, nor the *CPR* were differentially expressed, though at least one member of each other gene family was differentially expressed. The final gene count for each gene family in the *S. lativentris* CHC biosynthesis pathway is listed in Figure 45.

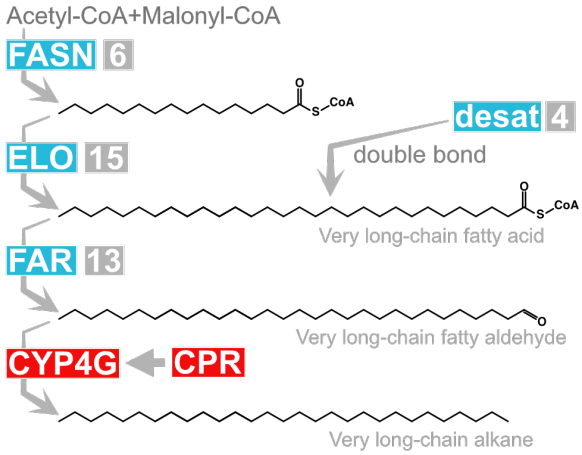

Figure 45. CHC biosynthesis enzymes in *S. lativentris*. Gene counts for each enzyme class are listed in grey boxes. Both CYP4G and CPR are single copy genes. FAS–Fatty acid synthase, ELO–elongase, FAR–fatty acyl CoA reductase, desat–desaturase, CYP4G–Cytochrome P450 4G, CPR–NADPH cytochrome P450 reductase.

To verify that all major CHC biosynthesis enzyme families are expressed in the oenocytes of *S. lativentris*, HCR probes were designed to target sequences homologous to those targeted by HCR in *P. sonomae*. The corresponding transcript IDs for the HCR targets are listed in Table 5 in the appendix. Following the same HCR protocol described previously, the set of HCR probes was used to label oenocytes in the abdomen of *S. lativentris* (Figure 46). Again, the imaging microscope could only image four channels at a time, so two separate rounds of HCR were performed, one round targeting *CYP4G1*, *ELO4*, and *Desat1,* and a second round targeting *CYP4G, FAS3,* and *FAR4.* The HCR labelling in Figure 46 clearly demonstrates that all of the transcripts are expressed in oenocytes, demonstrating that *S. lativentris* has an intact CHC biosynthesis pathway, with at least one member of each major enzyme family being expressed in oenocytes.

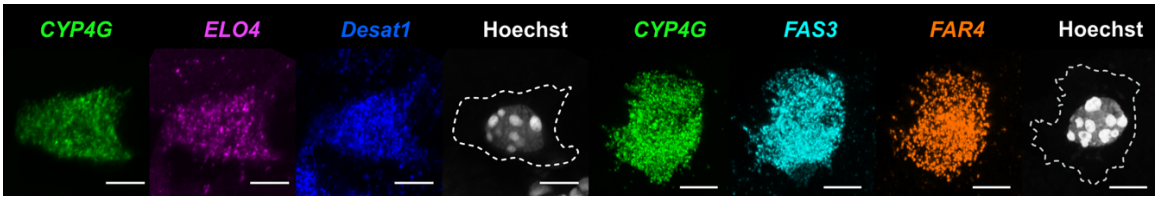

Figure 46. HCR probes targeting the major CHC biosynthesis enzyme families label oenocytes in the abdomen of *S. lativentris* (Hoechst, white, nuclei). Scale bars represent 5µm.

CHC Biosynthesis in *Sceptobius lativentris*

S. lativentris possesses an intact CHC biosynthesis pathway, which is expressed at low levels in oenocytes, yet it does not produce CHCs. At this point, we turned to the natural history of the beetle for insights. Three quarters of the beetle's life, by developmental standards, occurs outside of the ant nest (Figure 25) and yet up to this point, only beetles fully integrated into the nest had been analyzed. By letting *S. lativentris* larvae pupate in soil that had been cleared of living and dead *L. occidentale*, naïve teneral *S. lativentris* were obtained which had never before encountered an ant. These beetles were extracted in 10µL of hexane and analyzed with the GCMS method for measuring CHCs described above. We found that freshly eclosed teneral beetles produce CHCs (Figure 47).

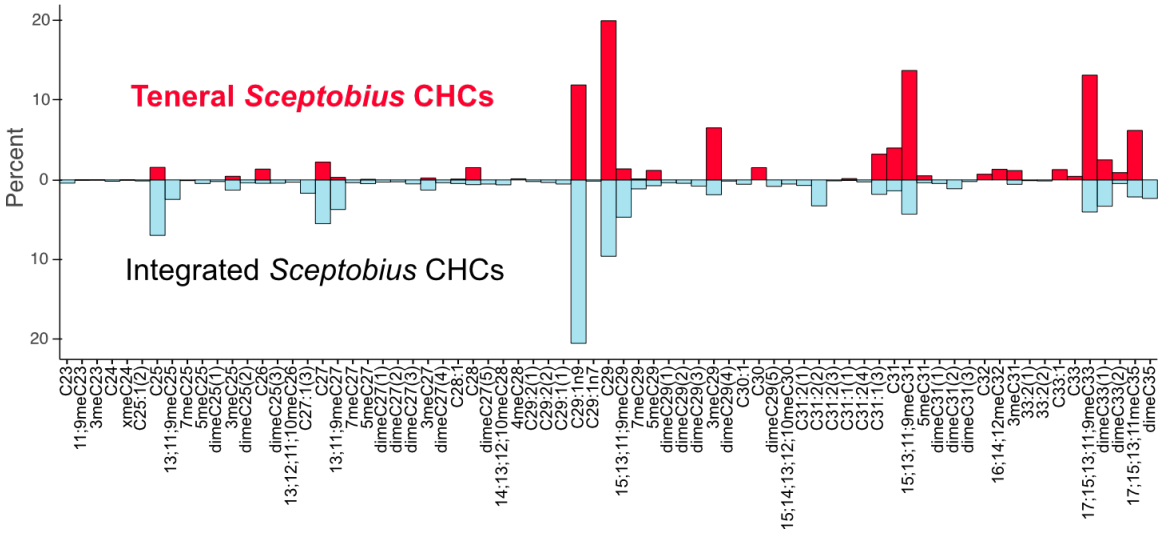

Figure 47. The average teneral *S. lativentris* CHC profile, compared to the average integrated *S. lativentris* CHC profile. Profiles are represented as percent composition, where the sum of all peaks add to 100%.

The teneral *S. lativentris* profile is distinct from the profile of integrated *S. lativentris*. Some of the components of the profile are shared, but the relative ratios of those compounds that are present are distinct from the ratios seen in integrated beetles. We additionally collected GCMS measurements of the CHC profiles of *S. lativentris* teneral beetles which had been isolated for 24 hours, larvae, and pupae. Interestingly, both first and early second instar larvae lacked measurable CHC; it was only in

late second instar larvae, called prepupae, that we were able to measure CHCs. CHC profiles of integrated *S. lativentris* and the *S. lativentris* that had been isolated from *L. occidentale* for 2-3 days (Figure 38) were additionally included in the dataset. All CHC extractions were performed in 10 microliters of hexane containing a 1 ng/microliter C18 internal standard, so that absolute amounts of CHCs could be determined. NMDS ordination of pairwise Bray-Curtis dissimilarity measurements for GCMS spectra from all developmental stages revealed that each developmental stage had a distinct profile (Figure 48). The isolated teneral beetles were included to see if this CHC profile would shift towards that of the ant, but no apparent difference was found.

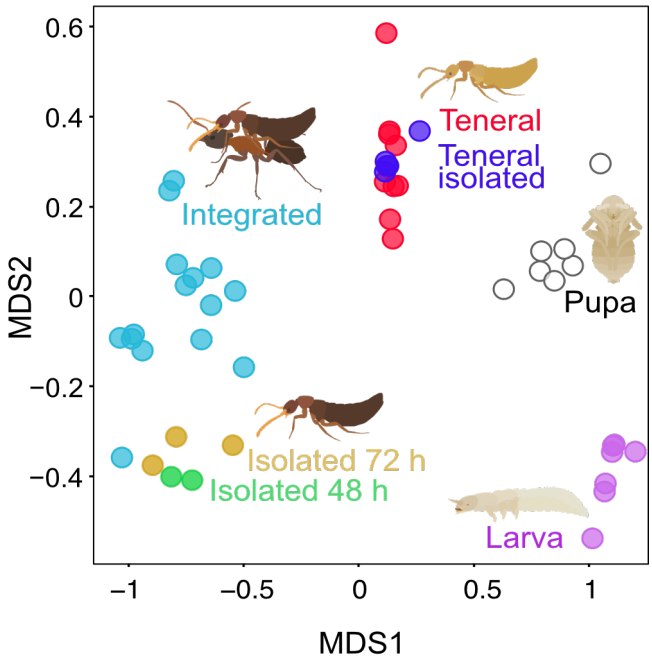

Figure 48. NMDS ordination of CHC profiles for *S. lativentris* developmental stages, 2D stress: 0.05.

The profiles of the integrated *S. lativentris* beetles which had been isolated appeared distinct from the teneral *S. lativentris* profile, demonstrating that the teneral profile is likely not endogenously produced by integrated beetles. This is further demonstrated by comparing the absolute amounts of each hydrocarbon between the two conditions (Figure 49). For almost all compounds shared by both teneral *S. lativentris* and isolated *S. lativentris*, a greater amount is measured in the teneral beetles.

The low levels of hydrocarbons on the isolated *S. lativentris* are likely the last remnants of the CHCs obtained from *L. occidentlae* prior to the isolation period, which were in the process of turning over at the time that the beetle was sacrificed to measure the CHCs.

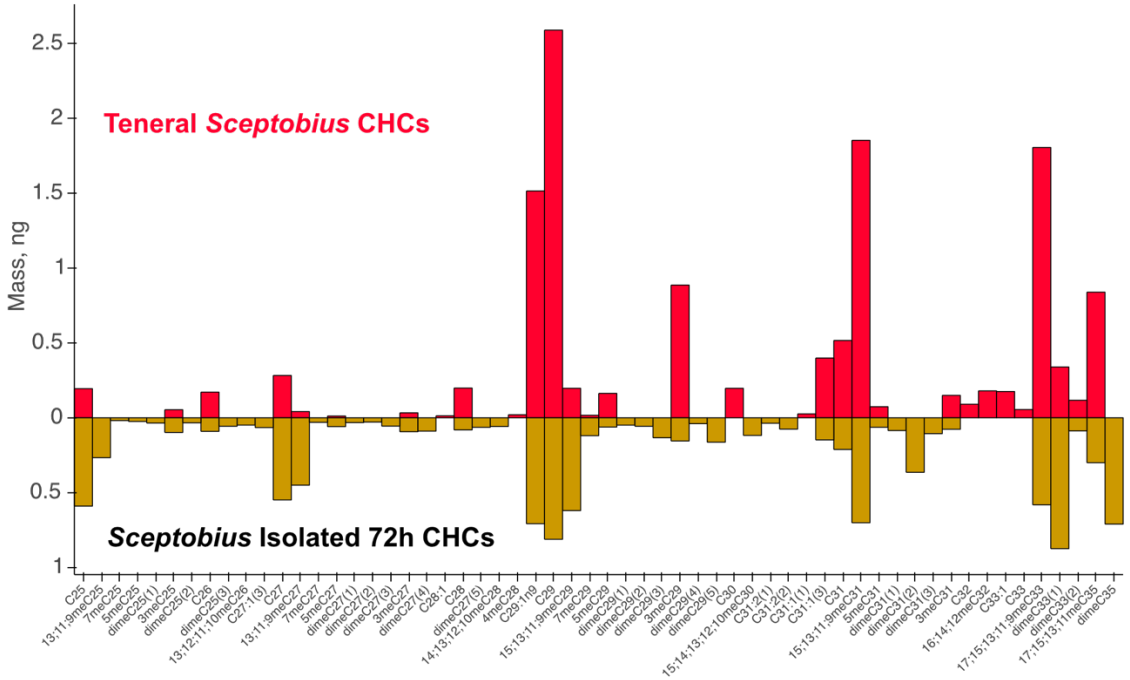

Figure 49. The average mass of CHCs in ng on Teneral *Sceptobius* compared to integrated *Sceptobius* isolated for 72 hours.

Quantification of the total amount of CHCs for the different *S. lativentris* life stages revealed that *S. lativentris* larvae, pupae, and teneral beetles produced almost an order of magnitude less hydrocarbon than what integrated beetles steal from *L. occidentale*, which in turn is an order of magnitude less hydrocarbon than the total amount of hydrocarbon on individual *L. occidentale* (Figure 50). This is an important point, as the amount of hydrocarbon on integrated *S. lativentris* is necessarily sufficient for maintaining water balance long term, but it is unclear if that is the case for teneral beetles. Teneral beetles die within roughly 24 hours of eclosing if not introduced to ants within that period. This is likely, at least in part, due to desiccation caused by the lack of sufficient CHCs. However, any amount

of CHCs is better than none, potentially extending the critical window in which teneral beetles have to find host ants that they can groom.

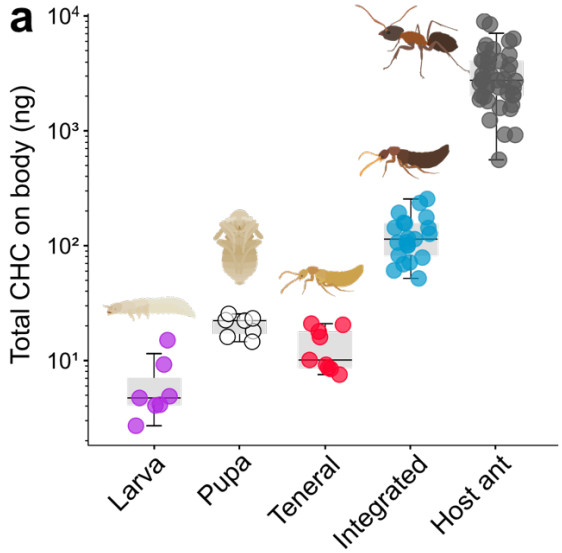

Figure 50. CHC amount at different *S. lativentris* life stages compared to the CHC amount on *L. occidentale.* Values are not normalized by surface area.

Looking at the CHC levels in the free-living *D. coriaria* across development (Figure 51), a different trend is seen from *S. lativentris.* Despite its much smaller size, *D. coriaria* produces similar amounts of hydrocarbon during its larval stage to *S. lativentris* larvae but then produces much more hydrocarbon during its pupal and teneral stage compared to *S. lativentris* pupae and tenerals. This additional evidence would suggest that teneral *Sceptobius* are deficient in CHCs for long term survival. The presence of CHCs in *S. lativentris* during the late larval, pupal, and teneral stages could also result from the likely necessity of CHCs for separation from the puparial case during eclosion[248]. While the authors did not look at CHCs specifically, they found that ablation of ~50% of oenocytes caused failure of *D. melanogaster* to complete pupal development.

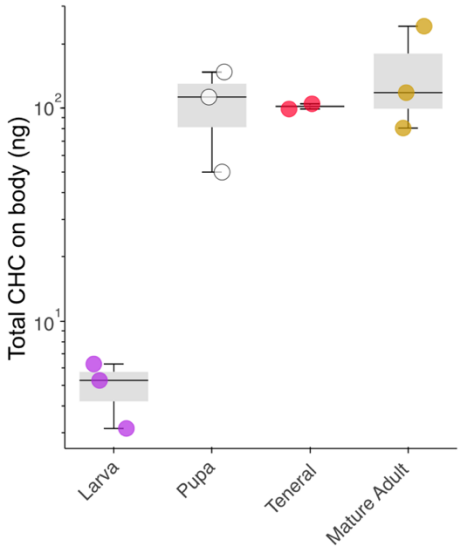

Figure 51. CHC amount at different *D. coriaria* life stages.

The Problem of Endogenous Biosynthesis and its Resolution

Though not large in amount, the CHCs produced by teneral *S. lativentris* are, by the nature of their incongruence with the integrated *S. lativentris* CHC profile, potentially sufficient to adulterate the profile of integrated beetles if they were to produce CHCs *de novo*. Comparing the magnitude of the average mass of all CHCs in the integrated *S. lativentris* profile to that of the average teneral *S. lativentris* profile, the amounts of a few key hydrocarbons would be shifted by endogenous biosynthesis (Figure 52).

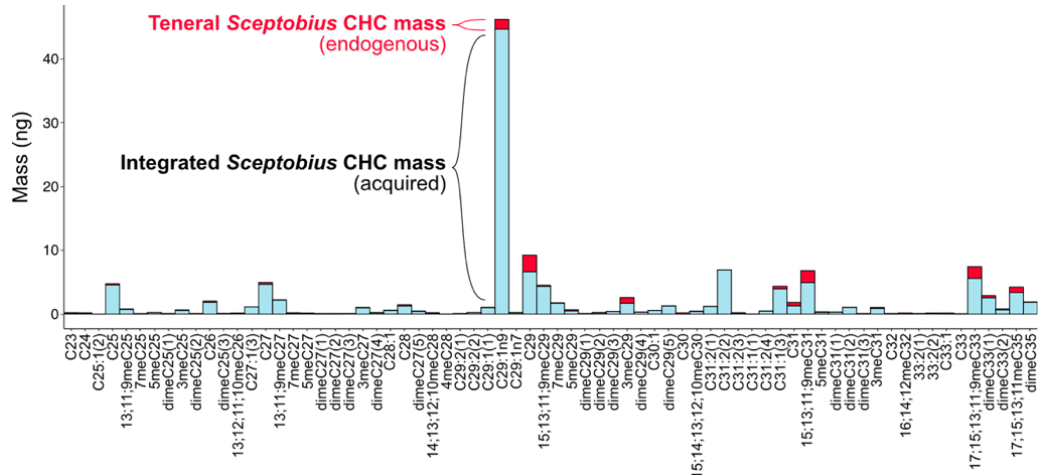

Figure 52. The average mass of CHCs in ng for teneral *S. lativentris* stacked on top of the average mass of CHCs for integrated *S. lativentris*.

To visualize the effect of this adulteration, we took the CHC profiles of a number of integrated *Sceptobius* for which we had quantitative mass data, and then applied an offset using the average mass of the CHCs from the teneral *S. lativentris* profile, creating an "integrated + endogenous" condition. To create a naturalistic, "endogenously" adulterated profile against which we could compare the artificial teneral offset, we used the endogenously produced CHC profile of *P. sonomae* to modify the *S. lativentris* profile. This was achieved by placing a number of *S. lativentris* into a 5 mL vial filled with 7-8 *P. sonomae* to force grooming and CHC transfer from *P. sonomae* to *S. lativentris* over the course of 2 hours. The CHCs were then extracted off of these "*Platyusa* groom" *S. lativentris* and analyzed via GCMS. NMDS ordination of pairwise Bray-Curtis dissimilarity measurements for the CHC profiles of *L. occidentale*, *P. sonomae*, *L. newtonarum*, wild-type *S. lativentris*, and the two modified *S. lativentris* conditions was performed (Figure 53). It is immediately obvious that the two adulterating conditions, "*Platyusa* groom" and "integrated + endogenous", push the *Sceptobius* CHC profile out of the main *L. occidentale* chemical space, on average. The chemical shift is not large, but given the potentially millions of ants within an *L. occidentale* nest as well as the spatial distribution of *S. lativentris* within the nest, a slight increase in recognition and ant aggression, from a baseline of no aggression for wild-type *S. lativentris*, could be devastating.

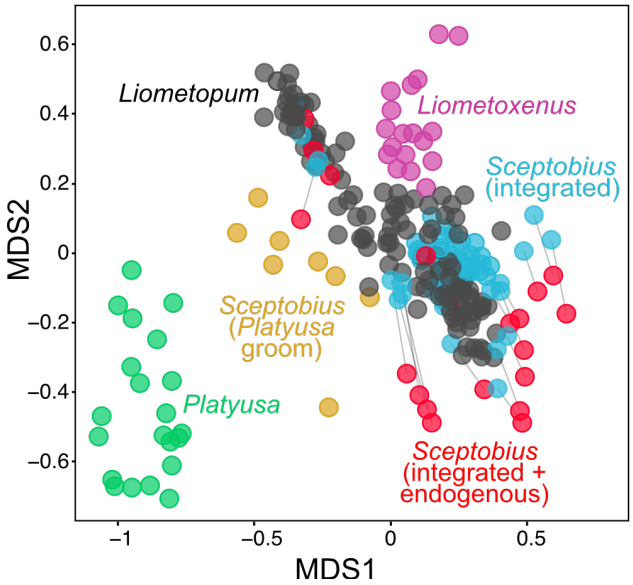

Figure 53. NMDS ordination of CHC profiles for *L. occidentale* and its myrmecophiles, including *S. lativentris* with adulterated profiles, 2D stress: 0.12. The hypothetical integrated + endogenous profiles, in red, are connected to their unadulterated counterpart with a grey line. The "*Platyusa* groom" beetles correspond to *S. lativentris* which had groomed *P. sonomae* for 2 hours.

We knew that teneral *S. lativentris* produce CHCs and integrated beetles do not, so we decided to look at the expression of various CHC biosynthesis enzymes during the transition of teneral *Sceptobius* into the *L. occidentale* nest. Teneral *Sceptobius* were collected on the day that they eclosed and either immediately used in experiments, or placed with ~5 ants in small petri dishes with filter paper until their use in experiments. Three beetles were sampled each from zero, one, two, three, and eight days post-eclosion. Four fully integrated *Sceptobius* were also collected from the field. Due to the difficulty of obtaining larvae for the experiment, beetles were accumulated over the span of multiple weeks. As they were collected, samples were processed immediately via the previously mentioned HCR protocol up through the methanol dehydration step, at which point they were stored at -20˚C. Once all samples had been collected, the remaining steps in the HCR process were carried out in parallel for all samples, with all beetles from the same time point being processed in the same tube. All sample tubes were incubated with identical probe and hairpin solution concentrations, targeting *desat1*, *elo4,* and *CYP4G1*. Samples were mounted together and imaged on a Zeiss 880

confocal microscope (Zeiss, Germany) in Airyscan fast mode using identical imaging parameters. Representative images for the *CYP4G1* imaging channel in the different stages are shown in Figure 54. Visually, the fluorescence level for the *CYP4G1* probe in the individual oenocytes appears to decrease with age.

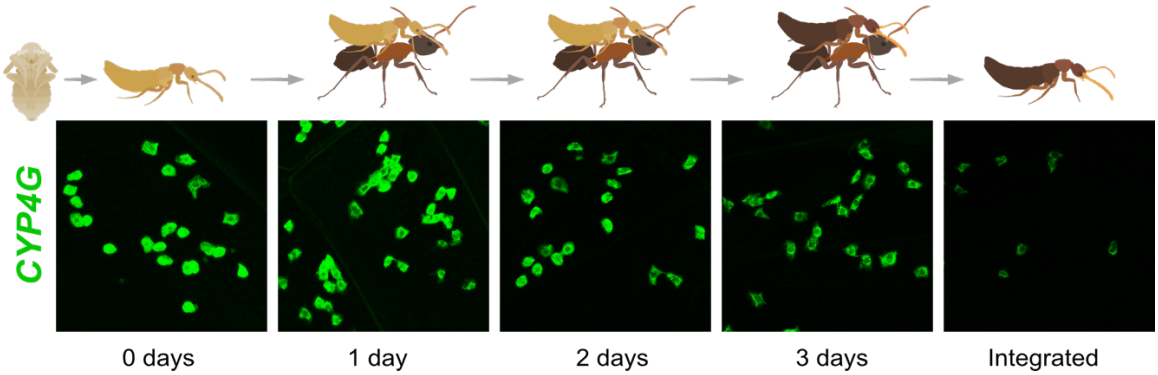

Figure 54. HCR probes targeting *CYP4G1* in oenocytes during the first few days after eclosing show a steady decrease in fluorescence.

To measure shifts in expression across the different time points, we quantified the fluorescence intensity on a per-oenocyte basis for each of the three target probes, across all samples and time points. At least two confocal image stacks were collected for each sample. Confocal image stacks were converted to Tiffs and masks for oenocytes were determined using the *CYP4G1* channel and the python package Cellpose v.2.0.5[249] in Python v3.8.13. Image stacks were first projected along the z-axis by summing over all slices in the stack and then cells were identified with the 'cyto' model in Cellpose using a diameter of 35, flow threshold of 0.1, minimum size of 200, cell probability threshold of 0.8, and interp and neg_avg set to true. The resulting oenocyte cell masks (Figure 55) were used to filter the *CYP4G1* channel by calculating the percentage of the z-projected frame occupied by all cell masks, and then setting a pixel intensity threshold that excludes the same percentage of voxels across the *CYP4G1* channel slices. The threshold mask determined with the *CYP4G1* channel was then applied to the *elo4* and *desat1* channels. Next, the cell masks were applied to each filtered

channel, integrating over the fluorescence intensity in each slice to recover the total fluorescence intensity in each oenocyte, for the three channels.

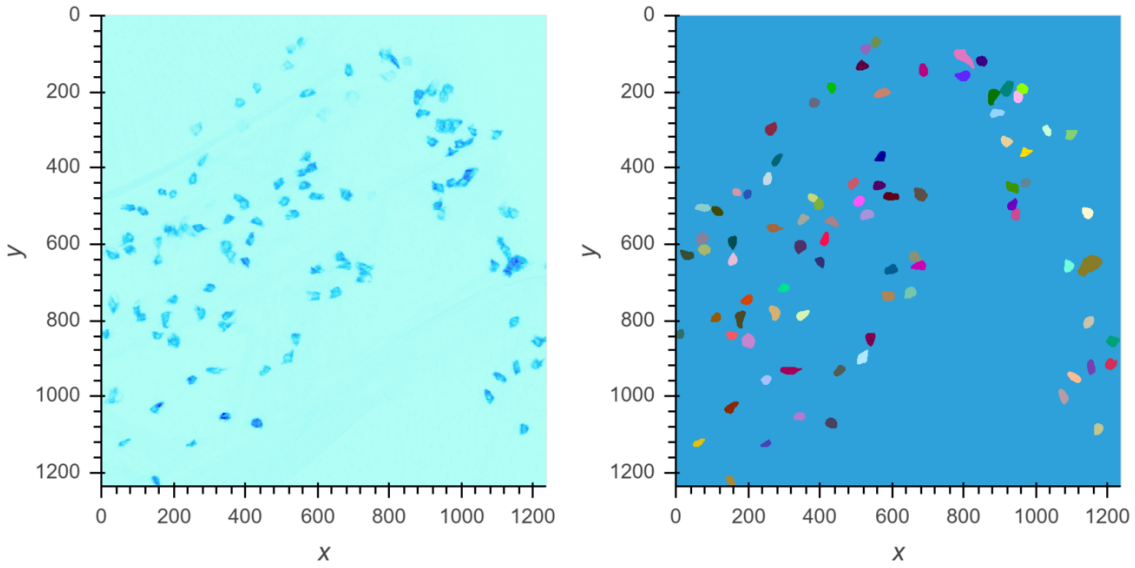

Figure 55. A representative z-projection of the *CYP4G1* channel on the left, with the corresponding cell masks generated by Cellpose on the right.

The total fluorescence intensity in individual oenocytes followed a pattern of approximately decreasing intensity with increasing age for the three targeted genes (Figure 56). *Desat1* was found to have some additional expression in fat body, which made accurate measurements of its oenocyte specific expression difficult. The most critical finding from this data is the confirmation that the expression of *CYP4G1* appears to decrease significantly between the time that teneral beetles eclose and their integration into ant nests. Whereas the other enzyme families in the CHC biosynthesis pathway contain multiple copies, there is only a single *CYP4G* gating the final production of CHCs. The loss of expression of this one enzyme can silence the entire CHC pathway, as the *CYP4G1* knockdown data in *P. sonomae* suggests (Figure 35).

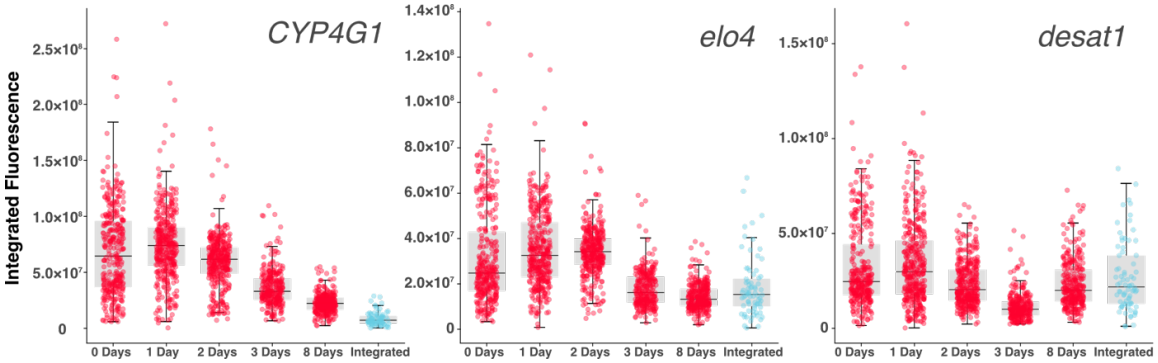

Figure 56. Integrated fluorescence intensity from individual oenocytes for each of the three HCR probes across multiple developmental time points in *S. lativentris.* Oenocytes from three or four beetles were imaged for each time point.

To verify that the drop in expression is systemic, expression of the three CHC biosynthesis enzymes was analyzed with qPCR. Teneral *Sceptobius* were collected and reared as previously described. Three or four beetles were sampled each from zero, one, and three days post-eclosion as well as fully integrated beetles. All beetles were frozen at -80˚C prior to RNA extraction. RNA was extracted from individual beetles with Trizol (Life Technologies, CA) and manual homogenization. Chilled chloroform was added, samples were centrifuged, and the RNA containing aqueous phase was collected. Chilled ethanol was added to precipitate RNA, which was then purified with an RNeasy purification kit (Qiagen, Germany). cDNA was then prepared using a Superscript III kit (Thermo Fisher, CA). The resulting cDNA was analyzed via qPCR. Briefly, 1 µL of cDNA template was combined with 6.5 µL of Luna® Universal qPCR master mix (New England BioLabs), 2 µL of combined forward and reverse primer (10µM, Integrated DNA Technologies, IA), and 10.5 µL of dH_2O per well. Samples were run on an Applied Biosystems StepOnePlus Real Time PCR System (Thermo Fisher, CA) using the following conditions: 95˚C for 1 minute, 40 cycles at 95˚ for 15 s, 59˚C for 30s. Melt curve analysis was performed by holding for 15s at 95˚C followed by 30s at 60˚C and 15s at 95˚C. Primers were designed for three *Sceptobius* CHC enzymes and two *Sceptobius* housekeeping genes, Ribosomal protein S3 and Ribosomal Protein L19.

The following primers were used.

***Sceptobius* elo4:**

F: 5'-TTCGGTGCTGCAAGGATAA-3'

R: 5'-CCCAAGAGTACCACACAAGAG-3'

***Sceptobius* CYP4G1:**

F: 5'-ACCCAGCTGATATTGAGGTTATC-3'

R: 5'-CTGACCAAGAGACCATTTCCA-3'

***Sceptobius* desat1:**

F: 5'-CGCTACAGCACTAACTTCACT-3'

R: 5'-ACACGACGCTTGACCATATC-3'

***Sceptobius* RPL19:**

F: 5'-GAATGTACCGCTACTGGTTTCT-3'

R: 5'-CAGCCTCTGTTATGCGATGT-3'

***Sceptobius* RPS3:**

F: 5'-GGTGTCGACGTAGTCGTTAATC-3'

R: 5'-CGAAGTAGTTGTGTCCGGTAAG-3'

Each sample was run in duplicate, and the geometric means of the technical replicates were determined. The ΔΔct calculation was then used to determine fold change of samples relative to the integrated condition. The difference between the cycle threshold for the genes of interest and the geometric mean of the two housekeeping genes was first calculated for each sample. From this difference in cycle threshold for each gene, the geometric mean of the cycle threshold difference in the integrated condition was subtracted. Multiplying the resulting values by negative one yielded the approximate fold change in expression for each time point compared to the integrated condition.

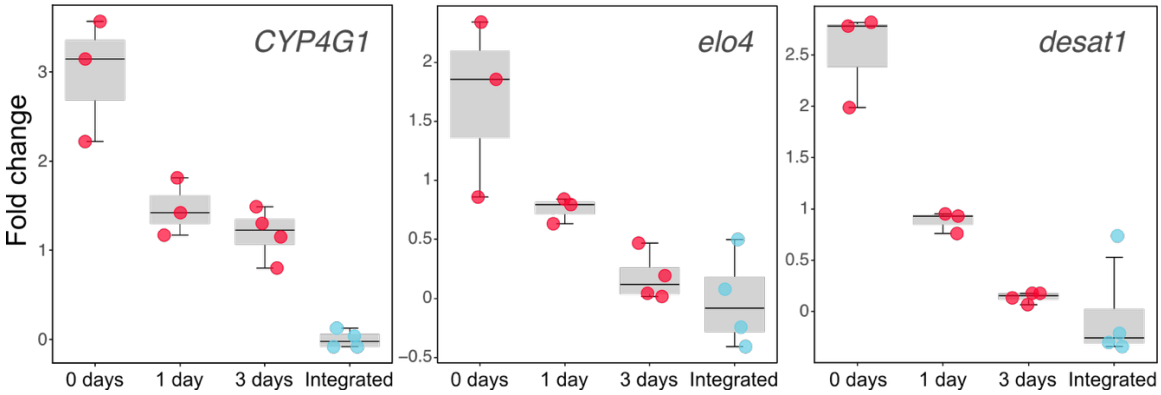

Figure 57. qPCR measurements of whole body *CYP4G1, elo4*, and *desat1* transcription at various timepoints after eclosion.

The qPCR results for the assayed genes showed a similar, though even more pronounced decrease in expression between the day of eclosion (0 days) and the integrated time point (Figure 57). *CYP4G1* appears to be the critical factor in the transition from life outside the ant nest to life inside the nest. Young *S. lativentris* produce hydrocarbons in the absence of *L. occidentale* but then shut off CHC biosynthesis as they switch to acquiring the compounds from the host ant. One might wonder about how this transition into the nest is made, since the beetle needs access to ants during the first day after eclosing to not die from desiccation, but is still expressing *CYP4G1* at high levels during this period (Figure 56 and 57). Below a certain threshold, CHCs have been found to be undetectable to social insects[67]. Briefly mentioned in the Natural History chapter, suppressing CHC production is a strategy employed by some myrmecophiles, which gives them access to the nest[61,250]. This strategy may be taxonomically restricted[61] and likely requires additional behavioral adaptations to avoid desiccation[36] if the strategy is employed long-term. Due to the low levels of CHCs produced by teneral *S. lativentris* (Figure 50), they likely fall into this chemically insignificant category. Initial grooming events occur while the beetle is still undetectable. As teneral beetles acquire increasing amounts of CHCs from the host ant during the first few days in the nest, their CHC profile shifts into the realm of chemical detectability of the host ant at the same time that *CYP4G1* expression is dropping off, eliminating the risk of adulterating their now significant CHC profile.

Endogenous Biosynthesis Revisited

After determining that *S. lativentris* shuts of CHC biosynthesis after eclosing and as it makes its way into the nests of *L. occidentale*, we revisited the problem of endogenous biosynthesis; we wanted to establish the consequences of CHC biosynthesis turning back on in *S. lativentris* while in the nest. To do this, we generated *S. lativentris* with a profile adulterated by the endogenous CHC profile of *P. sonomae*, briefly described and shown in Figure 53.

Wild caught *S. lativentris, L. occidentale*, and *P. sonomae* were transported to the lab as previously described and maintained until they were used for running in the behavioral arena. *L. occidentale* and *S. lativentris* were used in behavioral arenas within a week of collecting to avoid the slight shifts in CHC profiles that arise from the artificial lab diet. *S. lativentris* were coated with *P. sonomae* CHCs by placing *S. lativentris* in 5 mL vials with 7-8 *P. sonomae* for 2 hours. The number of *P. sonomae* was sufficient to fill the entire bottom of the vial, ensuring that *S. lativentris* was in contact with *P. sonomae* for the entire 2 hour period, regardless of grooming status. Control *S. lativentris* were placed in empty vials for 2 hours.

Following the coating procedure, *S. lativentris* was loaded into a behavioral arena with three *L. occidentale* collected contemporaneously from the same colony as the beetle. The behavioral arena was constructed from acrylic, with a 5cm diameter and a sliding door to allow acclimation of the beetle and ants in the arena prior to being introduced to each other. Due to the short duration of behavioral interactions, beetles and ants were loaded into the arena unanesthetized, to avoid changes in behavior that arise from CO_2 or cold anesthesia[251–253]. After a 2 minute acclimation period, the sliding door was opened, allowing the beetle and the ants to interact for a 5 minute interaction period. Behavior was recorded on a FLIR camera (BFS-U3-16S2C-CS: 1.6 MP) with an InfiniGage lens (Infinity Photo-Optical, CO), at 60hz.

After each run, *S. lativentris* and the three *L. occidentale* CHCs were analyzed via GCMS. Each beetle was extracted in 10 microliters of hexane for 20 minutes and three microliters of extract were analyzed. *L. occidentale* samples were extracted in 70 microliters of hexane for 20 minutes and two microliters were analyzed. CHCs were run on the GCMS, identified, and integrated as described previously.

Scoring of behavioral interactions was carried out in BORIS v. 8.20.1[254]. A simple ethogram consisting of biting, mandible flaring, and neutral interaction (any instance where no biting or mandible flaring was observed) was used. Interactions were scored any time that any ant's antenna made contact with *S. lativentris*. An aggression index was calculated as the sum of mandible flaring events and two times the number of biting events, divided by the sum of mandible flaring events, two times the number of biting events, and neutral events. Aggression values can thus take any value between zero, i.e. none of the interactions were aggressive, and one, i.e. every interaction was aggressive.

NMDS ordination of pairwise Bray-Curtis dissimilarity measurements of the CHC profiles of the *L. occidentale* and *S. lativentris* for each behavioral run, as well as a number of *P. sonomae,* was performed (Figure 58). The glyph size for each *S. lativentris* sample was scaled by the aggression index for the associated behavioral interaction. Control *S. lativentris*, which had groomed *L. occidentale* from the same colony as the test ants, experienced almost no aggression, whereas the *S. lativentris* with shifted profiles experienced relatively high degrees of aggression. This result demonstrates that the mimicry approach of *S. lativentris*, shutting off its biosynthesis and stealing hydrocarbons from the ant, is necessary for the beetle's high degree of integration into *L. occidentale* colonies. Slight deviations from this profile caused by "endogenous" biosynthesis are enough to result in significantly more aggression from the host.

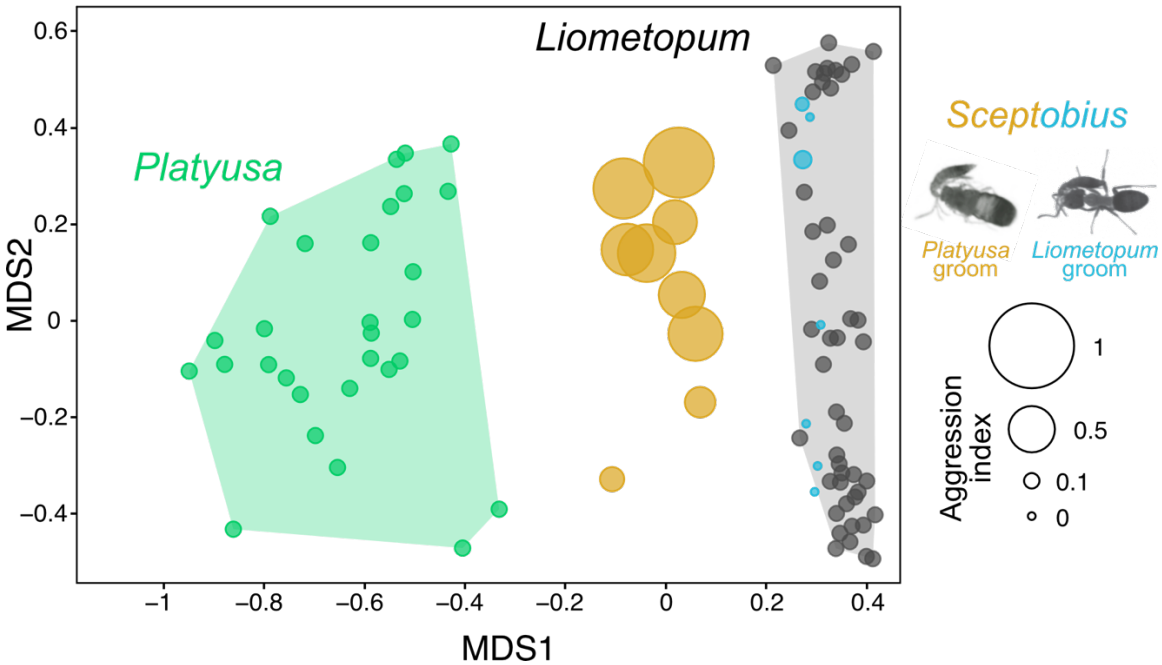

Figure 58. NMDS ordination of *P. sonomae*, *S. lativentris*, and *L. occidentale* CHC profiles using Bray-Curtis dissimilarity, 2D stress=0.08. The glyph size for the two different *S. lativentris* conditions (*Platyusa* CHC treatment; gold, control CHC treatment; blue) are determined by the aggression index for a behavioral run between the beetle and three ants from the beetle's colony of origin.

Chapter 5

LIFE HISTORY CONSEQUENCES OF MIMICRY

The accuracy with which *S. lativentris* mimics the CHCs of *L. occidentale* allows the beetle to live a protected life with access to abundant resources, simply by shutting down CHC biosynthesis and engaging in a few novel behaviors. There has to be a catch. As I have mentioned multiple times throughout this thesis, *Sceptobius* dies quickly when isolated from its host. The beetle can survive for up to three days under ideal conditions (Figure 38), but naturalistic conditions in the arid Southwest are almost always going to be much harsher. The loss of endogenous CHC production and associated desiccation is a contributing factor to death in these environments. Because CHCs act pleiotropically in the context of recognition and desiccation, the lateral function transfer of CHC production in *S. lativentris* has forced the beetle into an obligate, effectively irreversible symbiosis. Like many obligate bacterial endosymbionts[255], the beetle has started to shed traits that are no longer necessary, such as wings and defensive glands (Figure 22), further entrenching the symbiosis.

Desiccation is a Cause of Death

The loss of endogenous CHC production in adult *S. lativentris* has, up to this point, been assumed to lead to desiccation and death. This is a reasonable assumption to make, as CHC loss has been connected to desiccation and death in other species[256,257]. To verify that desiccation is a contributing factor to the death of isolated *S. lativentris*, we first recreated the *S. lativentris* condition in the free-living beetle *D. coriaria* by knocking down the beetle's *CYP4G*. We then demonstrated that the addition of exogenous CHCs can extend the survival time of both *S. lativentris* and the *CYP4G* RNAi *D. coriaria*. A model is then described for how the CHC mimicry mechanism employed by *S. lativentris* is likely the reason why the beetle is an obligate myrmecophile.

To make a *CYP4G* knockdown *D. coriaria*, we used the RNAi protocol described above, with a few minor differences. Cloning was performed as described above, using the following primers.

Dcor *oCYP4G*-1:

F: 5'- TAATACGACTCACTATAGGGCACTCCCTGTCGGAACCTTGGA-3'
R: 5'-TAATACGACTCACTATAGGGTTGCGACATCCTCCACAGACGT-3'

Dcor *oCYP4G*-2:

F: 5'-TAATACGACTCACTATAGGGACGTCTGTGGAGGATGTCGCAA-3'
R: 5'-TAATACGACTCACTATAGGGATCCAAAATCCCCGGACCCGAT-3'

EGFP:

F: 5'- TAATACGACTCACTATAGGGTCTTCTTCAAGGACGACGGCAACTAC -3'
R: 5'- TAATACGACTCACTATAGGGTTACTTGTACAGCTCGTCCATGCCGA -3'

With the help of Hannah Ryon, constructs were synthesized as described above. Constructs were microinjected into third instar *D. coriaria* larvae. The beetle larvae were reared in 5cm Petri dishes with clean filter paper until they pupated and eclosed, after which they were fed frozen fruit flies until they were used in experiments. Injected *D. coriaria* were used in experiments within 5-10 days of eclosing. Representative GCMS traces for *GFP* RNAi beetles, *CYP4G* RNAi beetles, and *CYP4G* RNAi beetles coated with *L. occidentale* CHCs (described in the next section) are shown in Figure 59. *CYP4G* RNAi was found to completely ablate CHCs in the beetle, and *L. occidentale* CHCs were successfully transferred onto these RNAi beetles.

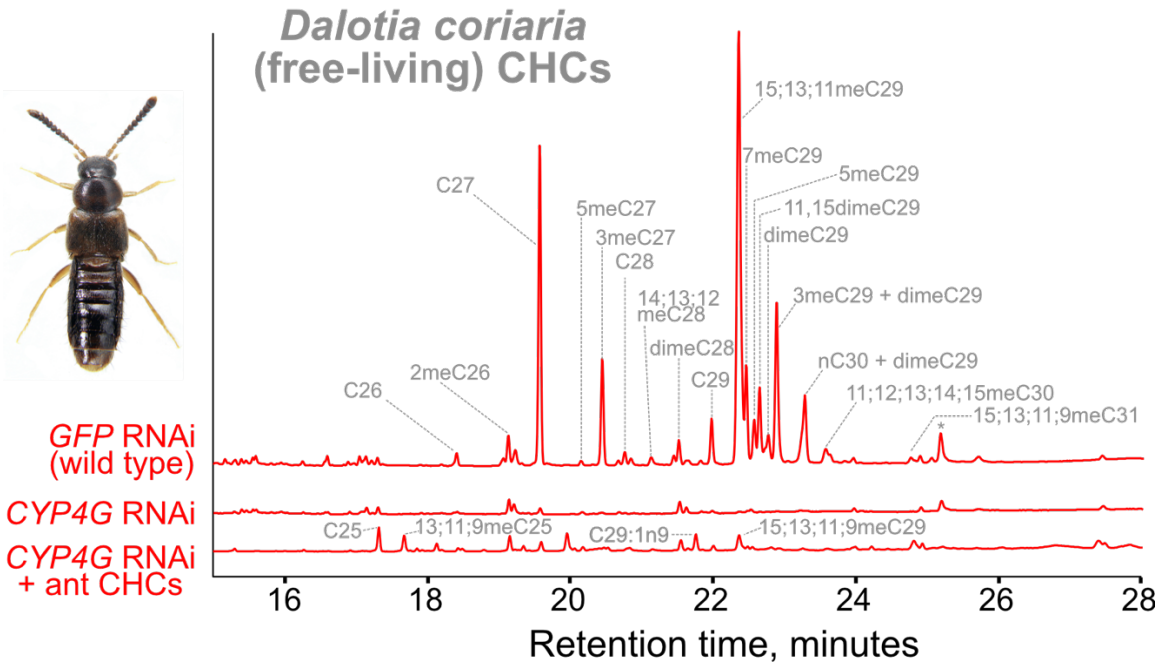

Figure 59. Free living *Dalotia coriaria* CHC production can be silenced, and replaced with *Liometopum* CHCs. Major *D. coriaria* and *L. occidentale* CHCs are labelled.

Desiccation resistance was measured in *S. laiventris* using an acrylic desiccation arena. The arena consisted of two sheets of 3/8 inch acrylic both containing six wells with a diameter of one centimeter each. The two sets of wells sandwiched a piece of filter paper, which acted as the floor for the beetles, located in the upper set of wells. The lower set of wells was used to introduce wetted circles of filter paper as a humidity source. The well setup was then sandwiched between two sets of IR passthrough acrylic, creating a dark behavior arena. The desiccation arena was lit from below by LED lights, which emitted partially in the IR range.

To test the effect of superphysiological levels of CHCs on *S. laiventris,* beetles were coated in *L. occidentale* CHCs, which were extracted and fractionated previously[18]. Briefly, surface chemicals were extracted from tens of thousands of *L. occidentale*, collected from the post colony mentioned in the Natural History section, and were subsequently separated via vacuum flash chromatography and

eluted with hexane and cyclohexane. The resulting purified CHC extracts contained approximately 250 ant equivalents per milliliter. 100 microliters of the *L. occidentale* CHCs were then applied to the inside of a 5mL glass vial and the hexane was evaporated off under a stream of N_2. This process resulted in a thin coating of *L. occidentale* CHCs on the inner surface of the vial.

S. laiventris were collected at multiple nest-sites, and were pooled for each run. Beetles were either placed in the CHC coated vial, or in a blank control vial, for an hour. *S. laiventris* in the CHC coated vial moved around enough to transfer CHCs from the walls of the vial to their cuticle. Groups of five beetles were then loaded into each well in the arena. Beetles were run in groups to avoid confounding effects from social isolation. Desiccation trials were run at room temperature under a FLIR camera (BFS-U3-04S2M-CS: 0.4 MP) with an InfiniGage lens (Infinity Photo-Optical, CO) running at 1 hz. Recordings were collected until all beetles in the desiccation arena were dead, typically 20-40 hours. For runs with higher humidity, 10 pieces of hole punched filter paper were placed in the lower chamber below each well and 50µl of water were added to the pieces of filter paper.

To replicate the effects of CHC addition on another beetle species, we knocked down *CYP4G1* in *D. coriaria,* using the RNAi protocol described above. Control beetles were injected with dsRNA targeting *GFP*, and thus had a species typical CHC profile. We then took the *CYP4G* KD *D. coriaria* and coated them in ant CHCs, as described above. *GFP* RNAi *D. coriaria*, *CYP4G* RNAi *D. coriaria*, and *CYP4G* RNAi *D. coriaria* with *L. occidentale* CHCs were then run in the desiccation arena. After each run, *D. coriaria* were extracted in 70 microliters of hexane containing an internal octadecane standard and analyzed with the CHC-GCMS method describe above to verify that the knockdowns were successful. Beetles for which the wild type CHC profile was detectible were excluded from downstream analysis.

The simple addition of CHCs to *S. lativentris* increased median survival time in arid conditions by roughly five hours (Figure 60). This trend was recapitulated with the *D. coriaria CYP4G* RNAi samples, though the baseline time to death was much faster than in *S. lativentris*. One primary difference between the uncoated *S. lativentris* condition and the uncoated *CYP4G* RNAi *D. coriaria* is that *S. lativentris,* though not producing any hydrocarbons, began the trial with recently acquired CHCs, whereas the uncoated *D. coriaria* had no CHCs. However CHC coating of *CYP4G* RNAi *D. coriaria* did not fully rescue survival to the levels of the uncoated *S. lativentris*, the most comparable condition. This is almost certainly because *D. coriaria* had *CYP4G* knocked down during the last larval instar and thus the beetles pupated, eclosed, and lived for 10 days without CHCs, which likely placed a large strain on their bodies, making them even more susceptible to the desiccating conditions in the arena than *S. lativentris.* Increasing the humidity in the chamber significantly increased the survival time of both *S. lativentris* conditions, though the CHC coated condition still lived longer, suggesting that even at these high humidities, desiccation stress might not be completely eliminated. The reduced desiccation pressure in the humid *S. lativentris* conditions increased the survival time of the beetles to levels comparable with a beetle producing CHCs in arid conditions (*D. coriaria GFP* RNAi).

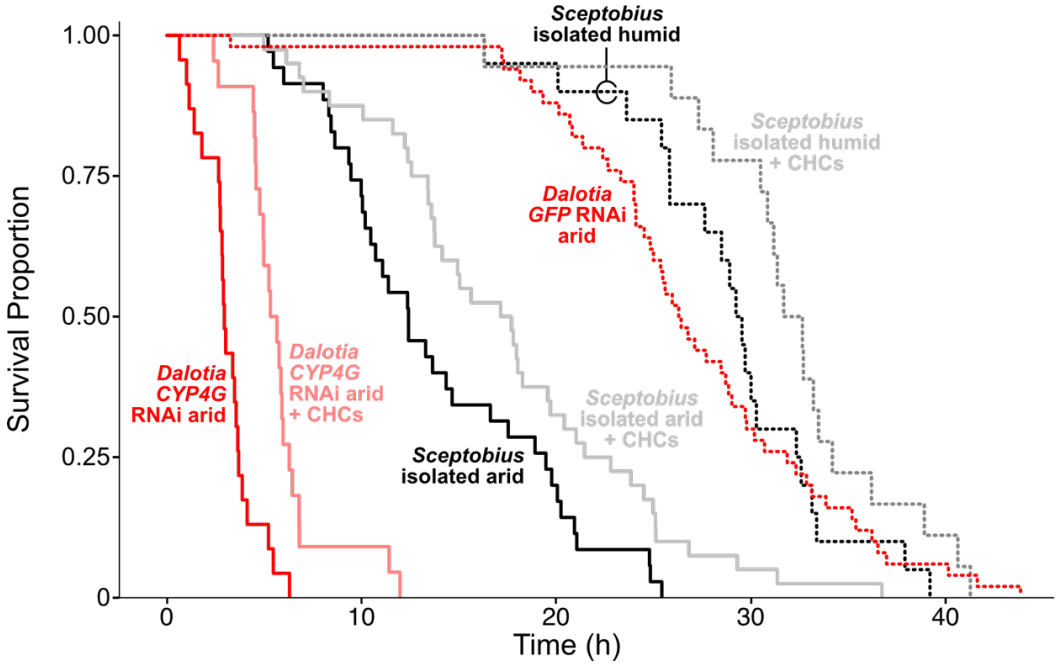

Figure 60. CHCs increase survival time in arid conditions for both *S. lativentris* and *CYP4G* RNAi *D. coriaria*.

The Catch-22

The results in Figure 60 combined with the results in Figure 58 demonstrate that acquisition of CHCs from *L. occidentale* is both essential for desiccation resistance in the *S. lativentris*, as well as aggression free access to the ant nest where *S. lativentris* lives. Ant use of CHCs as a recognition system is so effective because of the pleiotropic role of CHCs. Producing an endogenous mimetic profile is difficult to achieve to a good enough degree for full integration, stealing hydrocarbons while producing an endogenous profile also is not an option because of recognition, and chemical insignificance cannot be a widespread strategy because of desiccation. The only integration strategy guaranteed to achieve perfect CHC mimicry and provide access to the entire nest is acquired mimicry with suppression of *de novo* CHC production. But this strategy comes at a cost (Figure 61). The transition to perfect, acquired mimicry requires the development of basic attraction to ants and CHC acquisition behaviors as well as the loss of CHC biosynthesis. One can imagine this evolving from a free-living state, where ant attraction and CHC loss are slowly titrated in opposite directions until the

two reach their final state, with the pull of nest resources and protection encouraging this transition. But once the *S. lativentris* syndrome has been established, reversion becomes extremely difficult because of the CHC trait pleiotropy. CHC production has extreme negative fitness consequences inside the nest, but is essential outside of it. If *S. lativentris* were to lose ant attraction, it would desiccate outside of the nest. If *S. lativentris* instead regains CHC production, it is met with detection and death at the hands of its host. This biological Catch-22 can only be overcome by the simultaneous reversion of ant attraction and CHC silencing, a tall order by evolutionary standards. In this way, what may at one point have been a facultative association between ancestors of the beetle and the ant has been transformed into an irreversible, obligate dependence of the beetle on the ant for maintaining basic homeostatic functions. The further loss of wings and the aleocharine defensive gland (Figure 22) has only further entrenched the symbiosis.

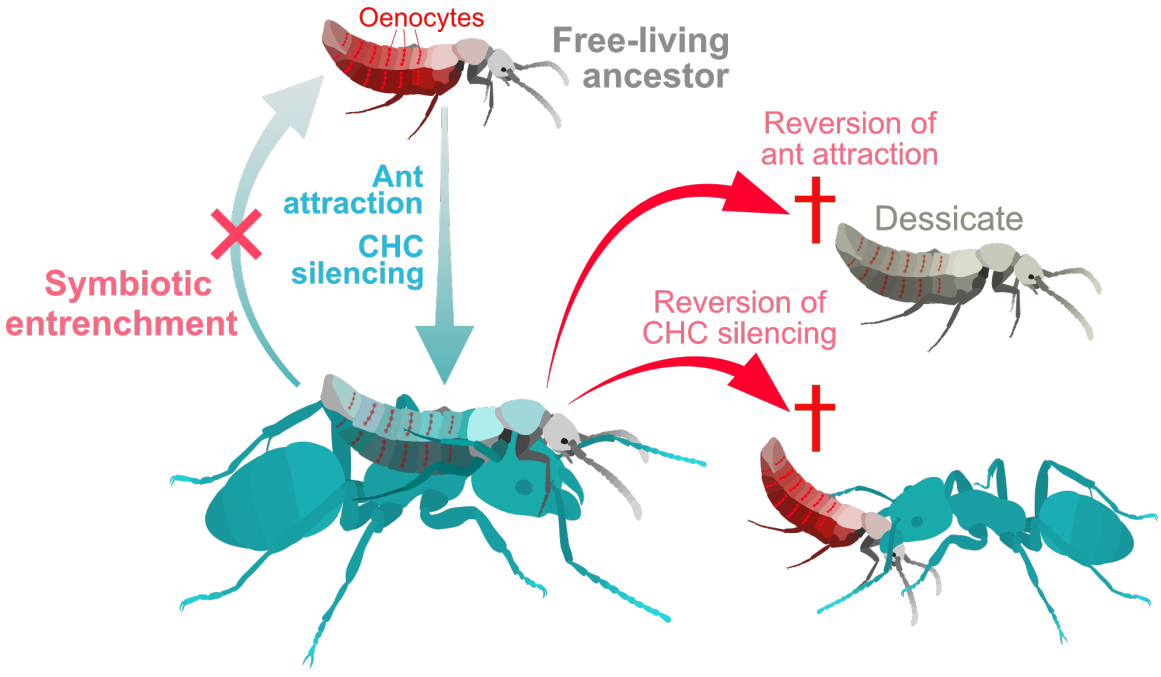

Figure 61. A model for entrenchment of obligate myrmecophily in *S. lativentris*.

This obligate syndrome is not unique to *S. lativentris*. In addition to the other members of the Sceptobiini, which are obligate inquilines of their hosts[88] and likely employ acquired CHC mimicry (personal observation), many army ant myrmecophiles present the hallmarks of this approach to mimicry including grooming behaviors[82,83], CHC mimicry[64], rapid death in the absence of the host[82], and degeneration of various traits such as eyes[258], wings[258], and defensive glands[125,259]. It is possible that only those ant species which are locally dominant, and highly aggressive encourage this approach to myrmecophily, as without high mortality associated with recognition, other less accurate mimicry mechanisms would suffice. A survey of obligate myrmecophiles employing acquired mimicry across different ant species that takes into account ant aggressiveness might prove informative.

To generalize the *S. lativentris* syndrome slightly, I think that the underlying critical feature of the obligate symbiotic entrenchment is the presence of a pleiotropic trait where one function is connected to some basic homeostatic mechanism and the second function negatively impacts fitness, but exclusively within the symbiotic niche. Furthermore, I think that what makes CHCs fall into this category is not necessarily their chemical composition, though it is important for their function, but instead their location. The surface of the organism both maintains order within its body, and interfaces with the world around it. This provides the link between homeostasis on one side of the equation and negative fitness due to recognition by the symbiont on the other side of the equation. Another example of this syndrome may exist in endosymbiotic bacteria, some of which have lost their ability to produce the components of their cell wall, both avoiding immune detection by their host and simultaneously becoming obligately dependent on the osmotically regulated host cellular environment[260].

A p p e n d i x

Species	**Source**
Drosophila melanogaster	NCBI RefSeq
Agrilus planipennis	NCBI RefSeq
Tribolium castaneum	NCBI RefSeq
Aethina tumida	NCBI RefSeq
Dendroctonus ponderosae	NCBI RefSeq
Anaplophora glabripennis	NCBI RefSeq
Leptinotarsa decemlineata	NCBI RefSeq
Onthophagus taurus	NCBI RefSeq
Nicrophorus vespilloides	NCBI RefSeq
Coproporus ventriculus	Kitchen et al.[125]
Gymnusa sp.	Kitchen et al.[125]
Adinopsis sp.	Kitchen et al.[125]
Deinopsis erosa	Kitchen et al.[125]
Cypha longicornis	Kitchen et al.[125]
Holobus sp.	Kitchen et al.[125]
Aleochara nigra	Kitchen et al.[125]
Aleochara sp.	Kitchen et al.[125]
Leptusa sp.	Kitchen et al.[125]
Liometoxenus newtonarum	Kitchen et al.[125]
Oxypoda opaca	Kitchen et al.[125]
Myllaena sp.	Kitchen et al.[125]
Falagria sp.	Kitchen et al.[125]
Lissagria laeviuscula	Kitchen et al.[125]
Atheta pasadenae	Kitchen et al.[125]
Dalotia coriaria	Kitchen et al.[125]
Earota dentata	Kitchen et al.[125]
Geostiba sp.	Kitchen et al.[125]

Table 1. Genomes used in the phylogenomic analysis

ID	Diagnostic ions
C23	324[M^+]
C24	338[M^+]
C25:1	350[M^+]
C25	352[M^+]
13;11;9meC25	197/196;225/224,169/168;253/252,141/140
7meC25	281/280,113/112
5meC25	309/308,85/84
dimeC25(1)	141, 168, 196, 211, 239, 267, 365 [M-15]
3meC25	337/336,57/56
dimeC25(2)	85/84,165/164,197/196,323, 365 [M-15]
C26	366[M^+]
dimeC25(3)	167/166,197/196,225/224, 351, 365 [M-15]
13;12;11;10meC26	211/210,197/196;183/182,225/224;239/238,169/168;155/154,253/252,365
C27:1n9	278[M^+][196]
C27	280[M^+]
13;11;9meC27	225/224,169/168;253/252,141/140
7meC27	309/308,113/112
5meC27	337/336,85/84
dimeC27(1)	267, 393 [M-15]
dimeC27(2)	295, 393 [M-15]
dimeC27(3)	323, 393 [M-15]
3meC27	364/365,56/57
dimeC27(4)	351, 393 [M-15]
C28	394[M^+]
dimeC27(5)	379, 393 [M-15]
14;13;12;10meC28	211/210,225/224;239/238,197/196;183/182,253/252;155/154,281/280
4meC28?	365/364
C29:1n7?	406[M^+]
C29:1n9	406[M^+][196]
C29	408[M^+]
15;13;11;9meC29	225/224;253/252,197/196;281/280,169/168;309/308,141/140
7meC29	337/336,113/112
5meC29	365/364,85/84
dimeC29 (1)	295, 421[M-15]
dimeC29 (2)	323, 421[M-15]
dimeC29 (3)	351, 421[M-15]
3meC29	393/392,57/56
dimeC29 (4)	379, 421[M-15]
dimeC29 (5)	421[M-15]

15;14;13;12;10 meC30	197/196,267/266;225/224,239/238;253/252,211/210;281/280,183/182;309 /308,155/154
C31:2 (1)	432[M^+]
C31:2 (2)	432[M^+]
2meC30	421/420;393/392
C31:1 (1)	434[M^+]
C31:1 (2)	434[M^+]
C31:1 (3)	434[M^+]
C31	436[M^+]
15;13;11;9meC3 1	253/252,225/224;281/280,197/196;309/308,169/168;337/336,141/140
5meC31	393/392,85/84
dimeC31 (1)	421,435,449 [M-15]
dimeC31 (2)	421,435,449 [M-15]
dimeC31 (3)	421,435,449 [M-15]
3meC31	421,57/56
dimeC31 (4)	421,435,449 [M-15]
dimeC31 (5)	421,435,449 [M-15]
xmeC32	449 [M-15]
17;15;13;11;9m eC33	253/252;281/280,225/224;309/308,197/196;337/336,169/168;365/364,141 /140
dimeC33 (1)	477 [M-15]
dimeC33 (2)	463, 477 [M-15]
17;16;15;14;13; 12;11;10meC34	252/253,266/267;280/281,238/239;224/225,294/295;308/309,210/211;196 /197,322/323;336/337,182/183;168/169,350/351;364/365,154/155
17;15;13;11meC 35	280/281,252/253;308/309,224/225;336/337,196/197;364/365,168/169
dimeC35	505 [M-15]

Table 2. *Liometopum occidentale* CHCs

Gene	Dcor v2 genome annotations from Kitchen et al. 2024 Cell[125]
ELO4	Dcor_evm.model.ctg10_len_3669713.1407, Dcor_evm.model.ctg10_len_3669713.1095a00001
ELO1	Dcor_evm.model.ctg25_len_963869.128_129
ELO2	Dcor_evm.model.ctg6_len_5675906.52
ELO3	Dcor_evm.model.ctg6_len_5675906.49
ELO5	Dcor_evm.model.ctg6_len_5675906.50
CyP4G1	Dcor_evm.model.scaffold137_size1808848.143
desat1	Dcor_evm.model.ctg12_len_6330523.1225
FAS1	Dcor_evm.model.ctg10_len_3669713.1007
FAS2	Dcor_evm.model.ctg12_len_6330523.983
FAS3	Dcor_evm.model.ctg1_len_6253557.1347
FAR1	Dcor_evm.model.ctg19_len_2461079.320
FAR2	Dcor_evm.model.ctg28_len_882067.176
FAR3	Dcor_evm.model.scaffold36_size190523.34
FAR4	Dcor_evm.model.scaffold36_size190523.36, Dcor_evm.model.scaffold36_size190523.35
desat2	Dcor_evm.model.ctg19_len_2461079.154-00001
desat4	Dcor_evm.model.ctg12_len_6330523.1222
desat3	Dcor_evm.model.ctg10_len_3669713.819
desat5	Dcor_TRINITY_GG_92_c1359_g1_i1_p1
ELO6	Dcor_evm.model.ctg12_len_6330523.1208
ELO7	Dcor_evm.model.ctg6_len_5675906.560
ELO8	Dcor_evm.model.ctg6_len_5675906.55
ELO9	Dcor_evm.model.ctg3_len_6069552.694
ELO10	None
FAR5	Dcor_evm.model.ctg19_len_2461079.402
FAR6	Dcor_evm.model.ctg24_len_2556950.36
FAR7	Dcor_evm.model.scaffold36_size190523.27
ELO11	Dcor_evm.model.ctg22_len_1181805.388
CPR	Dcor_evm.model.ctg3_len_6069552.174
FAR8	Dcor_evm.model.ctg12_len_6330523.1
ELO12	Dcor_evm.model.ctg24_len_2556950.88a

Table 3. CHC biosynthesis enzymes and orthologous sequences in *Dalotia coriaria*

Gene	Pson Orthologs
ELO4	Pson_TRINITY_DN782_c0_g1_i3.p1*, Pson_TRINITY_DN782_c0_g1_i4.p1
ELO1	none
ELO2	Pson_TRINITY_DN9471_c0_g1_i1.p2
ELO3	Pson_TRINITY_DN2473_c1_g1_i1.p1
ELO5	Pson_TRINITY_DN2473_c0_g1_i1.p1
CyP4G1	Pson_TRINITY_DN2722_c0_g2_i1.p1*
desat1	Pson_TRINITY_DN257_c2_g1_i1.p1*
FAS1	Pson_TRINITY_DN3393_c0_g1_i4.p1, Pson_k119_722322_gene2a
FAS2	Pson_TRINITY_DN33_c0_g1_i7.p1, Pson_TRINITY_DN3888_c0_g1_i1.p1
FAS3	Pson_TRINITY_DN465_c0_g1_i4.p1*
FAR1	Pson_TRINITY_DN7112_c0_g1_i9.p1, Pson_TRINITY_DN8317_c1_g1_i19.p1
FAR2	Pson_TRINITY_DN1026_c0_g1_i10.p1
FAR3	Pson_TRINITY_DN5094_c0_g1_i4.p1
FAR4	Pson_TRINITY_DN4620_c0_g1_i6.p1*, Pson_TRINITY_DN4620_c0_g2_i13.p1, Pson_k119_936437_483757_1086134_248186_1114230RC_gene4a
desat2	Pson_TRINITY_DN1356_c1_g1_i8.p1
desat4	Pson_TRINITY_DN4819_c0_g1_i1.p1
desat3	Pson_TRINITY_DN440_c0_g1_i11.p2
desat5	Pson_TRINITY_DN7573_c0_g1_i6.p1, Pson_TRINITY_DN7573_c0_g1_i8.p1
ELO6	Pson_TRINITY_DN10704_c0_g2_i4.p1
ELO7	Pson_TRINITY_DN1185_c0_g1_i19.p1
ELO8	Pson_TRINITY_DN3893_c0_g1_i1.p1
ELO9	Pson_TRINITY_DN6750_c0_g1_i1.p1
ELO10	Pson_TRINITY_DN6520_c0_g1_i8.p1
FAR5	Pson_TRINITY_DN155_c97_g1_i7.p1
FAR6	Pson_TRINITY_DN32631_c0_g1_i1.p1
FAR7	Pson_k119_245651_360072_58654_403476_814044RC_958313RC_gene1a
ELO11	Pson_TRINITY_DN112378_c0_g1_i1.p1
CPR	Pson_TRINITY_DN753_c1_g2_i4.p1
FAR8	Pson_TRINITY_DN2744_c0_g1_i5.p1, Pson_TRINITY_DN2254_c0_g1_i22.p1
ELO12	Pson_TRINITY_DN5856_c0_g1_i1.p1

Table 4. CHC biosynthesis enzymes in *Platyusa sonomae.* Asterisks denote transcripts which were targeted with HCR.

Gene	Slat Orthologs
ELO4	Slat_TRINITY_DN165_c1_g1_i28.p1*
ELO1	Slat_TRINITY_DN20689_c0_g1_i7.p1
ELO2	Slat_evm.model.hic_scaffold_2_pilon_pilon.379-00001
ELO3	Slat_TRINITY_DN9690_c1_g1_i9.p1, Slat_evm.model.hic_scaffold_2_pilon_pilon.373, Slat_evm.model.hic_scaffold_2_pilon_pilon.374
ELO5	Slat_TRINITY_DN54_c0_g2_i2.p1
CyP4G1	Slat_TRINITY_DN299_c0_g1_i3.p1*
desat1	Slat_TRINITY_DN897_c0_g1_i37.p1*
FAS1	Slat_TRINITY_DN902_c7_g1_i101.p1
FAS2	None
FAS3	Slat_TRINITY_DN18025_c1_g1_i4.p1, Slat_TRINITY_DN508_c3_g1_i5.p1, Slat_evm.model.hic_scaffold_3_pilon_pilon.1657*, Slat_evm.model.hic_scaffold_3_pilon_pilon.1761, Slat_evm.model.hic_scaffold_5_pilon_pilon.1559
FAR1	Slat_TRINITY_DN2352_c0_g1_i3.p1, Slat_TRINITY_DN4862_c0_g1_i12.p1
FAR2	Slat_TRINITY_DN454_c4_g1_i11.p1, Slat_TRINITY_DN1701_c0_g1_i42.p1
FAR3	Slat_TRINITY_DN4373_c0_g1_i4.p1
FAR4	Slat_evm.model.hic_scaffold_9_pilon_pilon.512*
desat2	Slat_TRINITY_DN1161_c4_g1_i2.p1
desat4	Slat_TRINITY_DN557_c1_g2_i1.p1
desat3	Slat_evm.model.hic_scaffold_10_pilon_pilon.1681
desat5	None
ELO6	Slat_TRINITY_DN15725_c0_g1_i12.p1
ELO7	Slat_TRINITY_DN15611_c0_g1_i2.p1
ELO8	Slat_TRINITY_DN3691_c0_g1_i1.p1
ELO9	Slat_TRINITY_DN1299_c0_g2_i2.p1
ELO10	Slat_TRINITY_DN28641_c0_g1_i3.p1
FAR5	Slat_TRINITY_DN35465_c0_g1_i4.p1, Slat_TRINITY_DN710_c1_g1_i5.p1
FAR6	Slat_evm.model.hic_scaffold_9_pilon_pilon.915
FAR7	Slat_evm.model.hic_scaffold_9_pilon_pilon.697, Slat_evm.model.hic_scaffold_9_pilon_pilon.1117, Slat_evm.model.hic_scaffold_4_pilon_pilon.2085
ELO11	Slat_TRINITY_DN2208_c0_g1_i15.p1
CPR	Slat_TRINITY_DN4772_c0_g1_i1.p1
FAR8	Slat_TRINITY_DN4813_c4_g1_i13.p1

ELO12	Slat_TRINITY_DN2842_c0_g1_i11.p3, Slat_TRINITY_DN7230_c0_g1_i20.p1, Slat_evm.model.hic_scaffold_9_pilon_pilon.77

Table 5. CHC biosynthesis enzymes in *Sceptobius lativentris.* Asterisks denote transcripts which were targeted with HCR.

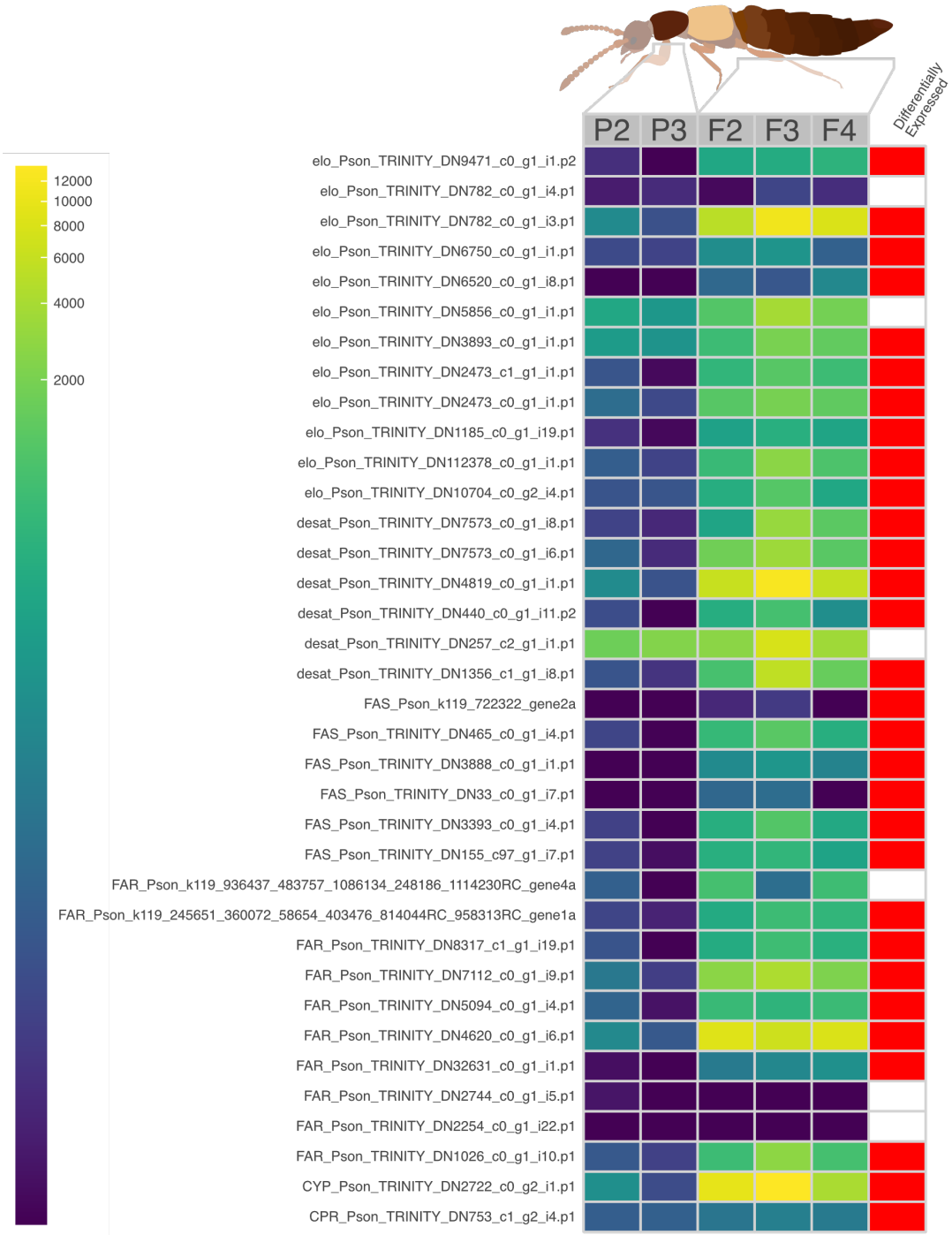

Figure 62. *Platyusa sonomae* CHC biosynthesis enzyme expression in pronotum (P, first thoracic segment), and fat body (F). Differentially expressed genes are marked in red.

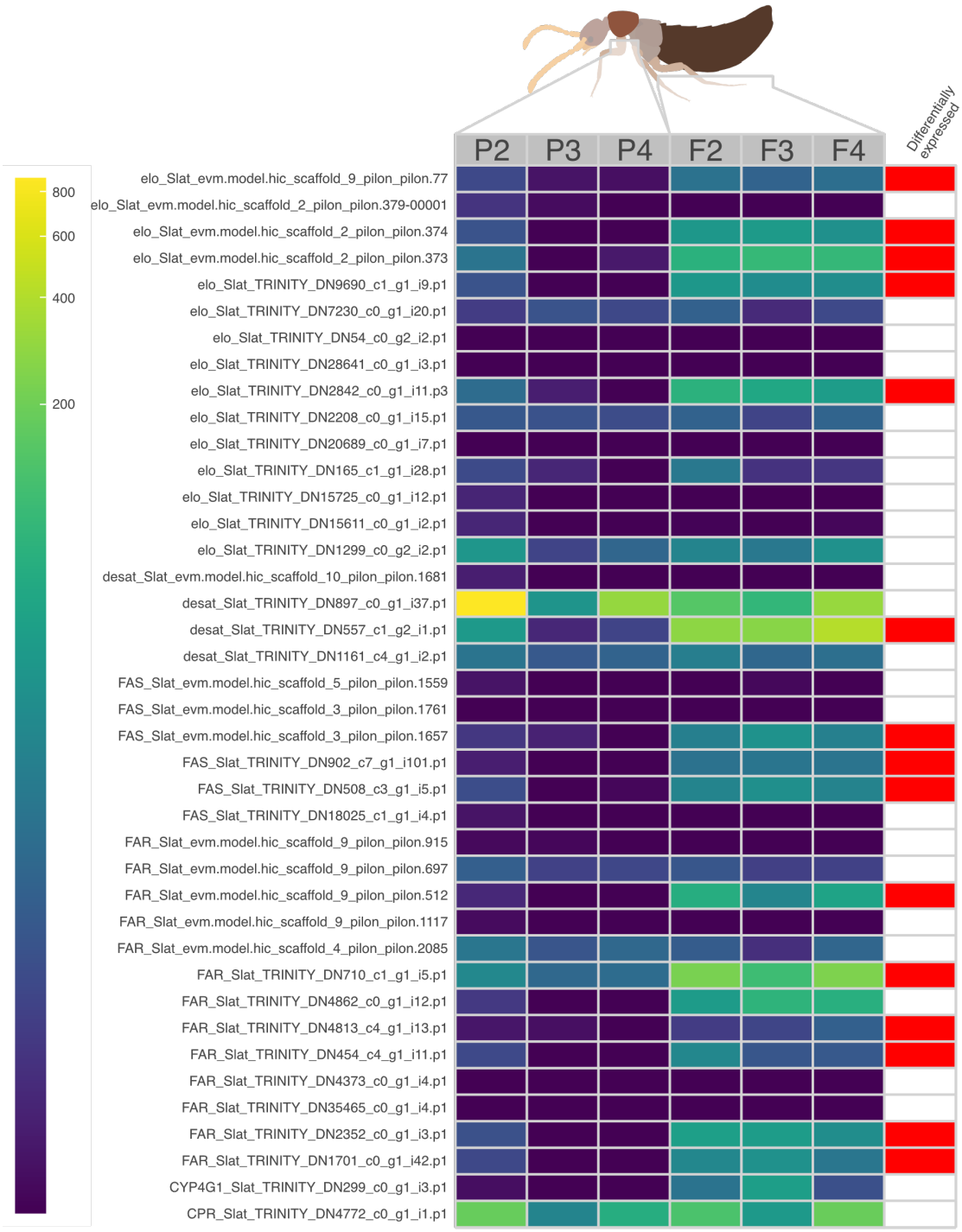

Figure 63. *Sceptobius lativentris* CHC biosynthesis enzyme expression in pronotum (P, first thoracic segment), and fat body (F). Differentially expressed genes are marked in red.

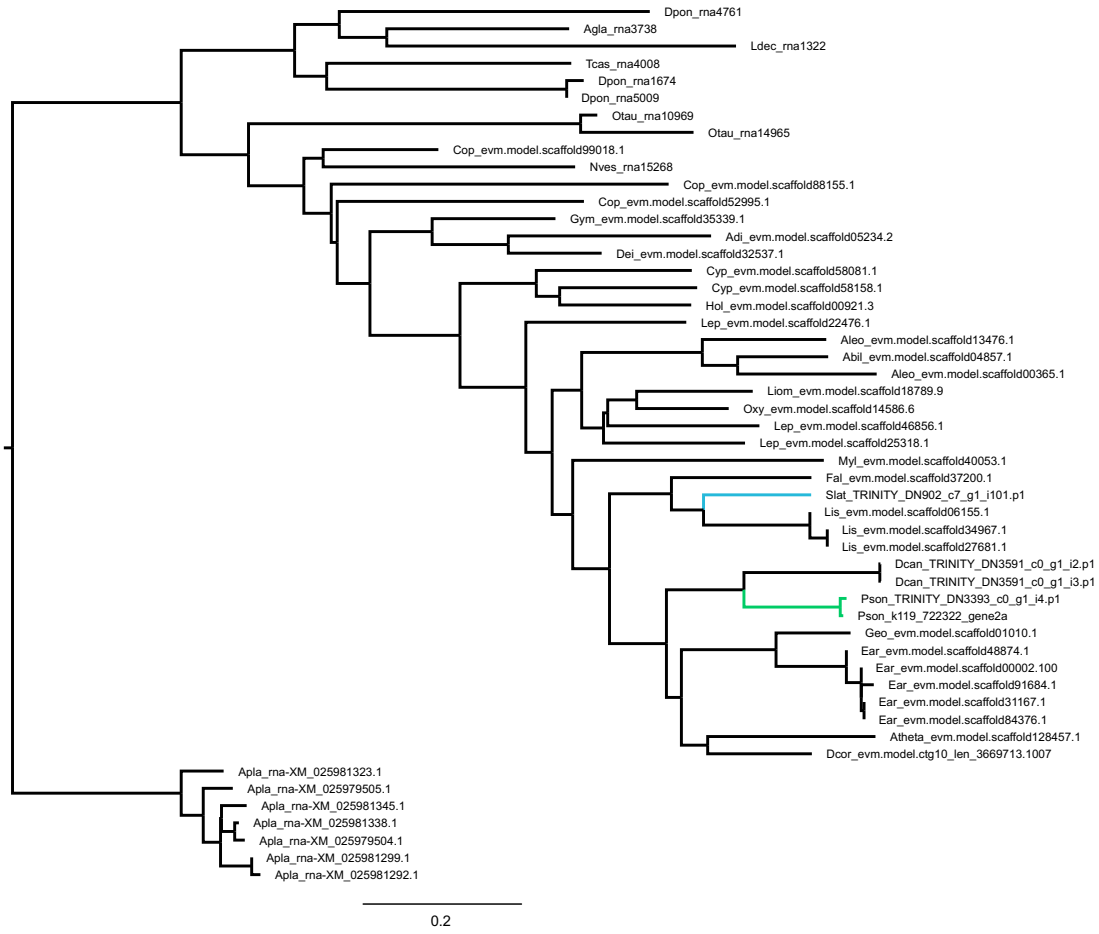

Figure 64. Fatty acid synthase 1 (*FAS1*) gene tree

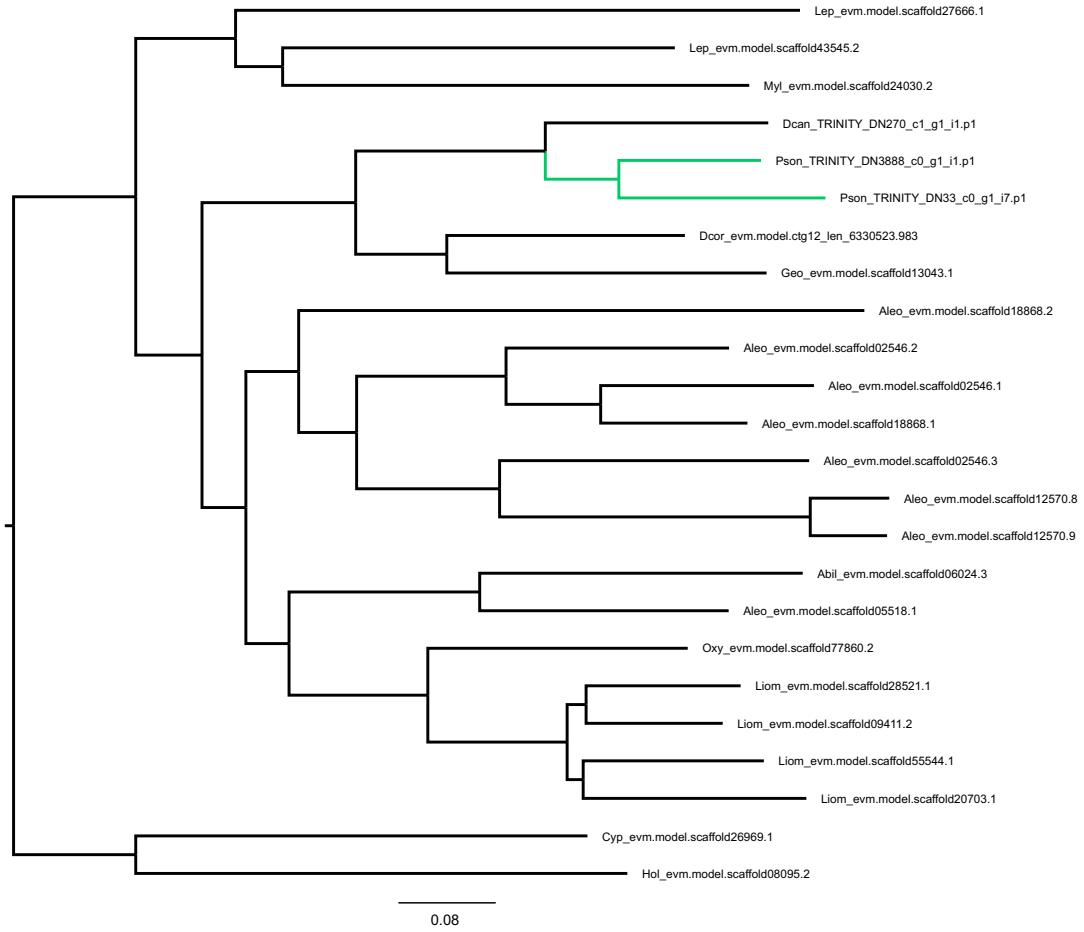

Figure 65. Fatty acid synthase 2 (*FAS2*) gene tree

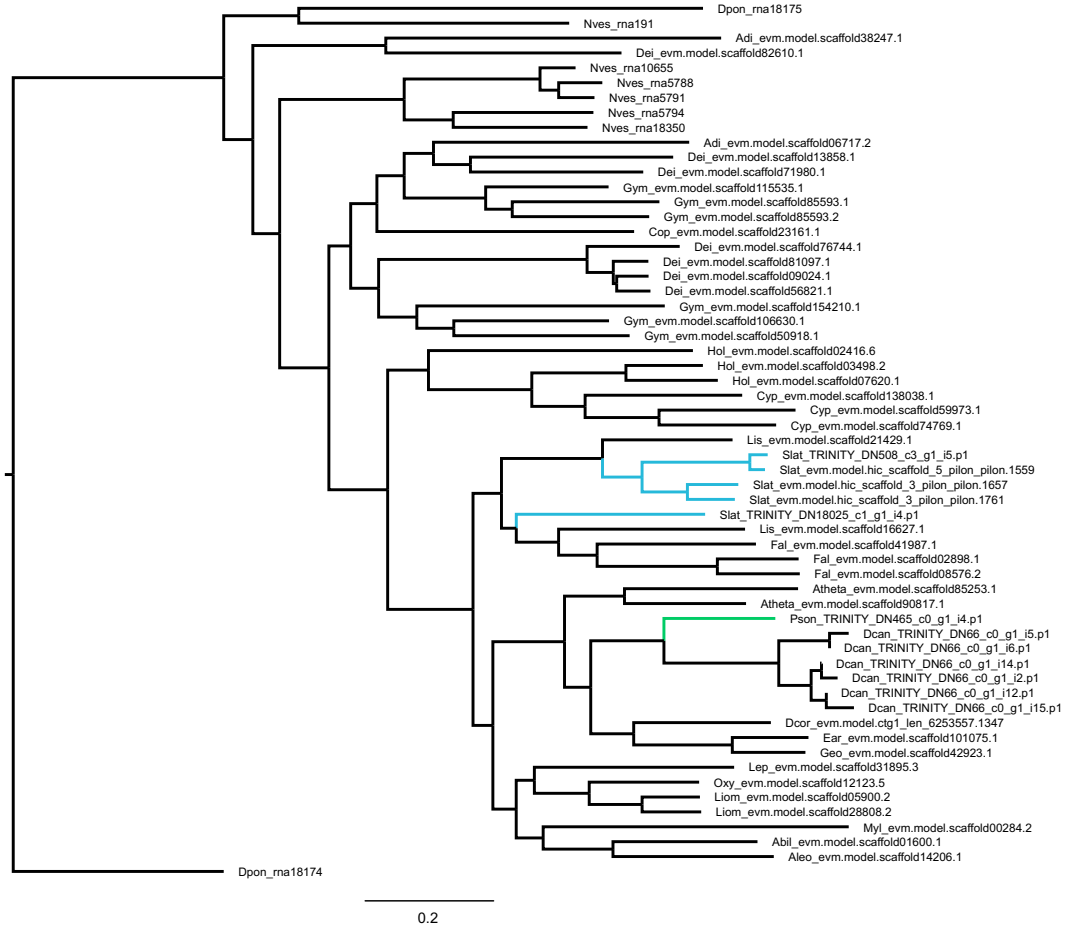

Figure 66. Fatty acid synthase 3 (*FAS3*) gene tree

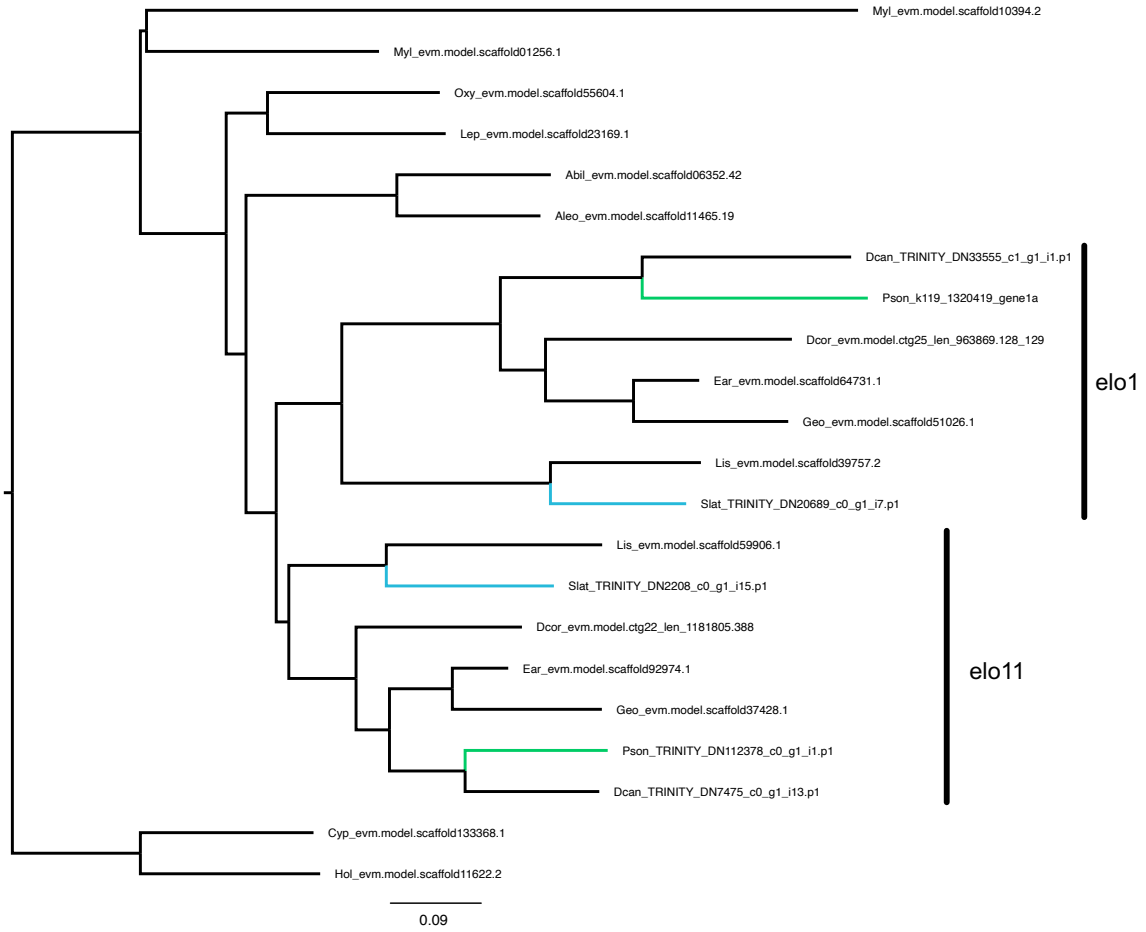

Figure 67. elongase 1 (*elo1*) and elongase 11 (*elo11*) gene tree

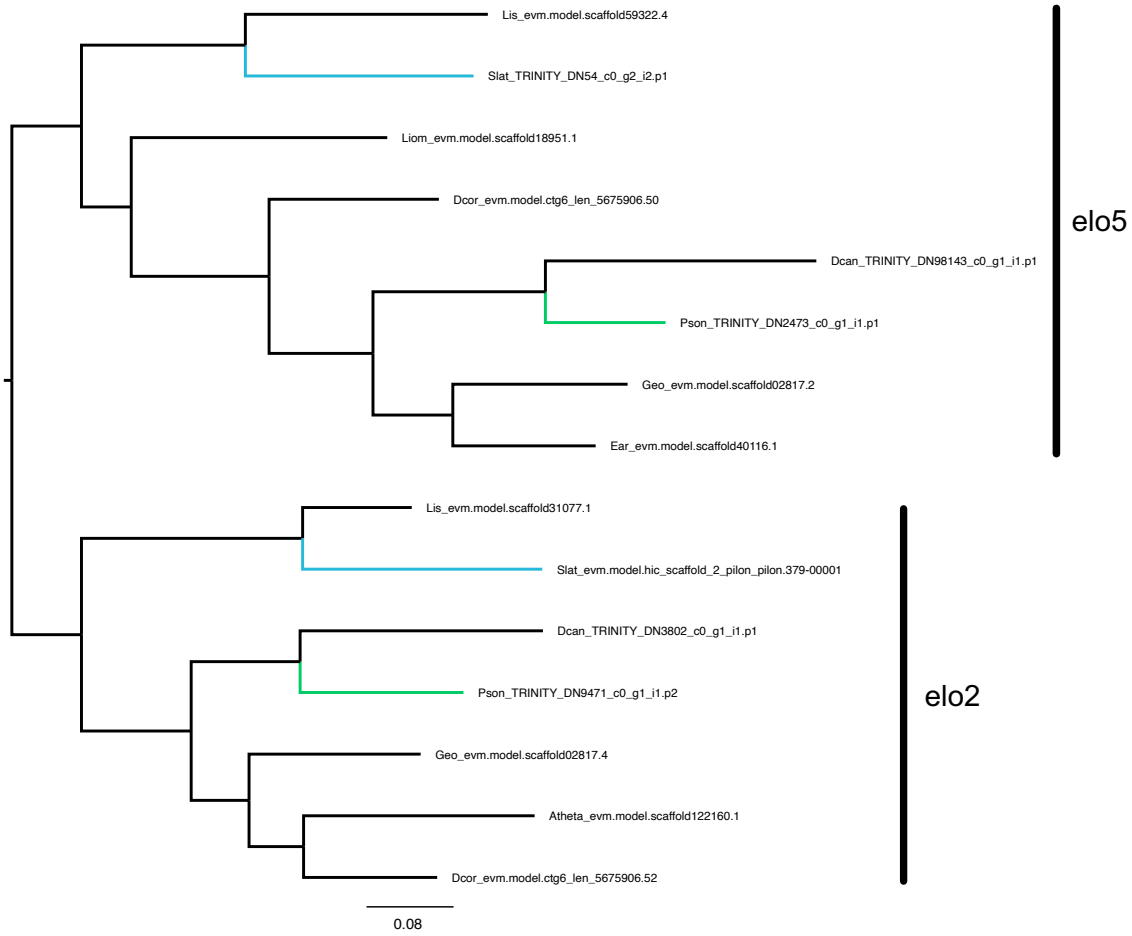

Figure 68. elongase 2 (*elo2*) and elongase 5 (*elo5*) gene tree

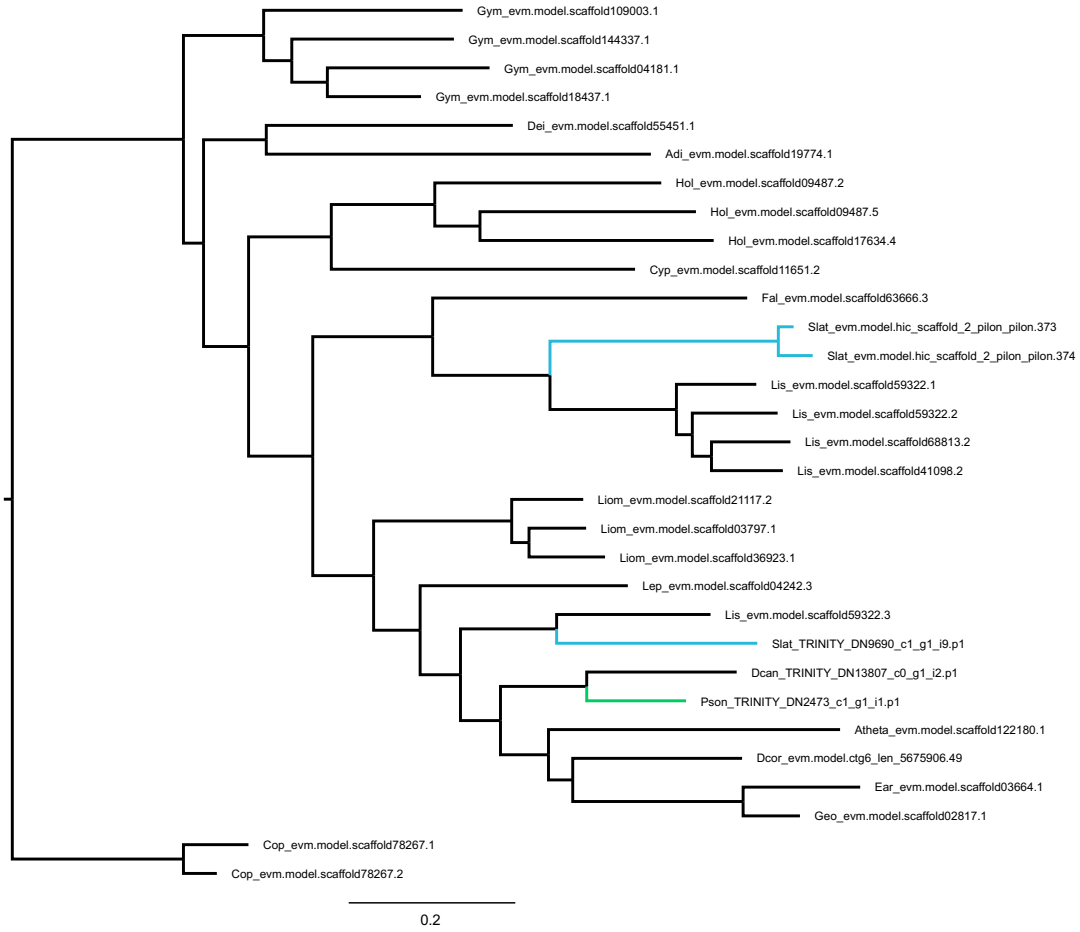

Figure 69. elongase 3 (*elo3*) gene tree

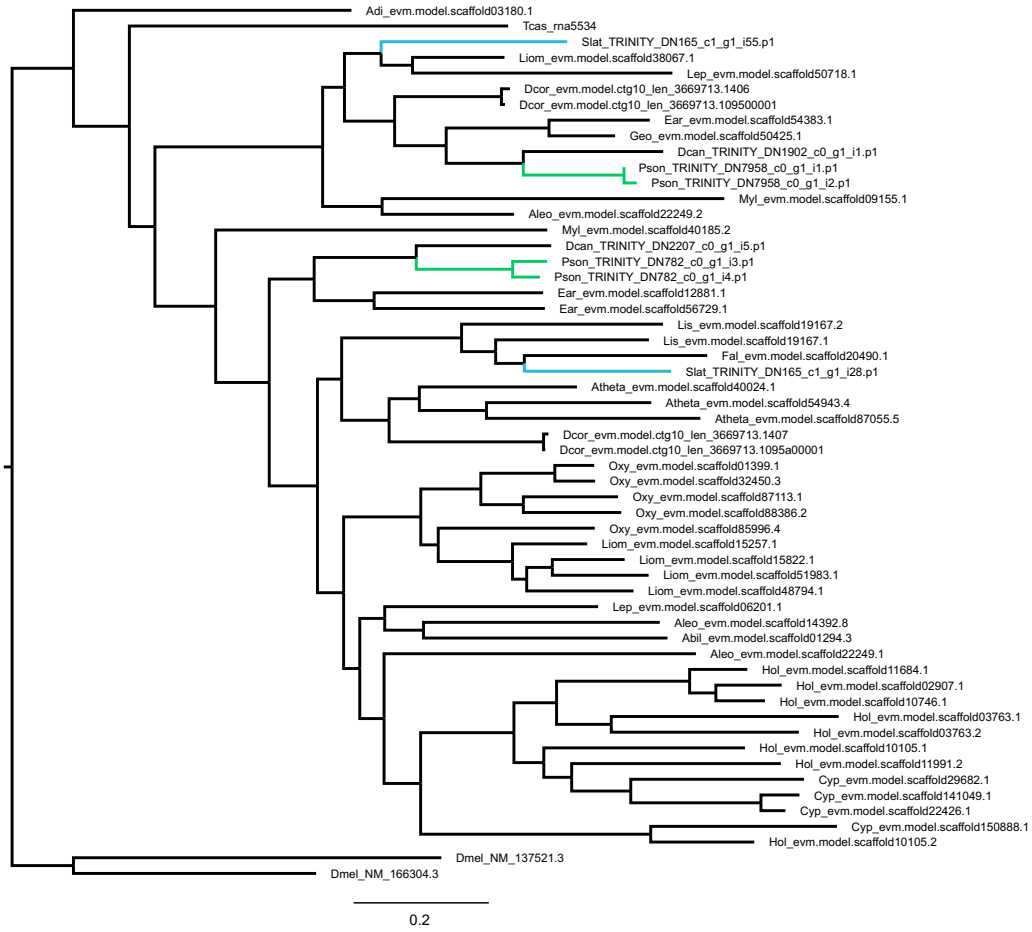

Figure 70. elongase 4 (*elo4*) gene tree

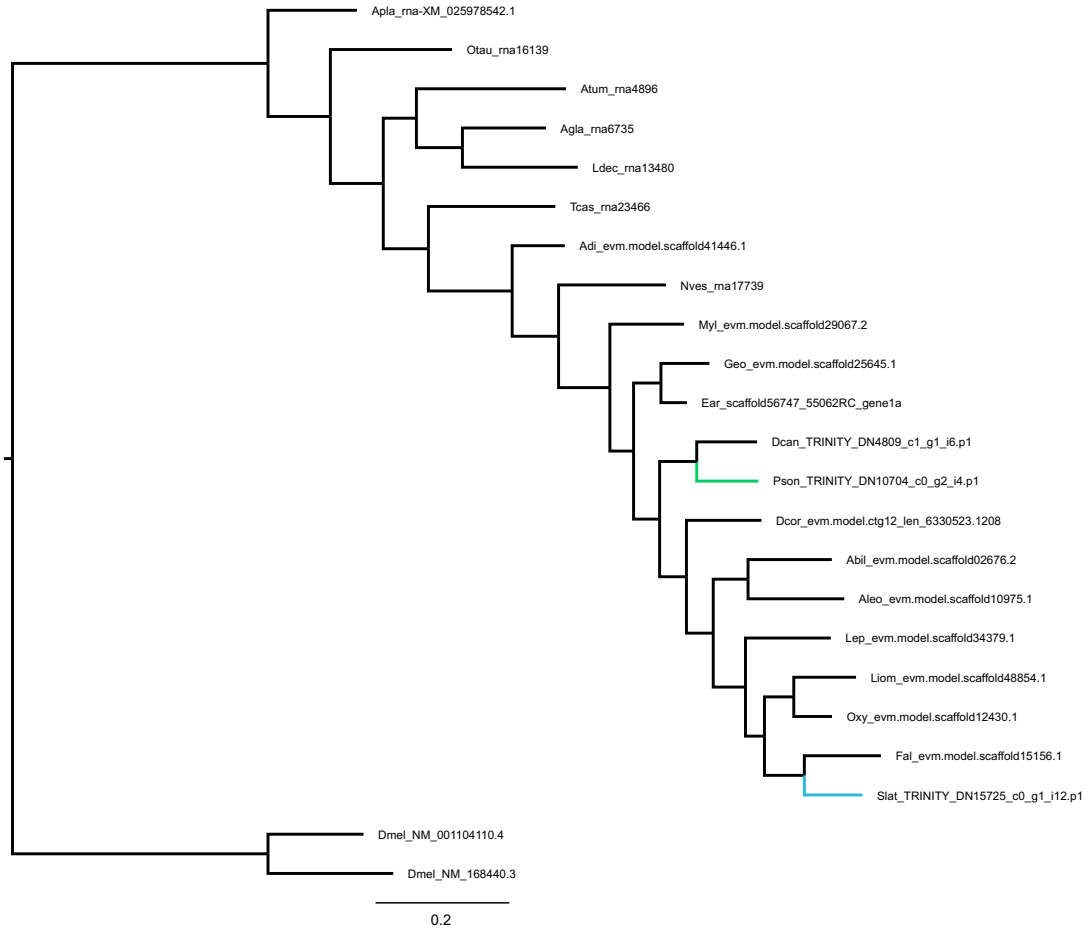

Figure 71. elongase 6 (*elo6*) gene tree

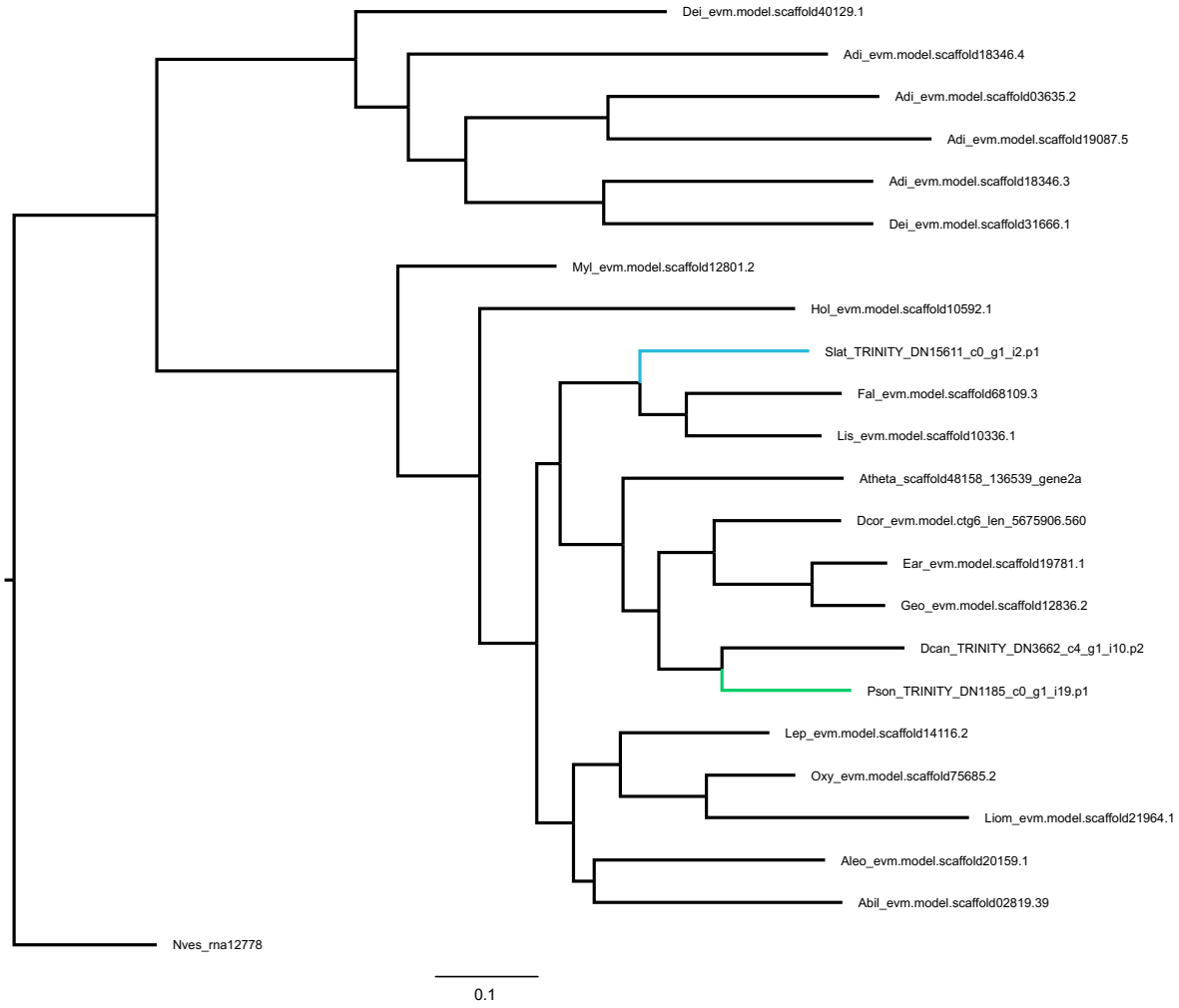

Figure 72. elongase 7 (*elo7*) gene tree

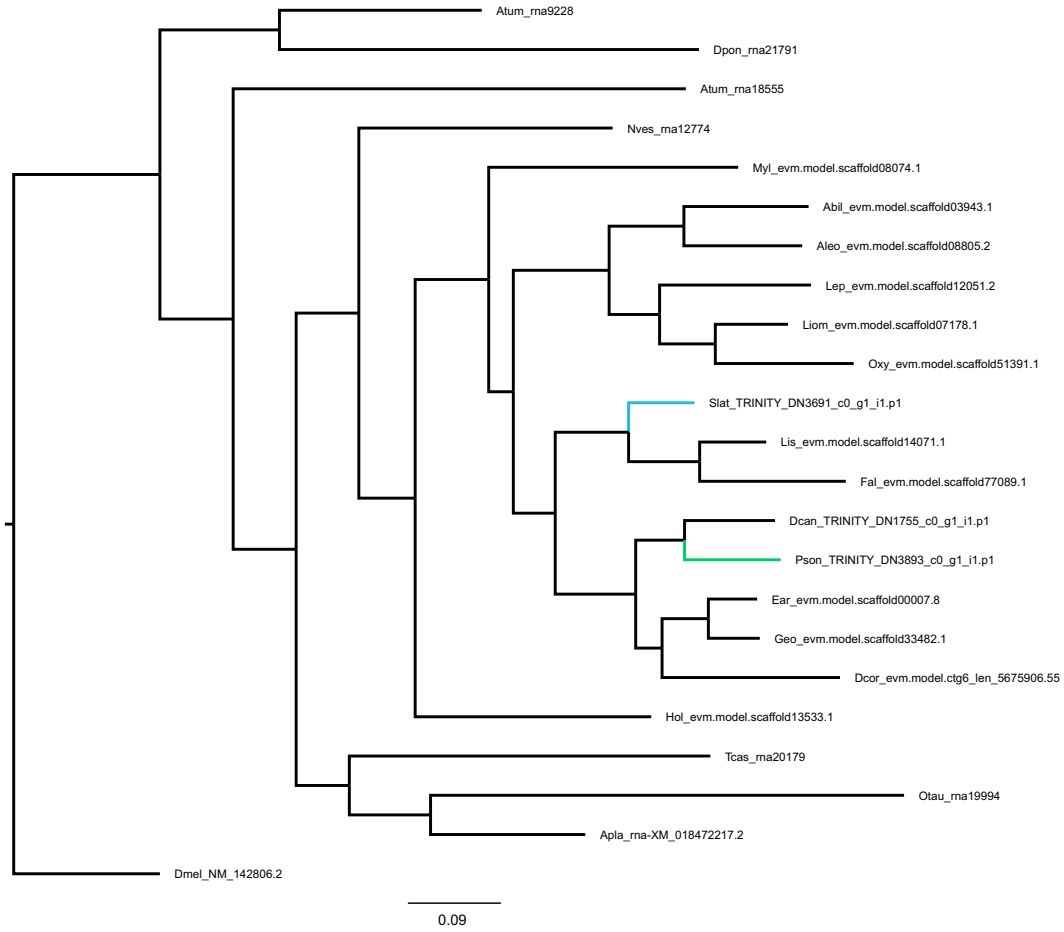

Figure 73. elongase 8 (*elo8*) gene tree

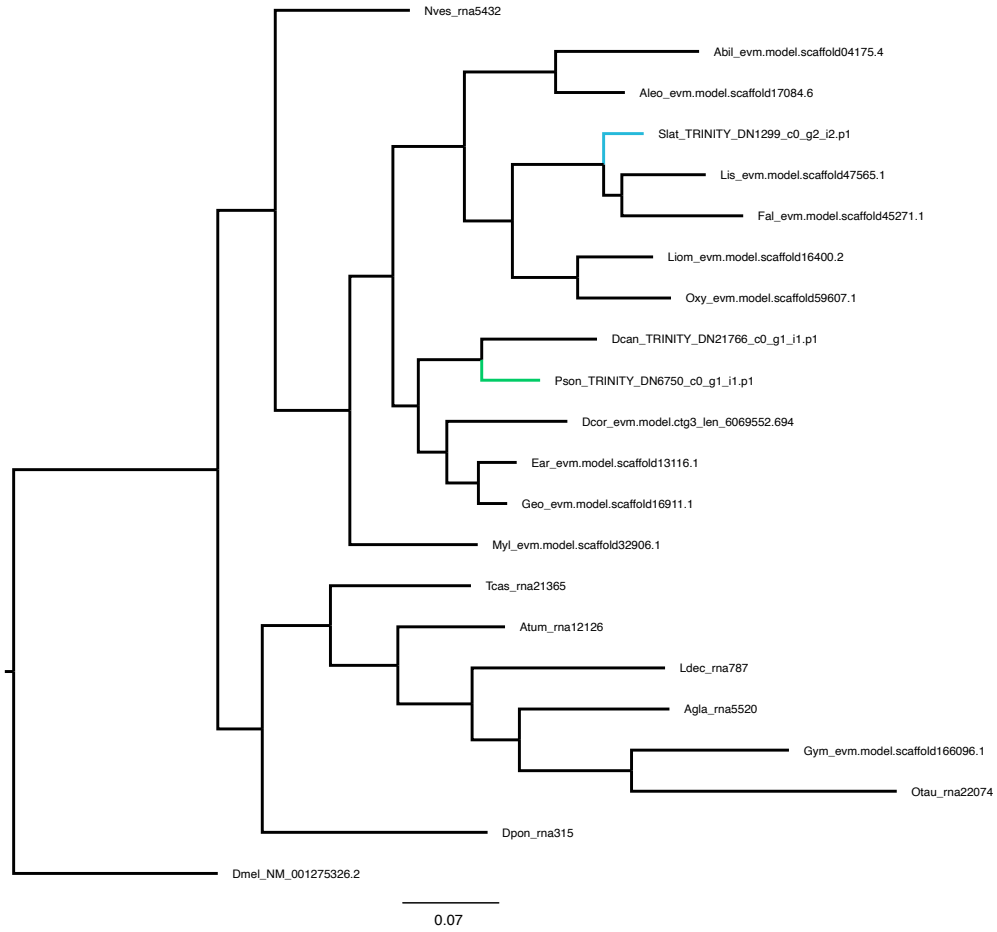

Figure 74. elongase 9 (*elo9*) gene tree

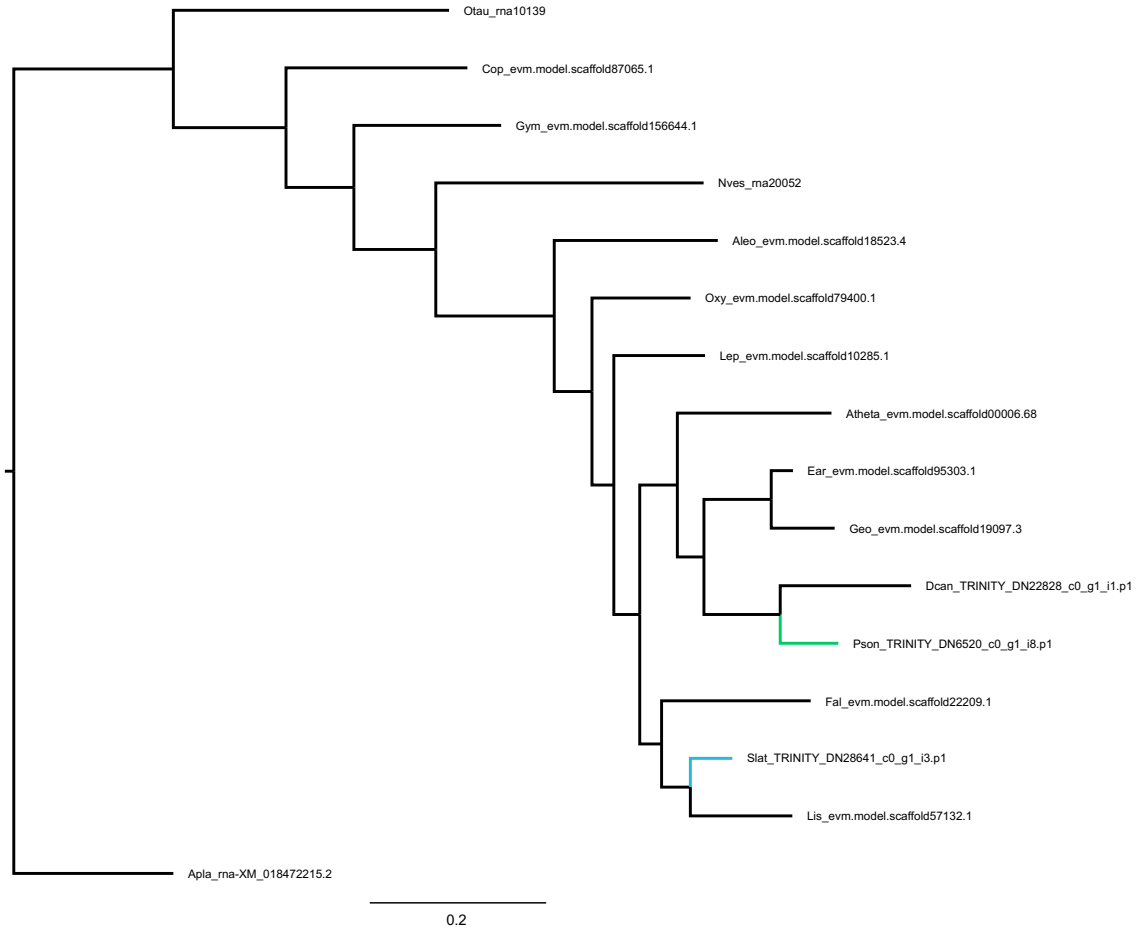

Figure 75. elongase 10 (*elo10*) gene tree

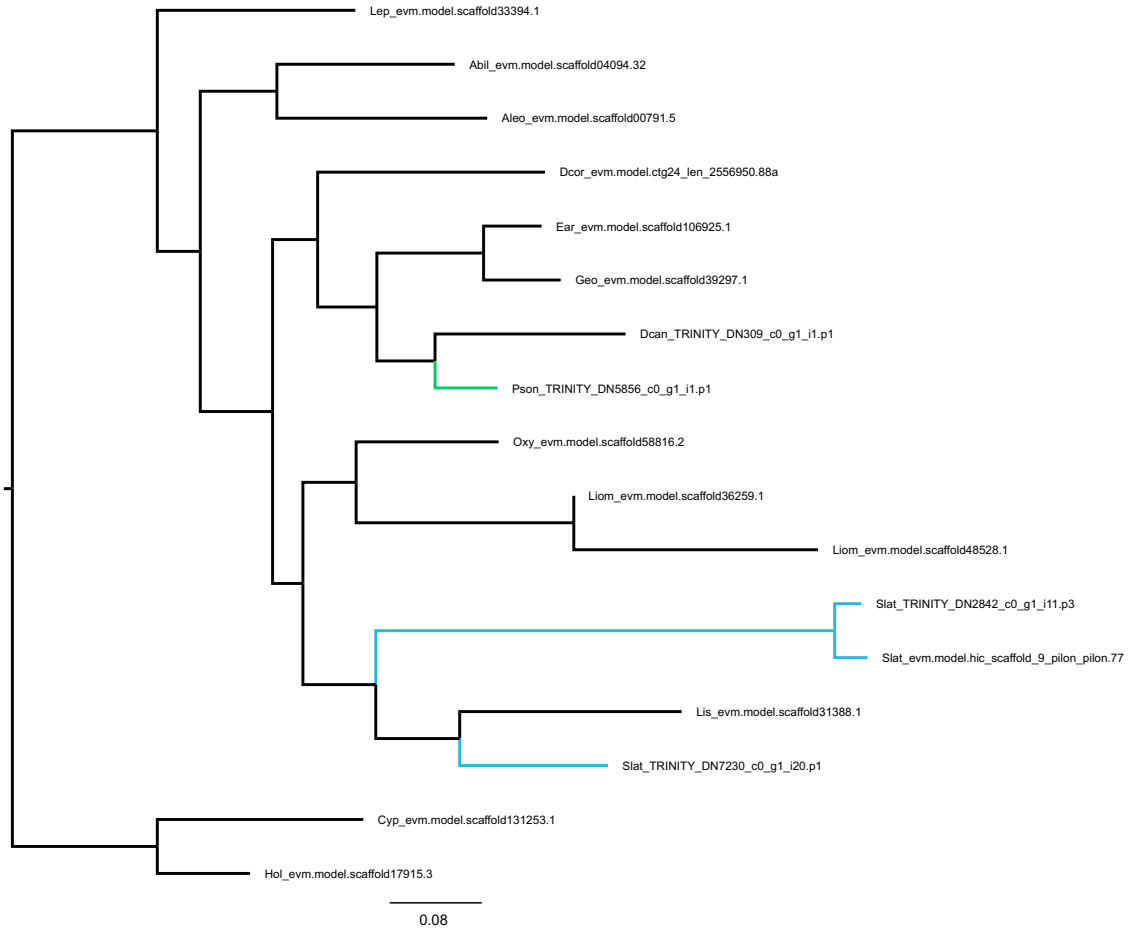

Figure 76. elongase 12 (*elo12*) gene tree

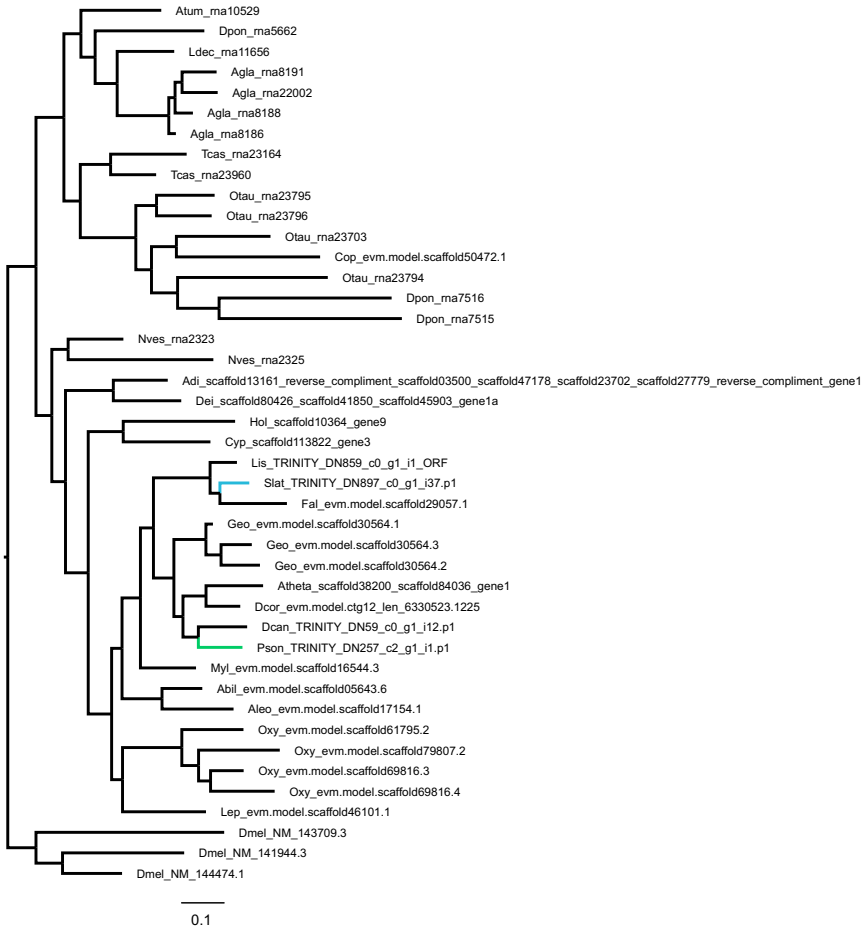

Figure 77. desaturase 1 (*desat1*) gene tree

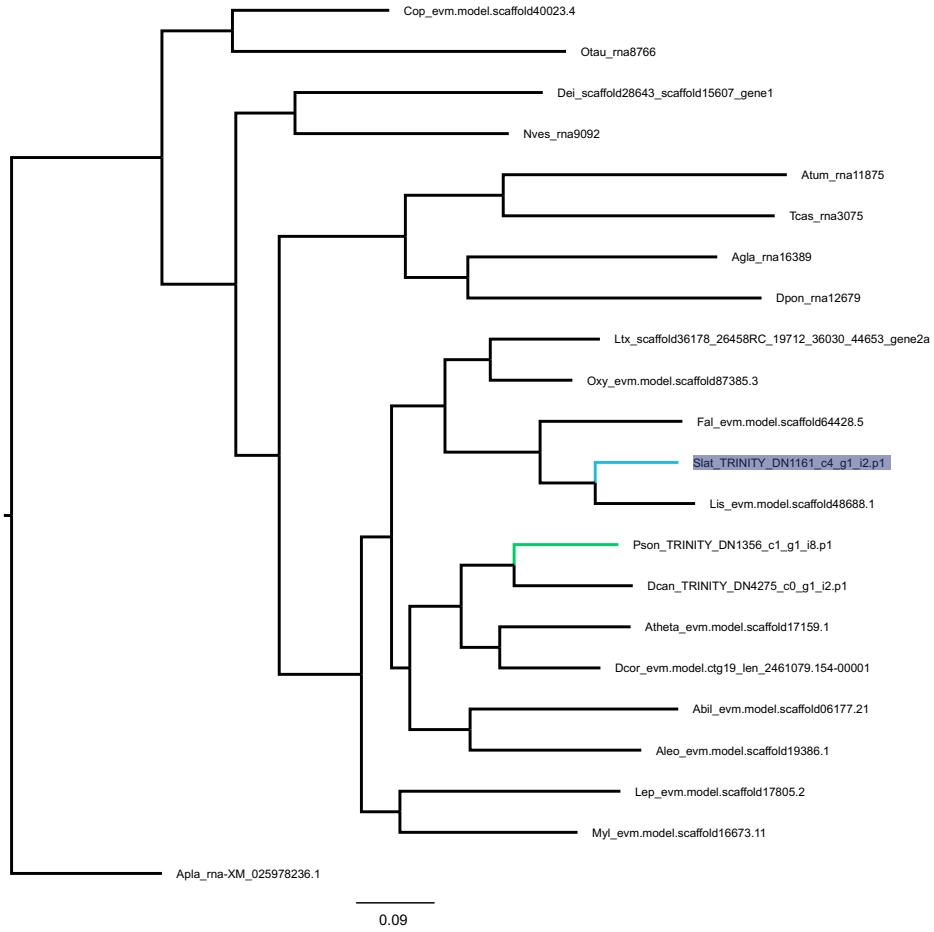

Figure 78. desaturase 2 (*desat2*) gene tree

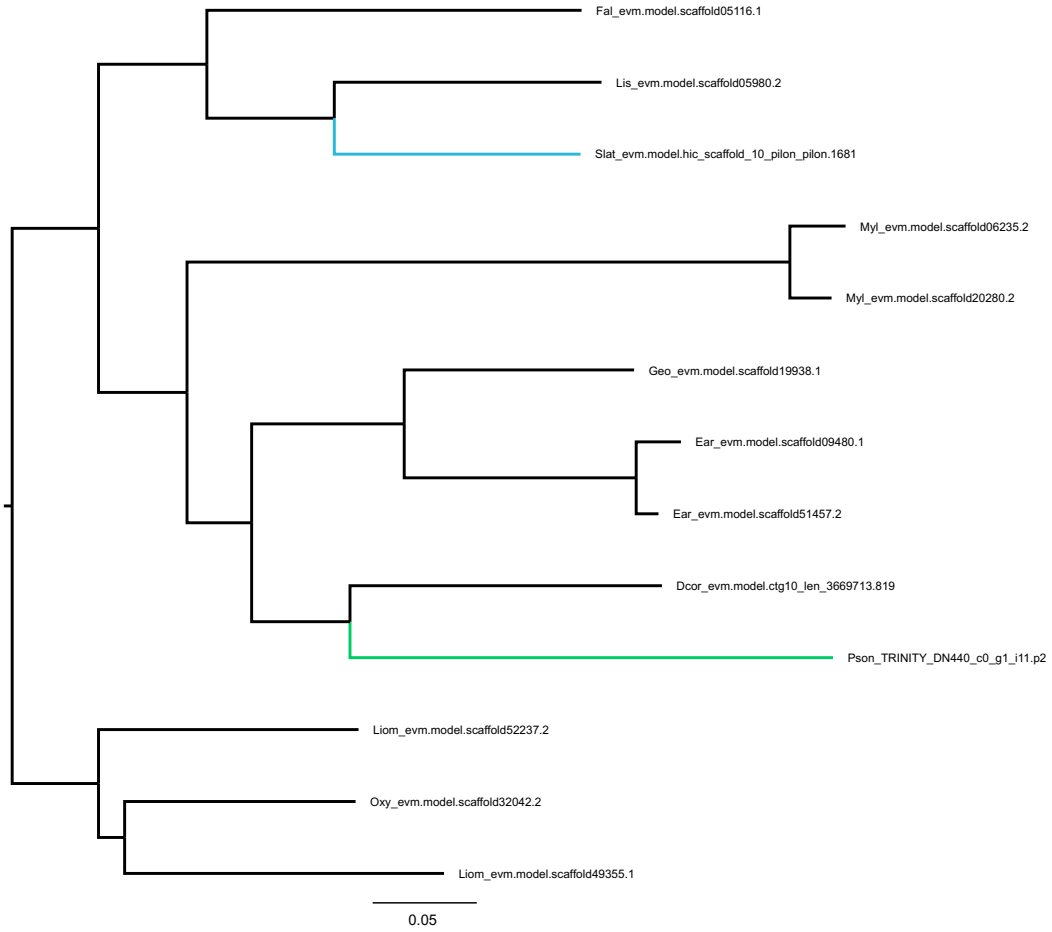

Figure 79. desaturase 3 (*desat3*) gene tree

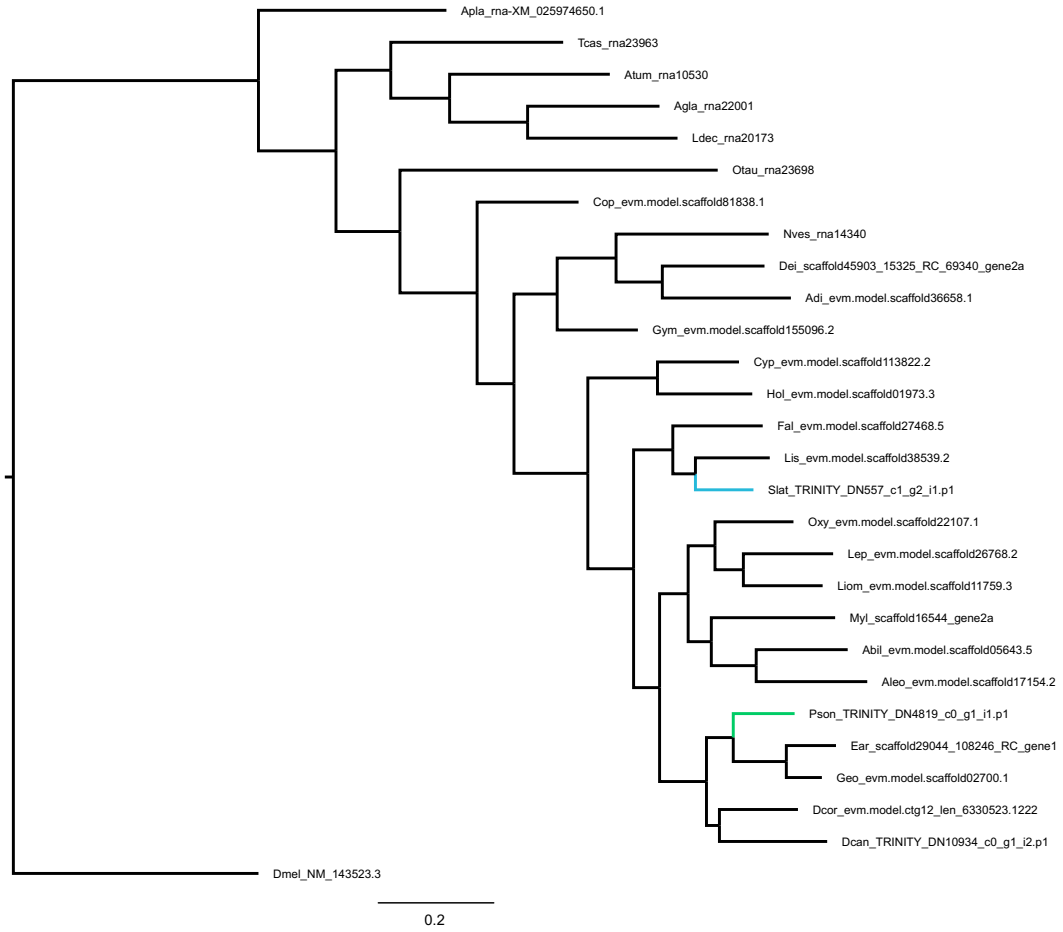

Figure 80. desaturase 4 (*desat4*) gene tree

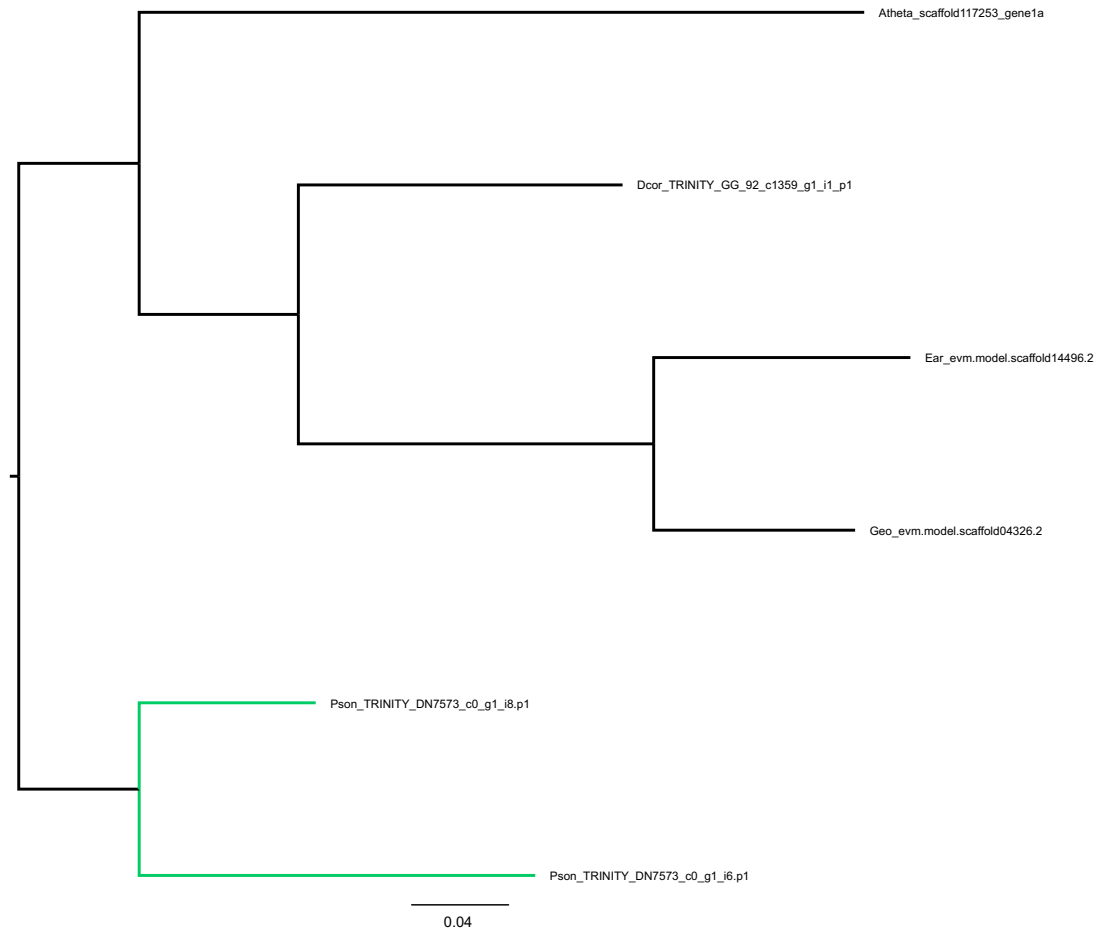

Figure 81. desaturase 5 (*desat5*) gene tree

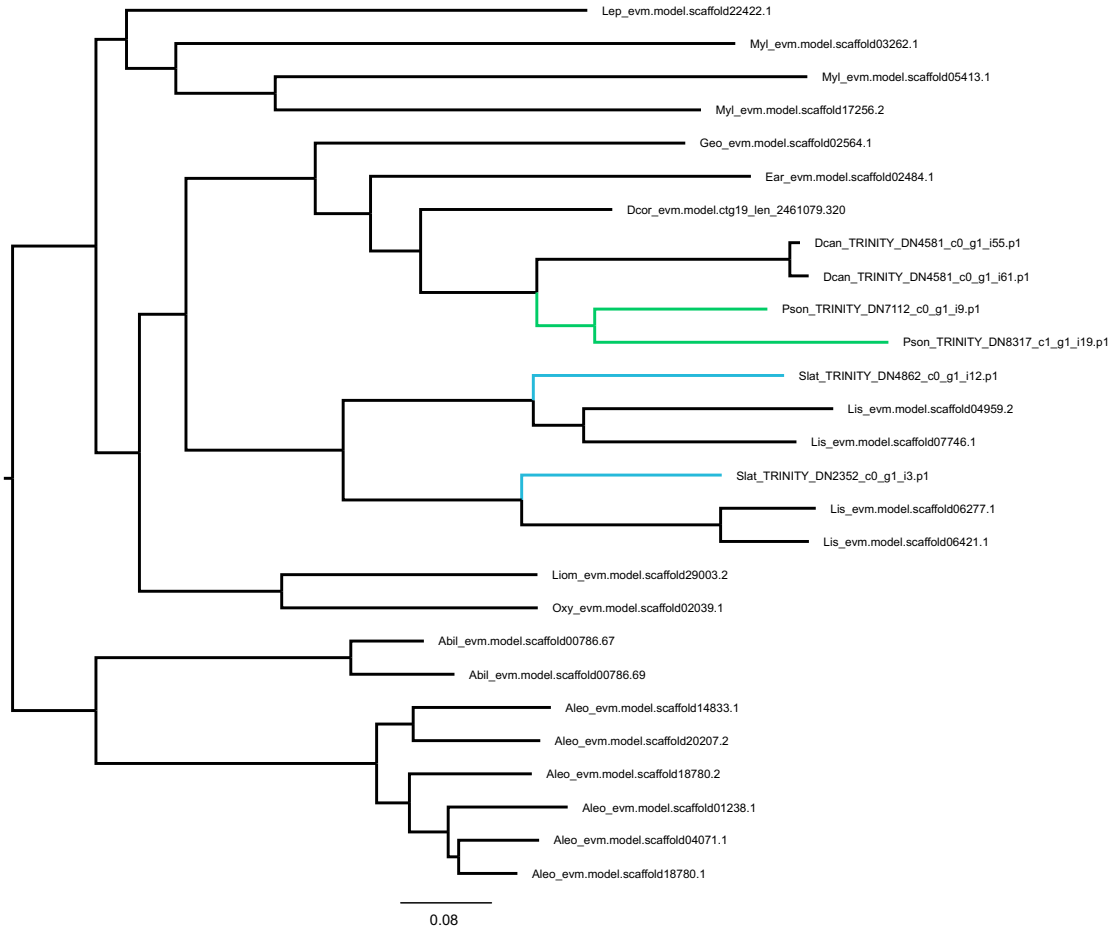

Figure 82. Fatty acyl-coA reductase 1 (*FAR1*) gene tree

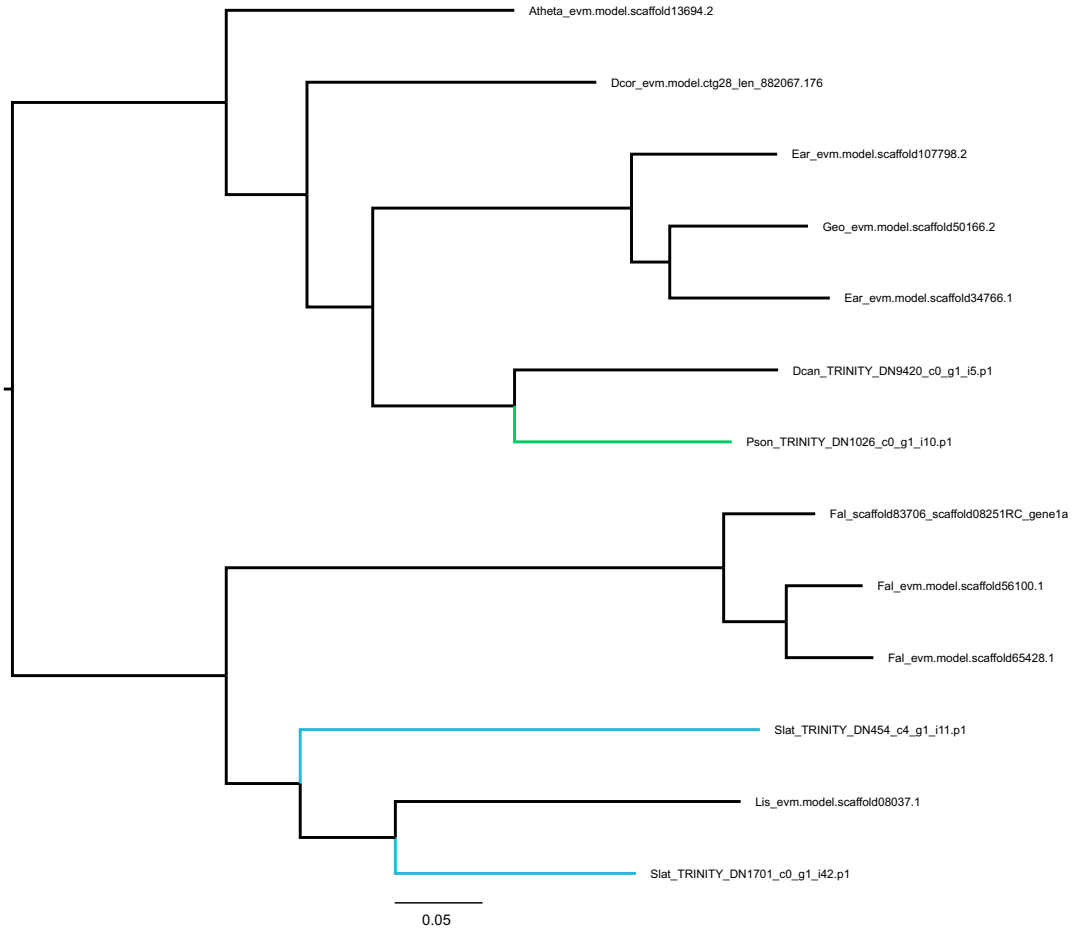

Figure 83. Fatty acyl-coA reductase 2 (*FAR2*) gene tree

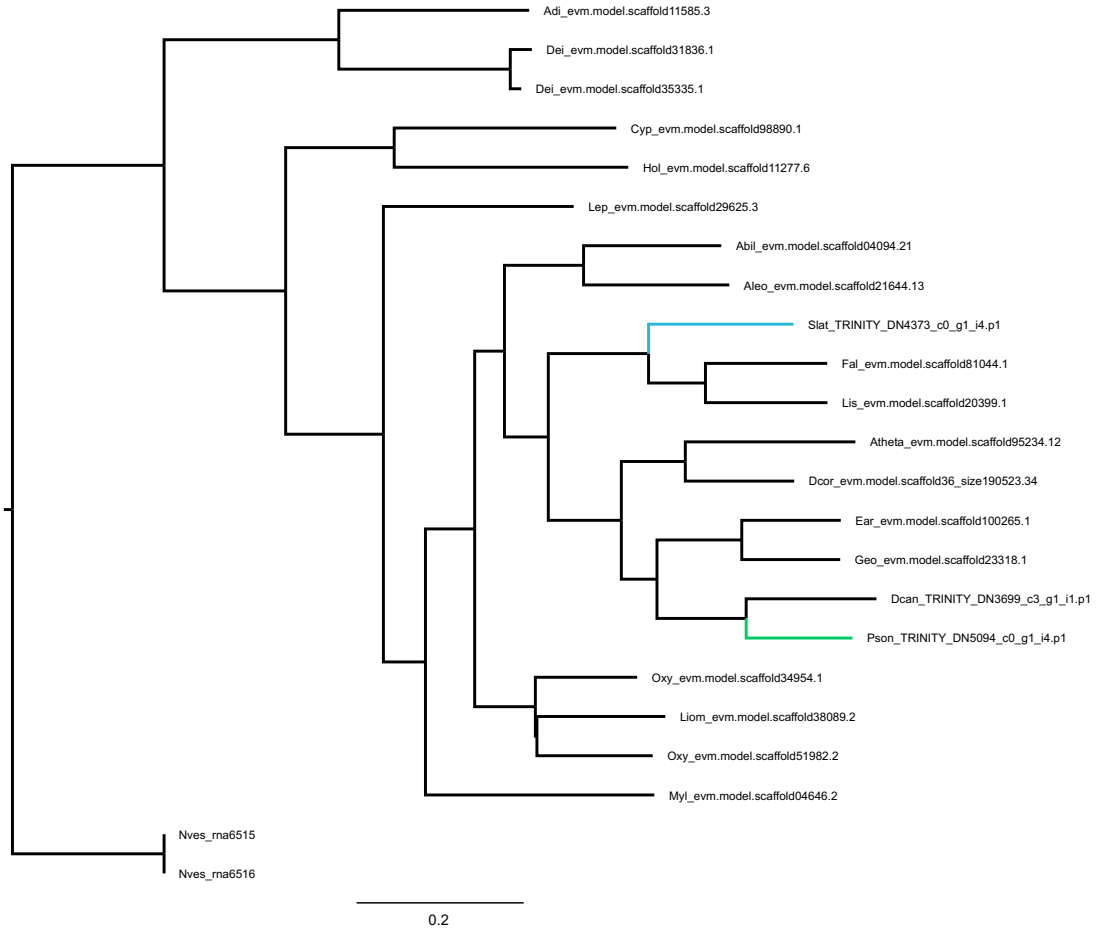

Figure 84. Fatty acyl-coA reductase 3 (*FAR3*) gene tree

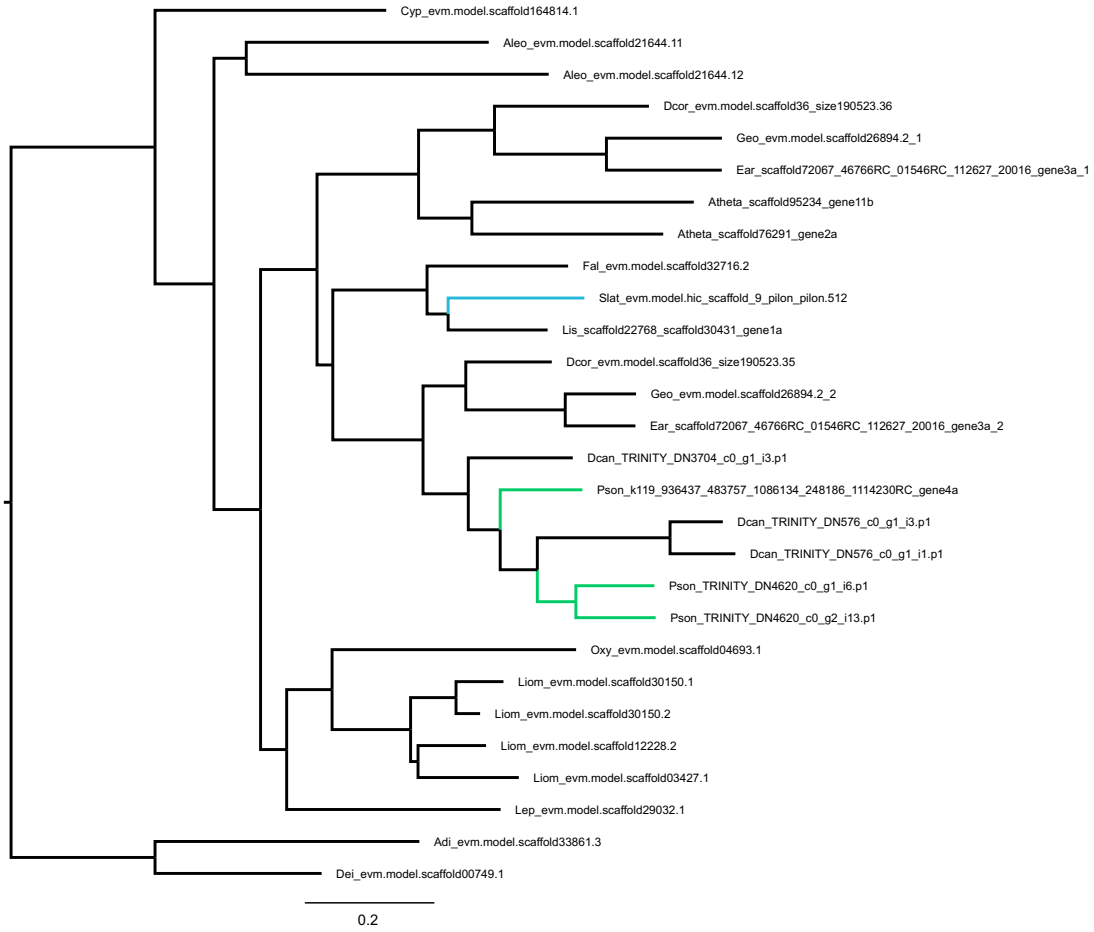

Figure 85. Fatty acyl-coA reductase 4 (*FAR4*) gene tree

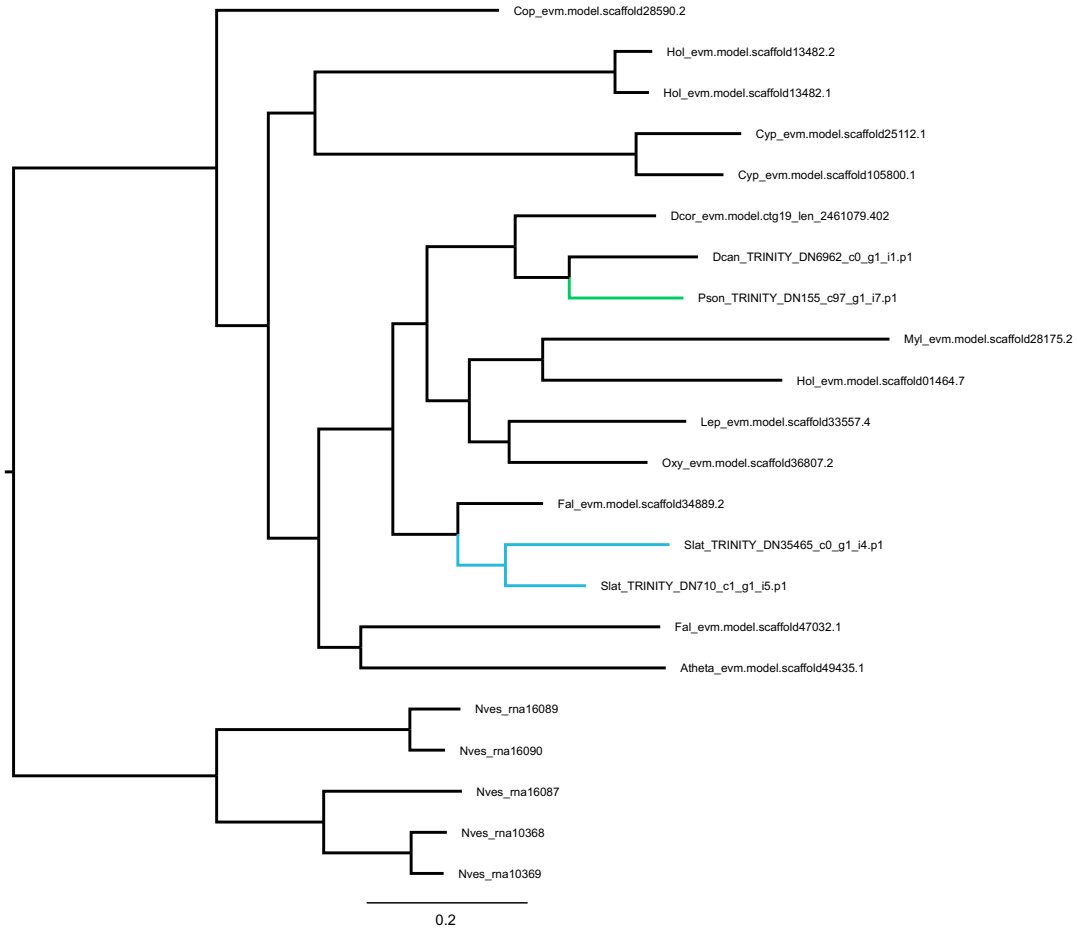

Figure 86. Fatty acyl-coA reductase 5 (*FAR5*) gene tree

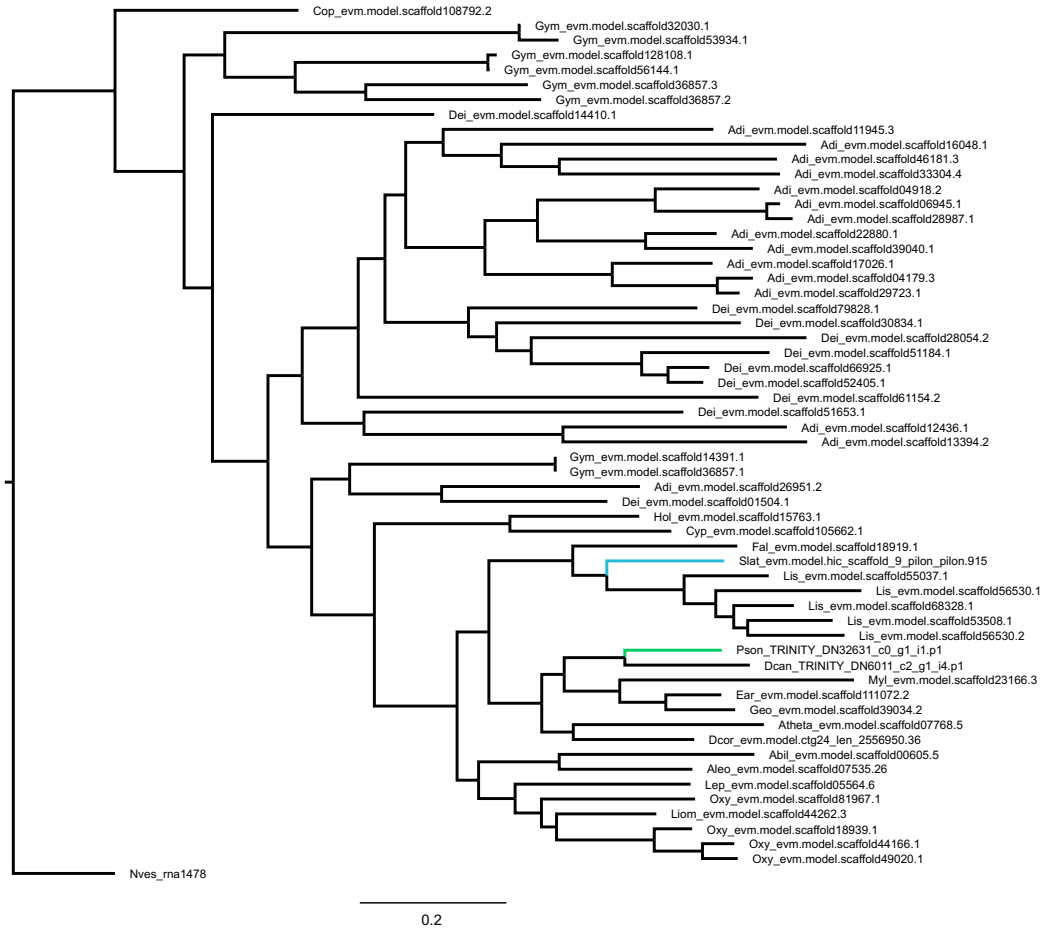

Figure 87. Fatty acyl-coA reductase 6 (*FAR6*) gene tree

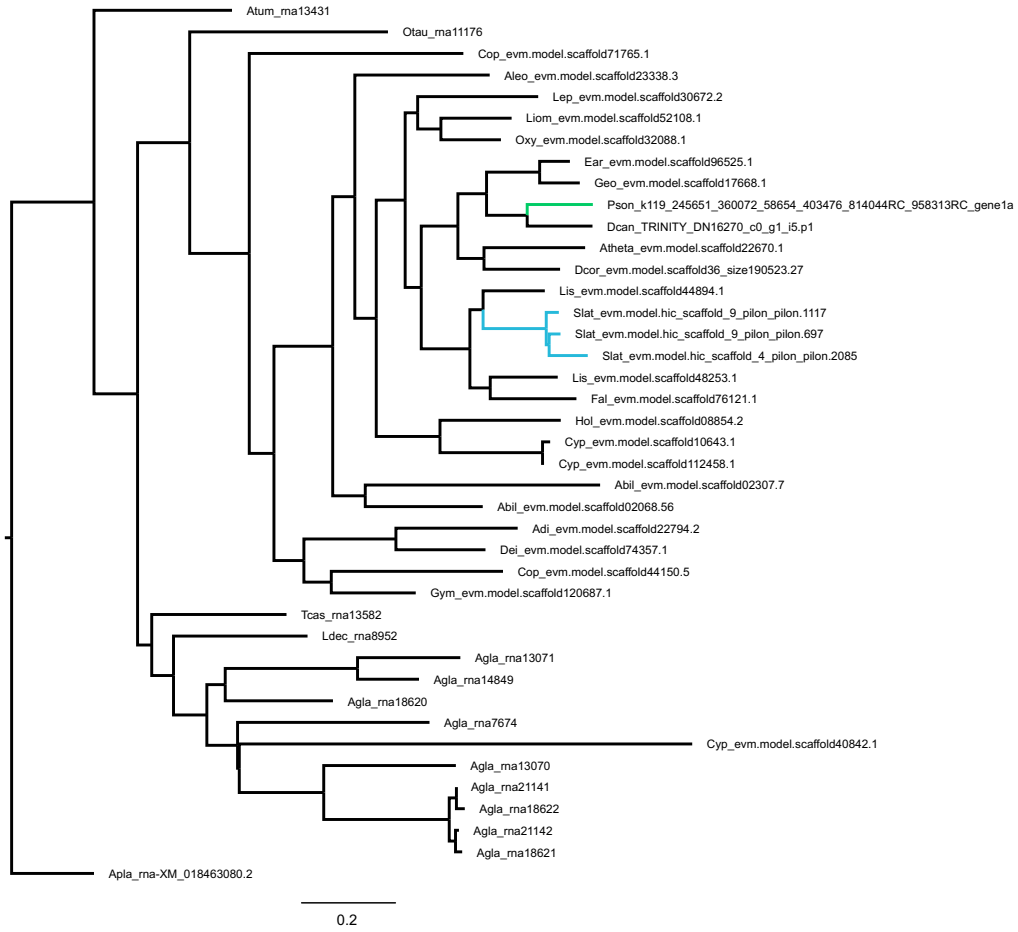

Figure 88. Fatty acyl-coA reductase 7 (*FAR7*) gene tree

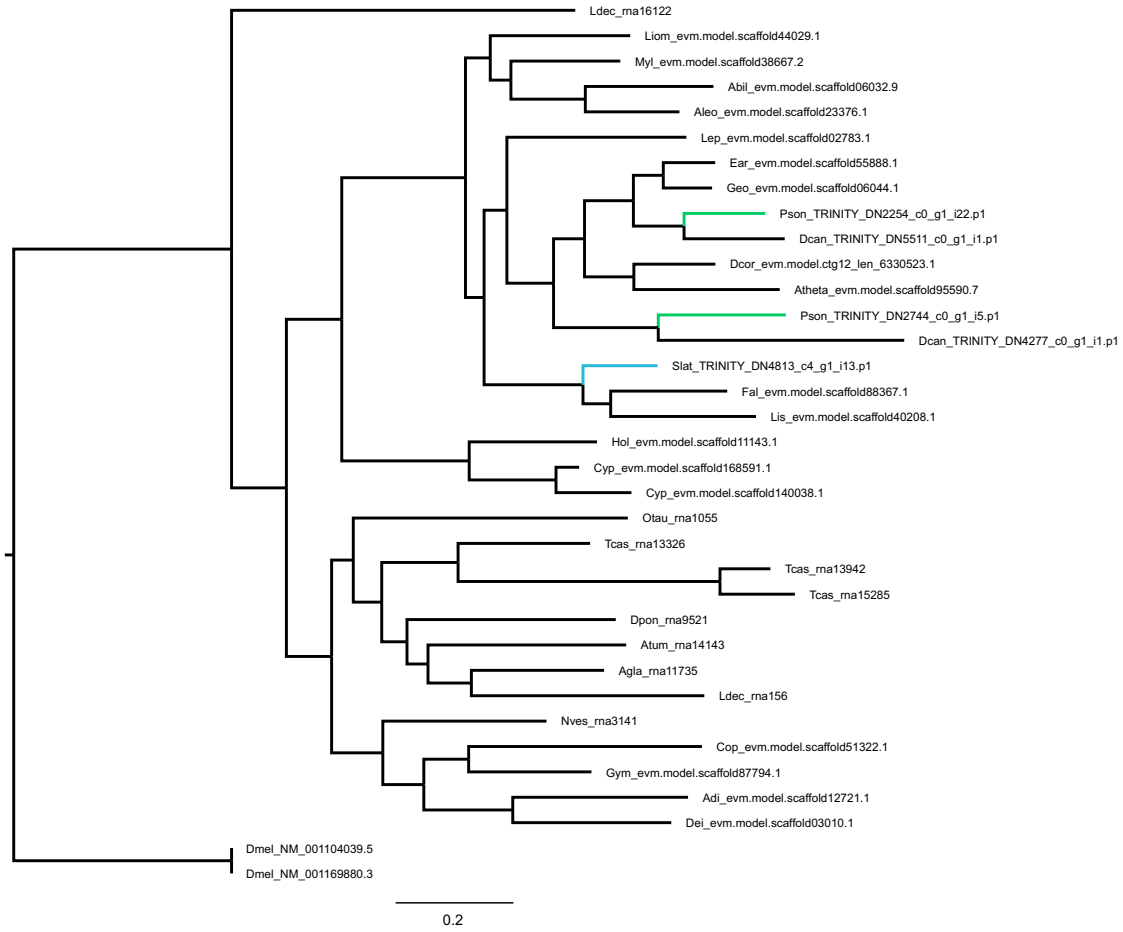

Figure 89. Fatty acyl-coA reductase 8 (*FAR8*) gene tree

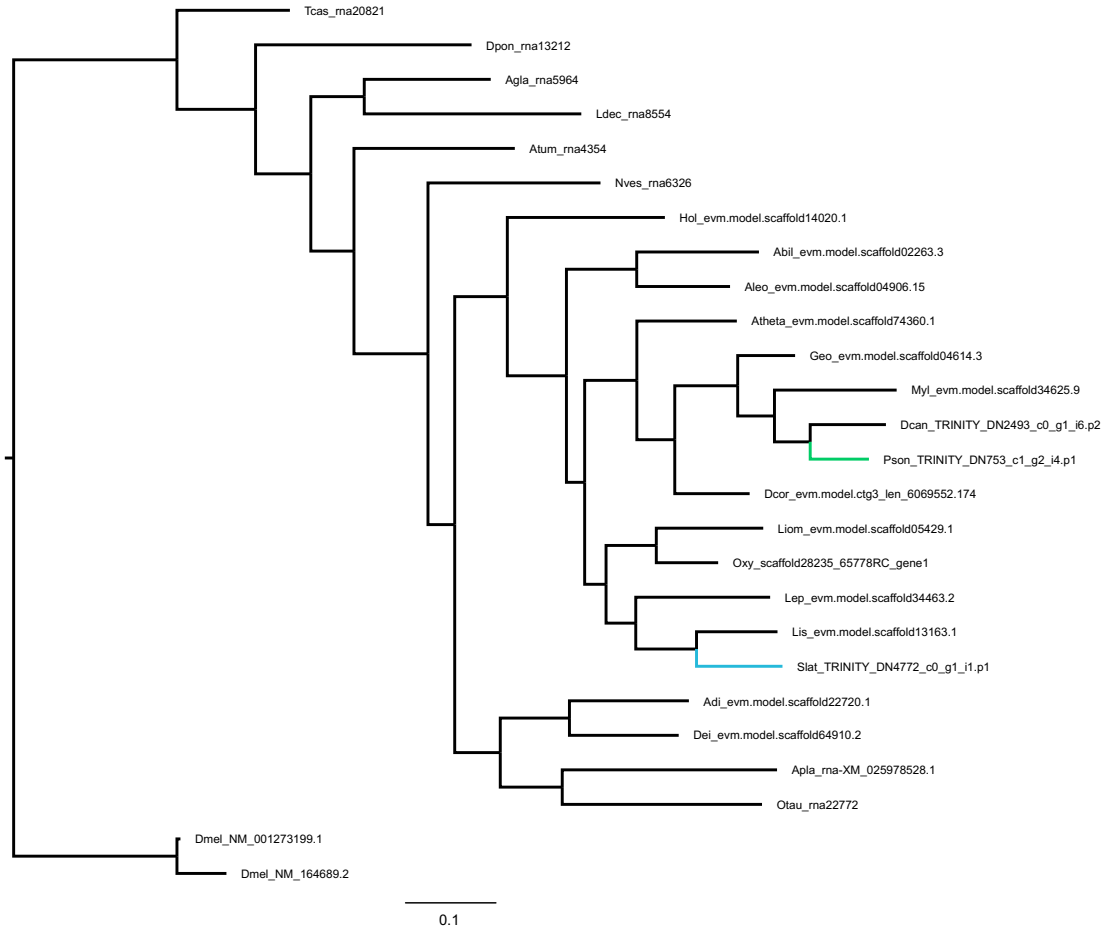

Figure 90. NADPH Cytochrome P450 Reductase (*CPR*) gene tree

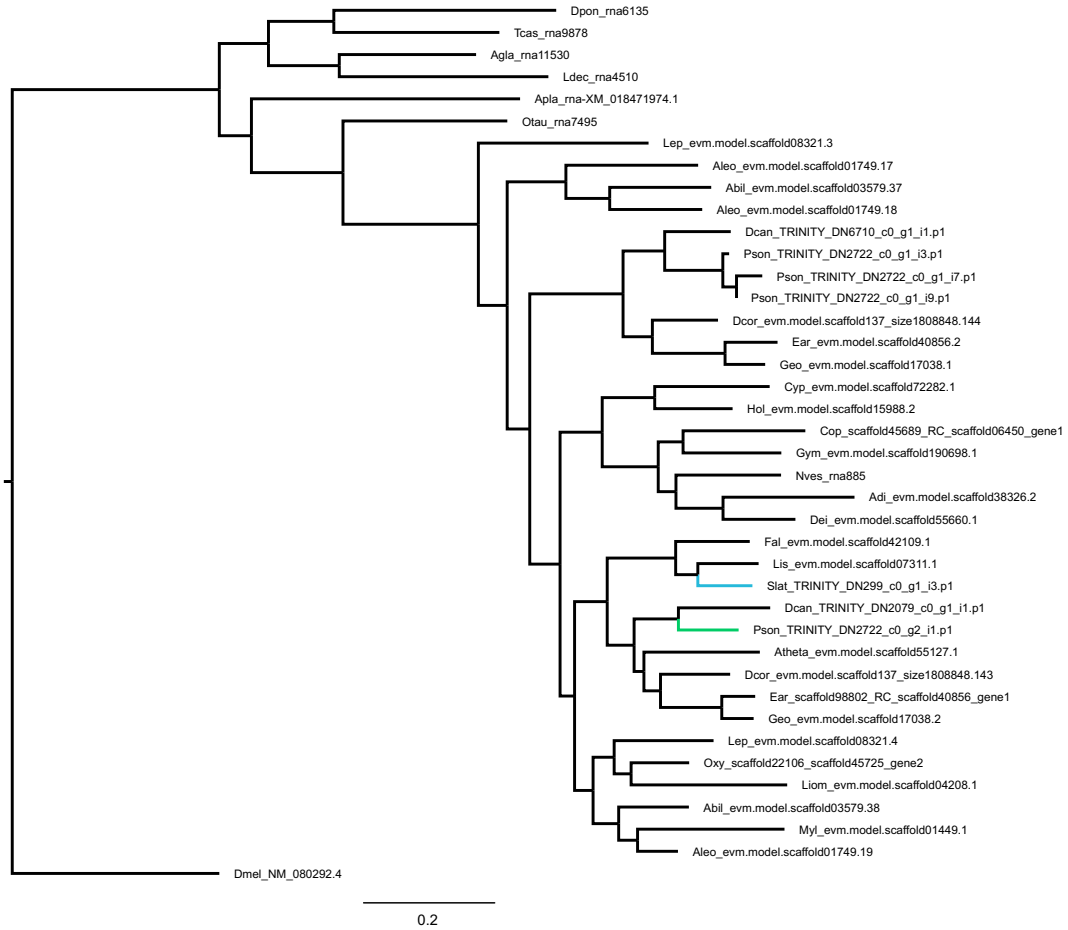

Figure 91. Cytochrome P450 4G1 (*CYP4G1*) gene tree

BIBLIOGRAPHY

1. Del Toro, I., Pacheco, J. & Mackay, W. Revision of the Ant Genus Liometopum (Hymenoptera: Formicidae). *Sociobiology* **53**, 299–370 (2009).
2. Gulmahamad, H. The Genus *Liometopum* Mayr (Hymenoptera: Formicidae) in California, with Notes on Nest Architechture and Structural Importance. *Pan-Pac. Entomol.* **71**, 82–86 (1995).
3. Ward, P. S. A synoptic review of the ants of California (Hymenoptera: Formicidae). *Zootaxa* **936**, 1–68 (2005).
4. Wheeler, W. M. The North American Ants of the Genus *Liometopum*. *Bull. Am. Mus. Nat. Hist.* **21**, 321–333 (1905).
5. Wheeler, G. C. & Wheeler, J. N. *The Ants of Nevada*. (Los Angeles : Natural History Museum of Los Angeles County, 1986).
6. Wang, T. B., Patel, A., Vu, F. & Nonacs, P. Natural History Observations on the Velvety Tree Ant (*Liometopum occidentale*): Unicoloniality and Mating Flights. *Sociobiology* **55**, 787–794 (2010).
7. Van Wilgenburg, E., Torres, C. W. & Tsutsui, N. D. The global expansion of a single ant supercolony. *Evol. Appl.* **3**, 136–143 (2010).
8. Giraud, T., Pedersen, J. S. & Keller, L. Evolution of supercolonies: The Argentine ants of southern Europe. *Proc. Natl. Acad. Sci.* **99**, 6075–6079 (2002).
9. Vogel, V., Pedersen, J. S., Giraud, T., Krieger, M. J. B. & Keller, L. The worldwide expansion of the Argentine ant. *Divers. Distrib.* **16**, 170–186 (2010).
10. Björkman-Chiswell, B. T., Van Wilgenburg, E., Thomas, M. L., Swearer, S. E. & Elgar, M. A. Absence of aggression but not nestmate recognition in an Australian population of the Argentine ant Linepithema humile. *Insectes Sociaux* **55**, 207–212 (2008).
11. Thomas, M. L., Payne-Makrisâ, C. M., Suarez, A. V., Tsutsui, N. D. & Holway, D. A. Contact between supercolonies elevates aggression in Argentine ants. *Insectes Sociaux* **54**, 225–233 (2007).
12. Shapley, H. Thermokinetics of Liometopum Apiculatum Mayr. *Proc. Natl. Acad. Sci. U. S. A.* **6**, 204–211 (1920).
13. Stoeffler, M., Maier, T. S., Tolasch, T. & Steidle, J. L. M. Foreign-language Skills in Rove-Beetles? Evidence for Chemical Mimicry of Ant Alarm Pheromones in Myrmecophilous Pella Beetles (Coleoptera: Staphylinidae). *J. Chem. Ecol.* **33**, 1382–1392 (2007).
14. Wells, R. L., Frost, C. J. & Yanoviak, S. P. Effects of Azteca trigona alarm pheromones on heterospecific ant behavior. *Insectes Sociaux* **68**, 359–365 (2021).
15. Morgan, E. D. Chemical sorcery for sociality: Exocrine secretions of ants (Hymenoptera: Formicidae). *Myrmecol. News* **11**, 79–90 (2008).

16. Choe, D.-H., Villafuerte, D. B. & Tsutsui, N. D. Trail Pheromone of the Argentine Ant, Linepithema humile (Mayr) (Hymenoptera: Formicidae). *PLOS ONE* **7**, e45016 (2012).
17. Simon, T. & Hefetz, A. Trail-following responses of Tapinoma simrothi (Formicidae: Dolichoderinae) to pygidial gland extracts. *Insectes Sociaux* **38**, 17–25 (1991).
18. Wagner, J. M. *et al.* Enforced specificity of an animal symbiosis. 2024.08.04.606548 Preprint at https://doi.org/10.1101/2024.08.04.606548 (2024).
19. Lockey, K. H. Lipids of the insect cuticle: origin, composition and function. *Comp. Biochem. Physiol. Part B Comp. Biochem.* **89**, 595–645 (1988).
20. Drijfhout, F. P., Kather, R. & Martin, S. The role of cuticular hydrocarbons in insects. in *Behavioral and Chemical Ecology* 91–114 (2010).
21. Menzel, F. *et al.* Communication vs. waterproofing: the physics of insect cuticular hydrocarbons. *J. Exp. Biol.* jeb.210807 (2019) doi:10.1242/jeb.210807.
22. Gibbs, A. & Pomonis, J. G. Physical properties of insect cuticular hydrocarbons: The effects of chain length, methyl-branching and unsaturation. *Comp. Biochem. Physiol. B Biochem. Mol. Biol.* **112**, 243–249 (1995).
23. O'Donnell, M. J. A perspective on insect water balance. *J. Exp. Biol.* **225**, jeb242358 (2022).
24. Chown, S. L. Respiratory water loss in insects. *Comp. Biochem. Physiol. A. Mol. Integr. Physiol.* **133**, 791–804 (2002).
25. Hadley, N. F. & Quinlan, M. C. Discontinuous Carbon Dioxide Release in the Eastern Lubber Grasshopper *Romalea Guttata* and its Effect on Respiratory Transpiration. *J. Exp. Biol.* **177**, 169–180 (1993).
26. Dembeck, L. M. *et al.* Genetic architecture of natural variation in cuticular hydrocarbon composition in Drosophila melanogaster. *eLife* **4**, e09861 (2015).
27. Martin, S. & Drijfhout, F. A Review of Ant Cuticular Hydrocarbons. *J. Chem. Ecol.* **35**, 1151–1161 (2009).
28. Xu, M. *et al.* Cuticular hydrocarbon chemistry, an important factor shaping the current distribution pattern of the imported fire ants in the USA. *J. Insect Physiol.* **110**, 34–43 (2018).
29. Rourke, B. C. & Gibbs, A. G. Effects of lipid phase transitions on cuticular permeability: model membrane and *in situ studies*. *J. Exp. Biol.* **202**, 3255–3262 (1999).
30. Menzel, F., Schmitt, T. & Blaimer, B. B. The evolution of a complex trait: cuticular hydrocarbons in ants evolve independent from phylogenetic constraints. *J. Evol. Biol.* **30**, 1372–1385 (2017).
31. Menzel, F., Blaimer, B. B. & Schmitt, T. How do cuticular hydrocarbons evolve? Physiological constraints and climatic and biotic selection pressures act on a complex functional trait. *Proc. R. Soc. B Biol. Sci.* **284**, 20161727 (2017).
32. Drechsler, P. & Federle, W. Biomechanics of smooth adhesive pads in insects: influence of tarsal secretion on attachment performance. *J. Comp. Physiol. A* **192**, 1213–1222 (2006).

33. Bontonou, G. & Wicker-Thomas, C. Sexual Communication in the Drosophila Genus. *Insects* **5**, 439–458 (2014).
34. Thomas, M. L. & Simmons, L. W. Sexual dimorphism in cuticular hydrocarbons of the Australian field cricket *Teleogryllus oceanicus* (Orthoptera: Gryllidae). *J. Insect Physiol.* **54**, 1081–1089 (2008).
35. Gordon, J. M., Šobotník, J. & Chouvenc, T. Colony-age-dependent variation in cuticular hydrocarbon profiles in subterranean termite colonies. *Ecol. Evol.* **10**, 10095–10104 (2020).
36. Lorenzi, M. C., Sledge, M. F., Laiolo, P., Sturlini, E. & Turillazzi, S. Cuticular hydrocarbon dynamics in young adult *Polistes dominulus* (Hymenoptera: Vespidae) and the role of linear hydrocarbons in nestmate recognition systems. *J. Insect Physiol.* **50**, 935–941 (2004).
37. Sprenger, P. P. & Menzel, F. 1 Cuticular hydrocarbons in ants (Hymenoptera: Formicidae) and other insects: how and why they differ among individuals, colonies, and species. *Myrmecol. News* **30**, (2020).
38. Vernier, C. L. *et al.* The cuticular hydrocarbon profiles of honey bee workers develop via a socially-modulated innate process. *eLife* **8**, e41855 (2019).
39. Sprenger, P. P. & Menzel, F. Cuticular hydrocarbons in ants (Hymenoptera: Formicidae) and other insects: how and why they differ among individuals, colonies, and species. *Myrmecol. News* **30**, (2020).
40. Chung, H. & Carroll, S. B. Wax, sex and the origin of species: Dual roles of insect cuticular hydrocarbons in adaptation and mating. *BioEssays* **37**, 822–830 (2015).
41. Griffiths, H. M. *et al.* Ants are the major agents of resource removal from tropical rainforests. *J. Anim. Ecol.* **87**, 293–300 (2018).
42. Hughes, D. P., Pierce, N. E. & Boomsma, J. J. Social insect symbionts: evolution in homeostatic fortresses. *Trends Ecol. Evol.* **23**, 672–677 (2008).
43. Ferguson-Gow, H., Sumner, S., Bourke, A. F. G. & Jones, K. E. Colony size predicts division of labour in attine ants. *Proc. R. Soc. B Biol. Sci.* **281**, 20141411 (2014).
44. Rettenmeyer, C. W., Rettenmeyer, M. E., Joseph, J. & Berghoff, S. M. The largest animal association centered on one species: the army ant Eciton burchellii and its more than 300 associates. *Insectes Sociaux* **58**, 281–292 (2011).
45. Lara-Juárez, P., Rivera, J. R. A., Lara, P. C. & Reyes-Agüero, J. A. Collecting (Escamoles) of *Liometopum apiculatum* (Hymenoptera, Formicidae, Dolichoderinae) in the San Luis Potosí High Plain, Mexico. *Interciencia* **43**, 763–769 (2018).
46. Porter, S. D. & Tschinkel, W. R. Fire ant polymorphism: the ergonomics of brood production. *Behav. Ecol. Sociobiol.* **16**, 323–336 (1985).
47. Hoenle, P. O. *et al.* Hunting habits die hard: Conserved prey preferences in army ants across two distant neotropical rainforests. *Ecosphere* **15**, e4812 (2024).
48. Hoenle, P. O. *et al.* Species-level predation network uncovers high prey specificity in a Neotropical army ant community. *Mol. Ecol.* **28**, 2423–2440 (2019).

49. D'Ettorre, P. & Heinze, J. Sociobiology of slave-making ants. *Acta Ethologica* **3**, 67–82 (2001).
50. Martin, S. J. & Drijfhout, F. P. How Reliable is the Analysis of Complex Cuticular Hydrocarbon Profiles by Multivariate Statistical Methods? *J. Chem. Ecol.* **35**, 375–382 (2009).
51. Parker, J. Myrmecophily in beetles (Coleoptera): evolutionary patterns and biological mechanisms. *Myrmecol. News* **22**, 65–108 (2016).
52. Parker, J. & Kronauer, D. J. C. How ants shape biodiversity. *Curr. Biol.* **31**, R1208–R1214 (2021).
53. Hölldobler, B. Communication between Ants and Their Guests. *Sci. Am.* **224**, 86–95 (1971).
54. Maruyama, M. & Parker, J. Deep-Time Convergence in Rove Beetle Symbionts of Army Ants. *Curr. Biol.* **27**, 920–926 (2017).
55. Orlov, I., Newton, A. F. & Solodovnikov, A. Phylogenetic review of the tribal system of Aleocharinae, a mega-lineage of terrestrial arthropods in need of reclassification. *J. Zool. Syst. Evol. Res.* **59**, 1903–1938 (2021).
56. Brückner, A. *et al.* Evolutionary assembly of cooperating cell types in an animal chemical defense system. *Cell* **184**, 6138-6156.e28 (2021).
57. Yamamoto, S., Maruyama, M. & Parker, J. Evidence for social parasitism of early insect societies by Cretaceous rove beetles. *Nat. Commun.* **7**, 13658 (2016).
58. Hertaeg, C., Risse, M., Vorburger, C., De Moraes, C. M. & Mescher, M. C. Aphids harbouring different endosymbionts exhibit differences in cuticular hydrocarbon profiles that can be recognized by ant mutualists. *Sci. Rep.* **11**, 1–10 (2021).
59. Vantaux, A., Dejean, A., Dor, A. & Orivel, J. Parasitism versus mutualism in the ant-garden parabiosis between Camponotus femoratus and Crematogaster levior. *Insectes Sociaux* **54**, 95–99 (2007).
60. Kistner, D. H. The Myrmecophilous Genus *Trilobitideus* (Coleoptera,Staphylinidae). *Sociobiology* **47**, 51–83 (2006).
61. Parmentier, T., Dekoninck, W. & Wenseleers, T. Arthropods Associate with their Red Wood ant Host without Matching Nestmate Recognition Cues. *J. Chem. Ecol.* **43**, 644–661 (2017).
62. von Beeren, C., Schulz, S., Hashim, R. & Witte, V. Acquisition of chemical recognition cues facilitates integration into ant societies. *BMC Ecol.* **11**, 1–13 (2011).
63. Parmentier, T., Gaju-Ricart, M., Wenseleers, T. & Molero-Baltanás, R. Chemical and behavioural strategies along the spectrum of host specificity in ant-associated silverfish. *BMC Zool.* **7**, 23 (2022).
64. von Beeren, C. *et al.* Chemical and behavioral integration of army ant-associated rove beetles – a comparison between specialists and generalists. *Front. Zool.* **15**, 8 (2018).
65. Howard, R. W., McDaniel, C. A. & Blomquist, G. J. Chemical Mimicry as an Integrating Mechanism: Cuticular Hydrocarbons of a Termitophile and Its Host. *Science* **210**, 431–433 (1980).

66. Howard, R. W., Mcdaniel, C. A. & Blomquist, G. J. Chemical Mimicry as an Integrating Mechanism: Cuticular Hydrocarbons of a Termitophile and Its Host. *Science* **210**, 431–433 (1980).
67. Uboni, A., Bagnères, A. G., Christidès, J. P. & Lorenzi, M. C. Cleptoparasites, social parasites and a common host: Chemical insignificance for visiting host nests, chemical mimicry for living in. *J. Insect Physiol.* **58**, 1259–1264 (2012).
68. Howard, R. W., Akre, R. D. & Garnett, W. B. Chemical Mimicry in an Obligate Predator of Carpenter Ants (Hymenoptera: Formicidae). *Ann. Entomol. Soc. Am.* **83**, 607–616 (1990).
69. von Beeren, C., Hashim, R. & Witte, V. The Social Integration of a Myrmecophilous Spider Does Not Depend Exclusively on Chemical Mimicry. *J. Chem. Ecol.* **38**, 262–271 (2012).
70. von Beeren, C., Pohl, S. & Witte, V. On the Use of Adaptive Resemblance Terms in Chemical Ecology. *Psyche J. Entomol.* **2012**, 635761 (2012).
71. Dettner, K. & Liepert, C. Chemical Mimicry and Camouflage. *Annu. Rev. Entomol.* **39**, 129–154 (1994).
72. Akino, T. Chemical camouflage by myrmecophilous beetles Zyras comes (Coleoptera: Staphylinidae) and Diaritiger fossulatus (Coleoptera: Pselaphidae) to be integrated into the nest of Lasius fuliginosus (Hymenoptera: Formicidae). *Chemoecology* **12**, 83–89 (2002).
73. Holze, H., Schrader, L. & Buellesbach, J. Advances in deciphering the genetic basis of insect cuticular hydrocarbon biosynthesis and variation. *Heredity* **126**, 219–234 (2021).
74. Grigoraki, L., Grau-Bové, X., Carrington Yates, H., Lycett, G. J. & Ranson, H. Isolation and transcriptomic analysis of Anopheles gambiae oenocytes enables the delineation of hydrocarbon biosynthesis. *eLife* **9**, e58019 (2020).
75. Legendre, A., Miao, X.-X., Da Lage, J.-L. & Wicker-Thomas, C. Evolution of a desaturase involved in female pheromonal cuticular hydrocarbon biosynthesis and courtship behavior in *Drosophila*. *Insect Biochem. Mol. Biol.* **38**, 244–255 (2008).
76. Chertemps, T., Duportets, L., Labeur, C., Ueyama, M. & Wicker-Thomas, C. A female-specific desaturase gene responsible for diene hydrocarbon biosynthesis and courtship behaviour in Drosophila melanogaster. *Insect Mol. Biol.* **15**, 465–473 (2006).
77. Lenoir, A. *et al.* Chemical Integration of Myrmecophilous Guests in Aphaenogaster Ant Nests. *Psyche J. Entomol.* **2012**, 840860 (2012).
78. Guerrieri, F. J. *et al.* Ants recognize foes and not friends. *Proc. R. Soc. B Biol. Sci.* **276**, 2461–2468 (2009).
79. Martin, S. J., Vitikainen, E., Helanterä, H. & Drijfhout, F. P. Chemical basis of nest-mate discrimination in the ant Formica exsecta. *Proc. R. Soc. B Biol. Sci.* **275**, 1271–1278 (2008).
80. Sturgis, S. J. & Gordon, D. M. Nestmate recognition in ants (Hymenoptera: Formicidae): a review. *Myrmecol. News* **16**, 101–110 (2012).

81. Von Beeren, C. *et al.* Multiple phenotypic traits as triggers of host attacks towards ant symbionts: body size, morphological gestalt, and chemical mimicry accuracy. *Front. Zool.* **18**, 46 (2021).
82. Akre, R. D. & Rettenmeyer, C. W. Behavior of Staphylinidae Associated with Army Ants (Formicidae: Ecitonini). *J. Kans. Entomol. Soc.* **39**, 745–782 (1966).
83. Akre, R. D. & Torgerson, R. L. The Behavior of Diploeciton Nevermanni, a Staphylinid Beetle Associated With Army Ants. *Psyche J. Entomol.* **75**, 023814 (1968).
84. Valentine, B. D. Grooming Behavior in Coleoptera. *Coleopt. Bull.* **27**, 63–73 (1973).
85. Vander Meer, R. K. & Wojcik, D. P. Chemical Mimicry in the Myrmecophilous Beetle Myrmecaphodius excavaticollis. *Science* **218**, 806–808 (1982).
86. Vane-Wright, R. I. A unified classification of mimetic resemblances. *Biol. J. Linn. Soc.* **8**, 25–56 (1976).
87. Siemann, E., Tilman, D. & Haarstad, J. Insect species diversity, abundance and body size relationships. *Nature* **380**, 704–706 (1996).
88. Danoff-Burg, J. A. An Ethogram of the Ant-Guest Beetle Tribe Sceptobiini (Coleoptera: Staphylinidae; Formicidae). *Sociobiology* **27**, 287–328 (1996).
89. Danoff-Burg, J. A. Evolving under myrmecophily: a cladistic revision of the symphilic beetle tribe Sceptobiini (Coleoptera: Staphylinidae: Aleocharinae). *Syst. Entomol.* **19**, 25–45 (1994).
90. Kistner, D. H., Jensen, E. A. & Jacobson, H. R. A New Genus and Two New Species of Myrmecophilous Staphylinidae Found with *Liometopum* in California (Coleoptera; Hymenoptera: Formicidae). *Sociobiology* **39**, 291–305 (2002).
91. Hebard, M. A Revision of the North American Species of the Genus Myrmecophila (Orthoptera; Gryllidae; Myrmecophilinae). *Trans. Am. Entomol. Soc. 1890-* **46**, 91–111 (1920).
92. Stalling, T. Myrmecophilus balcanicus, a new species of ant-loving cricket from the Former Yugoslav Republic of Macedonia, with notes on the synonymy of Myrmecophilus zorae. *Entomol. Hell.* **22**, 29 (2017).
93. Stalling, T. A New Species of Ant-Loving Cricket from Mallorca, Balearic Islands, Spain (Orthoptera, Myrmecophilidae). *Graellsia* **69**, 153–156 (2013).
94. Komatsu, T., Maruyama, M. & Itino, T. Behavioral differences between two ant cricket species in Nansei Islands: host-specialist versus host-generalist. *Insectes Sociaux* **56**, 389–396 (2009).
95. Kronauer, D. J. C. & Pierce, N. E. Myrmecophiles. *Curr. Biol.* **21**, R208–R209 (2011).
96. Henderson, G. & Akre, R. D. Biology of the Myrmecophilous Cricket, *Myrmecophila manni* (Orthoptera: Gryllidae). *J. Kans. Entomol. Soc.* **59**, 454–467 (1986).
97. Akino T., Mochizuki R., Morimoto M. & Yamaoka R. Chemical Gamouflage of Myrmecophilous Cricket Myrmecophilus sp. to be Integrated with Several Ant Species. *Jpn. J. Appl. Entomol. Zool.* **40**, 39–46 (1996).
98. Aalbu, R. L., Smith, A. D., Kanda, K. & Bouchard, P. Renefouqueosis peruviensis, a new genus and species of Stenosini (Coleoptera: Tenebrionidae) from Peru with a

key to the Stenosini of the World and notes on the genera Anchomma and Fitzsimonsium. *Acta Entomol. Musei Natl. Pragae* **57**, 313–330 (2017).
99. Doyen, J. T. & Lawrence, J. F. Relationships and higher classification of some Tenebrionidae and Zopheridae (Coleoptera). *Syst. Entomol.* **4**, 333–377 (1979).
100. Horn, G. H. Synopsis of the 'Colydiidæ' of the United States. *Proc. Am. Philos. Soc.* **17**, 555–592 (1878).
101. Tonkel, K. C., Kirchoff, V. S. & Rector, B. G. Carabidae and Tenebrionidae diversity in the Great Basin Province of California. *J. Insect Sci.* **23**, 9 (2023).
102. Fall, H. C. *List of the Coleoptera of Southern California: With Notes on Habits and Distribution and Descriptions of New Species*. (California academy of sciences, 1901).
103. Lenoir, A., Depickère, S., Devers, S., Christidès, J.-P. & Detrain, C. Hydrocarbons in the Ant Lasius niger: From the Cuticle to the Nest and Home Range Marking. *J. Chem. Ecol.* **35**, 913–921 (2009).
104. Zhou, Y.-L., Ślipiński, A., Ren, D. & Parker, J. A Mesozoic clown beetle myrmecophile (Coleoptera: Histeridae). *eLife* **8**, (2019).
105. Akre, R. D. Behavior of *Euxenister* and *Pulvinister*, Histerid Beetles Associated with Army Ants (Coleoptera: Histeridae; Hymenoptera: Formicidae: Dorylinae). *Pan-Pac. Entomol.* **44**, 87–101 (1968).
106. Disney, R. H. L. *Scuttle Flies: The Phoridae*. (Springer Netherlands, Dordrecht, 1994). doi:10.1007/978-94-011-1288-8.
107. Porter, S. D., Fowler, H. G., Campiolo, S. & Pesquero, M. A. Host Specificity of Several Pseudacteon (Diptera: Phoridae) Parasites of Fire Ants (Hymenoptera: Formicidae) in South America. *Fla. Entomol.* **78**, 70–75 (1995).
108. Porter, S. D. Biology and Behavior of Pseudacteon Decapitating Flies (Diptera: Phoridae) That Parasitize Solenopsis Fire Ants (Hymenoptera: Formicidae). *Fla. Entomol.* **81**, 292–309 (1998).
109. Feener, D. H., Jr. & Brown, B. V. Reduced Foraging of Solenopsis geminata (Hymenoptera: Formicidae) in the Presence of Parasitic Pseudacteon spp. (Diptera: Phoridae). *Ann. Entomol. Soc. Am.* **85**, 80–84 (1992).
110. LeBrun, E. G. & Feener, D. H. Linked indirect effects in ant-phorid interactions: impacts on ant assemblage structure. *Oecologia* **133**, 599–607 (2002).
111. Orr, M., Seike, S. & Gilbert, L. Foraging ecology and patterns of diversification in dipteran parasitoids of fire ants in south Brazil. *Ecol. Entomol.* **22**, 305–314 (1997).
112. Wuellner, C. T., Dall'Aglio-Holvorcem, C. G., Benson, W. W. & Gilbert, L. E. Phorid Fly (Diptera: Phoridae) Oviposition Behavior and Fire Ant (Hymenoptera: Formicidae) Reaction to Attack Differ According to Phorid Species. *Ann. Entomol. Soc. Am.* **95**, 257–266 (2002).
113. Disney, R. H. L. Three new species of scuttle-fly (Diptera:Phoridae) that parasitize ants (Hymenoptera:Formicidae) in North America. *J. Zool.* **197**, 473–481 (1982).

114. Vigil, L. Interactions Between the Velvety Tree Ant *Liometopum occidentale* (Hymenoptera: Formicidae) and *Pseudacteon* Phorid Flies (Diptera: Phoridae). (California State University, Northridge, 2016).
115. Elizalde, L. & Folgarait, P. J. Behavioral strategies of phorid parasitoids and responses of their hosts, the leaf-cutting ants. *J. Insect Sci.* **12**, 135 (2012).
116. Pérez-Lachaud, G. *et al.* How to escape from the host nest: Imperfect chemical mimicry in eucharitid parasitoids and exploitation of the ants' hygienic behavior. *J. Insect Physiol.* **75**, 63–72 (2015).
117. Klimaszewski, J., Klimaszewski, J., Pelletier, G., Maruyama, M. & Hlavac, P. Canadian species of the Zyras group of genera and review of the types from America north of Mexico (Coleoptera, Staphylinidae, Aleocharinae). *Rev. Suisse Zool.* **112**, 703--733 (2005).
118. Hlaváč, P., Newton, A. F. & Maruyama, M. World catalogue of the species of the tribe Lomechusini (Staphylinidae:Aleocharinae). *Zootaxa* **3075**, 1–151 (2011).
119. Caterino, M. S. & Chatzimanolis, S. Newly Recorded and Noteworthy California Staphylinidae. *Coleopt. Bull.* **61**, 398–407 (2007).
120. Hölldolber, B., Möglich, M. & Maschwitz, U. Myrmecophilic Relationship of *Pella* (Coleoptera: Staphylinidae) to *Lasius fuliginosus* (Hymenoptera: Formicidae). *Psyche J. Entomol.* **88**, 347–374 (1981).
121. Hölldobler, B. Zur Physiologie der Gast-Wirt-Beziehungen (myrmecophilie) bei Ameisen - II. Das Gastverhältnis des imaginalen Atemeles pubicollis Bris. (Col. Staphylinidae) zu Myrmica und Formica (Hym. Formicidae). *Z. Für Vgl. Physiol.* **66**, 215–250 (1970).
122. Hölldobler, B., Kwapich, C. L. & Haight, K. L. Behavior and exocrine glands in the myrmecophilous beetle Lomechusoides strumosus (Fabricius, 1775) (formerly called Lomechusa strumosa) (Coleoptera: Staphylinidae: Aleocharinae). *PLOS ONE* **13**, e0200309 (2018).
123. Araujo, J. & Pasteels, J. M. Ultrastructure de la glande defensive de *Drusilla canaliculata* (Fab., Coleoptera, Staphylinidae). *Arch. Biol. (Liege)* **96**, 81–99 (1985).
124. Steidle, J. L. M. & Dettner, K. Chemistry and morphology of the tergal gland of freeliving adult Aleocharinae (Coleoptera: Staphylinidae) and its phylogenetic significance. *Syst. Entomol.* **18**, 149–168 (1993).
125. Kitchen, S. A. *et al.* The genomic and cellular basis of biosynthetic innovation in rove beetles. *Cell* **187**, 3563-3584.e26 (2024).
126. Dettner, K. Defensive secretions and exocrine glands in free-living staphylinid bettles—their bearing on phylogeny (Coleoptera: Staphylinidae). *Biochem. Syst. Ecol.* **21**, 143–162 (1993).
127. Hölldobler, B. Zur Physiologie der Gast-Wirt-Beziehungen (Myrmecophilie) bei Ameisen - I. Das Gastverhältnis der *Atemeles*- und *Lomechusa*-Larven (Col. Staphylinidae) zu *Formica* (Hym. Formicidae). *Z. Für Vgl. Physiol.* **56**, 1–21 (1967).

128. Danoff-Burg, J. A. Evolutionary Lability and Phylogenetic Utility of Behavior in a Group of Ant-Guest Staphylinidae Beetles. *Ann. Entomol. Soc. Am.* **95**, 143–155 (2002).
129. Gordon, D. M. The life history of harvester ant colonies. *Philos. Trans. R. Soc. B Biol. Sci.* **379**, 20230332 (2024).
130. Danoff-Burg, J. An ethogram of the ant-guest beetle tribe Sceptobiini (Coleoptera: Staphylinidae; Formicidae). *Sociobiology* **27**, 287–328 (1996).
131. Wasmann, E. Zur Kenntniss der Gäste der Treiberameisen und ihrere Wirthe am obern Congo, nach den Sammlungen und Beobachtungen von P. Herr. Kohl C.S.S.C. bearbeitet. *Zool. Jahrb. Suppl.* **7**, 611–682 (1904).
132. Rosa, C. S. *et al.* On the Chemical Disguise of a Physogastric Termitophilous Rove Beetle. *Sociobiology* **65**, 38–47 (2018).
133. Zilberman, B., Pires-Silva, C. M., Moreira, I. E., Pisno, R. M. & Bezerra-Gusmão, M. A. State of knowledge of viviparity in Staphylinidae and the evolutionary significance of this phenomenon in *Corotoca* Schiødte, 1853. *Papéis Avulsos Zool.* **59**, e20195919 (2019).
134. Oliveira, M. H. D. *et al.* "The road to reproduction": foraging trails of Constrictotermes cyphergaster (Termitidae: Nasutitermitinae) as maternities for Staphylinidae beetles. *Sociobiology* **65**, 531 (2018).
135. Henning, S. F. The effect of ant association on lycaenid larval duration (Lepidoptera: Lycaenidae). *Entomol. Rec. J. Var.* **96**, 99–102 (1984).
136. Brand, J. M., Blum, M. S., Fales, H. M. & Pasteels, J. M. The chemistry of the defensive secretion of the beetle, *Drusilla canaliculata*. *J. Insect Physiol.* **19**, 369–382 (1973).
137. Haas, B. J. *et al.* De novo transcript sequence reconstruction from RNA-seq using the Trinity platform for reference generation and analysis. *Nat. Protoc.* **8**, 1494–1512 (2013).
138. Langmead, B. & Salzberg, S. L. Fast gapped-read alignment with Bowtie 2. *Nat. Methods* **9**, 357–359 (2012).
139. Brown, J., Pirrung, M. & McCue, L. A. FQC Dashboard: integrates FastQC results into a web-based, interactive, and extensible FASTQ quality control tool. *Bioinformatics* **33**, 3137–3139 (2017).
140. Song, L. & Florea, L. Rcorrector: efficient and accurate error correction for Illumina RNA-seq reads. *GigaScience* **4**, 48 (2015).
141. Freedman, A. FilterUncorrectabledPEfastq. https://github.com/harvardinformatics/TranscriptomeAssemblyTools. (2016).
142. Krueger, F. Trim Galore. v0.6.0 https://github.com/FelixKrueger/TrimGalore. (2019).
143. Nishimura, O., Hara, Y. & Kuraku, S. gVolante for standardizing completeness assessment of genome and transcriptome assemblies. *Bioinformatics* **33**, 3635–3637 (2017).

144. Manni, M., Berkeley, M. R., Seppey, M., Simão, F. A. & Zdobnov, E. M. BUSCO Update: Novel and Streamlined Workflows along with Broader and Deeper Phylogenetic Coverage for Scoring of Eukaryotic, Prokaryotic, and Viral Genomes. *Mol. Biol. Evol.* **38**, 4647–4654 (2021).
145. Fu, L., Niu, B., Zhu, Z., Wu, S. & Li, W. CD-HIT: accelerated for clustering the next-generation sequencing data. *Bioinformatics* **28**, 3150–3152 (2012).
146. Gadagkar, S. R., Rosenberg, M. S. & Kumar, S. Inferring species phylogenies from multiple genes: Concatenated sequence tree versus consensus gene tree. *J. Exp. Zoolog. B Mol. Dev. Evol.* **304B**, 64–74 (2005).
147. Philippe, H. *et al.* Resolving Difficult Phylogenetic Questions: Why More Sequences Are Not Enough. *PLoS Biol.* **9**, e1000602 (2011).
148. Emms, D. M. & Kelly, S. OrthoFinder: solving fundamental biases in whole genome comparisons dramatically improves orthogroup inference accuracy. *Genome Biol.* **16**, 157 (2015).
149. Emms, D. M. & Kelly, S. OrthoFinder: phylogenetic orthology inference for comparative genomics. *Genome Biol.* **20**, 238 (2019).
150. Capella-Gutiérrez, S., Silla-Martínez, J. M. & Gabaldón, T. trimAl: a tool for automated alignment trimming in large-scale phylogenetic analyses.
151. Hoang, D. T., Chernomor, O., von Haeseler, A., Minh, B. Q. & Vinh, L. S. UFBoot2: Improving the Ultrafast Bootstrap Approximation. *Mol. Biol. Evol.* **35**, 518–522 (2018).
152. Minh, B. Q. *et al.* IQ-TREE 2: New Models and Efficient Methods for Phylogenetic Inference in the Genomic Era. *Mol. Biol. Evol.* **37**, 1530–1534 (2020).
153. Kocot, K. M., Citarella, M. R., Moroz, L. L. & Halanych, K. M. PhyloTreePruner: A Phylogenetic Tree-Based Approach for Selection of Orthologous Sequences for Phylogenomics. *Evol. Bioinforma. Online* **9**, 429–435 (2013).
154. Kück, P. & Meusemann, K. FASconCAT: Convenient handling of data matrices. *Mol. Phylogenet. Evol.* **56**, 1115–1118 (2010).
155. Misof, B. *et al.* Selecting informative subsets of sparse supermatrices increases the chance to find correct trees. *BMC Bioinformatics* **14**, 348 (2013).
156. Lanfear, R., Calcott, B., Kainer, D., Mayer, C. & Stamatakis, A. Selecting optimal partitioning schemes for phylogenomic datasets. *BMC Evol. Biol.* **14**, 82 (2014).
157. Yang, Z. Among-site rate variation and its impact on phylogenetic analyses. *Trends Ecol. Evol.* **11**, 367–372 (1996).
158. Lanfear, R., Frandsen, P. B., Wright, A. M., Senfeld, T. & Calcott, B. PartitionFinder 2: New Methods for Selecting Partitioned Models of Evolution for Molecular and Morphological Phylogenetic Analyses. *Mol. Biol. Evol.* **34**, 772–773 (2017).
159. Stamatakis, A. RAxML-VI-HPC: maximum likelihood-based phylogenetic analyses with thousands of taxa and mixed models. *Bioinformatics* **22**, 2688–2690 (2006).
160. Zuckerkandl, E. & Pauling, L. Evolutionary Divergence and Convergence in Proteins. in *Evolving Genes and Proteins* (eds. Bryson, V. & Vogel, H. J.) 97–166 (Academic Press, 1965). doi:10.1016/B978-1-4832-2734-4.50017-6.

161. Britten, R. J. Rates of DNA Sequence Evolution Differ Between Taxonomic Groups. *Science* **231**, 1393–1398 (1986).
162. Rutschmann, F. Molecular dating of phylogenetic trees: A brief review of current methods that estimate divergence times. *Divers. Distrib.* **12**, 35–48 (2006).
163. Forest, F. Calibrating the Tree of Life: fossils, molecules and evolutionary timescales. *Ann. Bot.* **104**, 789–794 (2009).
164. Magallón, S. A. Dating Lineages: Molecular and Paleontological Approaches to the Temporal Framework of Clades. *Int. J. Plant Sci.* **165**, S7–S21 (2004).
165. Near, T. J. & Sanderson, M. J. Assessing the quality of molecular divergence time estimates by fossil calibrations and fossil-based model selection. *Philos. Trans. R. Soc. B Biol. Sci.* **359**, 1477–1483 (2004).
166. Parham, J. F. *et al.* Best Practices for Justifying Fossil Calibrations. *Syst. Biol.* **61**, 346–359 (2012).
167. Misof, B. *et al.* Phylogenomics resolves the timing and pattern of insect evolution. *Science* **346**, 763–767 (2014).
168. Kirejtshuk, A. G., Poschmann, M., Prokop, J., Garrouste, R. & Nel, A. Evolution of the elytral venation and structural adaptations in the oldest Palaeozoic beetles (Insecta: Coleoptera: Tshekardocoleidae). *J. Syst. Palaeontol.* **12**, 575–600 (2014).
169. Zhang, S.-Q. *et al.* Evolutionary history of Coleoptera revealed by extensive sampling of genes and species. *Nat. Commun.* **9**, 205 (2018).
170. Alexeev, A. Jurassic and lower cretaceous Buprestidae (Coleoptera) from Eurasia. *Paleontol. J.* **27**, (1993).
171. Rhynchophora. in *Mesozoic Coleoptera* vol. 161 142–176 (Nauka Publishers, 1977).
172. McKenna, D. D. *et al.* The evolution and genomic basis of beetle diversity. *Proc. Natl. Acad. Sci.* **116**, 24729–24737 (2019).
173. Wang, B. *et al.* The earliest known longhorn beetle (Cerambycidae: Prioninae) and implications for the early evolution of Chrysomeloidea. *J. Syst. Palaeontol.* **12**, 565–574 (2014).
174. Mahlerová, K., Jakubec, P., Krak, K. & Růžička, J. Resolving the intergeneric phylogeny of the large carrion beetles (Staphylinidae: Silphinae: Silphini). *Syst. Entomol.* **50**, 168–179 (2025).
175. Sikes, D. S., Thayer, M. K. & Newton, A. F. Large carrion and burying beetles evolved from Staphylinidae (Coleoptera, Staphylinidae, Silphinae): a review of the evidence. *ZooKeys* **1200**, 159–182 (2024).
176. Cai, C.-Y. *et al.* Early origin of parental care in Mesozoic carrion beetles. *Proc. Natl. Acad. Sci.* **111**, 14170–14174 (2014).
177. Liu, Y., Liu, Y., Ji, S. & Yang, Z. U-Pb zircon age for the Daohugou Biota at Ningcheng of Inner Mongolia and comments on related issues. *Chin. Sci. Bull.* **51**, 2634–2644 (2006).
178. Cai, C.-Y., Yan, E. V., Beattie, R., Wang, B. & Huang, D.-Y. First rove beetles from the Jurassic Talbragar Fish Bed of Australia (Coleoptera, Staphylinidae). *J. Paleontol.* **87**, 650–656 (2013).

179. Bean, L. B. The leptolepid fish Cavenderichthys talbragarensis (Woodward, 1895) from the Talbragar Fish Bed (Late Jurassic) near Gulgong, New South Wales. *Rec. West. Aust. Mus.* **23**, 43 (2006).
180. Yamamoto, S. & Maruyama, M. Phylogeny of the rove beetle tribe Gymnusini **sensu n.** (Coleoptera: Staphylinidae: Aleocharinae): implications for the early branching events of the subfamily. *Syst. Entomol.* **43**, 183–199 (2018).
181. Cai, C. & Huang, D. The oldest aleocharine rove beetle (Coleoptera, Staphylinidae) in Cretaceous Burmese amber and its implications for the early evolution of the basal group of hyper-diverse Aleocharinae. *Gondwana Res.* **28**, 1579–1584 (2015).
182. Shi, G. *et al.* Age constraint on Burmese amber based on U–Pb dating of zircons. *Cretac. Res.* **37**, 155–163 (2012).
183. Zerche, L. Eine neue Art der Gattung Adinopsis Cameron aus dem Baltischen Bernstein (Coleoptera: Staphylinidae, Aleocharinae, Deinopsini). *Beitr. Zur Entomol. Contrib. Entomol.* **49**, 97–105 (1999).
184. Ritzkowski, S. K-Ar-Altersbestimmungen der bernsteinführenden Sedimente des Samlandes (Paläogen, Bezirk Kaliningrad). *Metalla* **66**, 19–23 (1997).
185. Bogri, A., Solodovnikov, A. & Żyła, D. Baltic amber impact on historical biogeography and palaeoclimate research: oriental rove beetle Dysanabatium found in the Eocene of Europe (Coleoptera, Staphylinidae, Paederinae). *Pap. Palaeontol.* **4**, 433–452 (2018).
186. Paśnik, G. Fossils of Staphylinidae from Baltic amber: a new genus and three new species (Insecta, Coleoptera, Staphylinidae). *Senckenberg. Biol.* **85**, 97–100 (2005).
187. Paśnik, G. & Kubisz, D. A new genus and new species of Staphylinidae (Coleoptera) from Baltic amber. *Eur. J. Entomol.* **99**, 353–361 (2002).
188. Tasaku, Y. & Maruyama, M. Resolving the taxonomic confusion of Taxicera Mulsant & Rey, 1873 and Dalotia Casey, 1910 (Coleoptera, Staphylinidae, Aleocharinae), with the rediscovery of Dalotia pseudorphana (Cameron, 1933), comb. nov., from bird nest material. *Zootaxa* **5609**, 70–82 (2025).
189. Yang, Z. PAML 4: Phylogenetic Analysis by Maximum Likelihood. *Mol. Biol. Evol.* **24**, 1586–1591 (2007).
190. Whelan, S. & Goldman, N. A General Empirical Model of Protein Evolution Derived from Multiple Protein Families Using a Maximum-Likelihood Approach. *Mol. Biol. Evol.* **18**, 691–699 (2001).
191. Inoue, J., Donoghue, P. C. J. & Yang, Z. The Impact of the Representation of Fossil Calibrations on Bayesian Estimation of Species Divergence Times. *Syst. Biol.* **59**, 74–89 (2010).
192. Yang, Z. & Rannala, B. Bayesian Estimation of Species Divergence Times Under a Molecular Clock Using Multiple Fossil Calibrations with Soft Bounds. *Mol. Biol. Evol.* **23**, 212–226 (2006).
193. Parker, J. & Grimaldi, D. A. Specialized Myrmecophily at the Ecological Dawn of Modern Ants. *Curr. Biol.* **24**, 2428–2434 (2014).

194. Zenkevich, I. Kovats' retention index system. *Encycl. Chromatogr.* 1304–1310 (2010).
195. Structure and analysis of insect hydrocarbons. in *Insect Hydrocarbons: Biology, Biochemistry, and Chemical Ecology* (Cambridge University Press, 2010).
196. Brückner, A. Using weapons instead of perfume: chemical association strategies of the myrmecophilous bug Scolopostethus pacificus (Rhyparochromidae). *Chemoecology* **32**, 147–157 (2022).
197. Greene, M. J. & Gordon, D. M. Structural complexity of chemical recognition cues affects the perception of group membership in the ants Linephithema humile and Aphaenogaster cockerelli. *J. Exp. Biol.* **210**, 897–905 (2007).
198. Ichinose, K. & Lenoir, A. Hydrocarbons detection levels in ants. *Insectes Sociaux* **57**, 453–455 (2010).
199. Ricotta, C. & Podani, J. On some properties of the Bray-Curtis dissimilarity and their ecological meaning. *Ecol. Complex.* **31**, 201–205 (2017).
200. Oksanen, J. *et al.* vegan: Community Ecology Package. 2.6-10 https://doi.org/10.32614/CRAN.package.vegan (2001).
201. Brückner, A. & Heethoff, M. A chemo-ecologists' practical guide to compositional data analysis. *Chemoecology* **27**, 33–46 (2017).
202. Donisthorpe, H. S. J. K. *The Guests of British Ants: Their Habits and Life-Histories*. (G. Routledge and Sons, limited, 1927).
203. Fowler, W. W. *The Coleoptera of the British Islands*. (Reeve, 1888).
204. Michener, R. & Lajtha, K. *Stable Isotopes in Ecology and Environmental Science*. (John Wiley & Sons, Ltd, 2007). doi:10.1002/9780470691854.
205. Fischer, C. R., Bowen, B. P., Pan, C., Northen, T. R. & Banfield, J. F. Stable-Isotope Probing Reveals That Hydrogen Isotope Fractionation in Proteins and Lipids in a Microbial Community Are Different and Species-Specific. *ACS Chem. Biol.* **8**, 1755–1763 (2013).
206. Barnes, C., Sweeting, C. J., Jennings, S., Barry, J. T. & Polunin, N. V. C. Effect of temperature and ration size on carbon and nitrogen stable isotope trophic fractionation. *Funct. Ecol.* **21**, 356–362 (2007).
207. A. Hobbie, E. & Werner, R. A. Intramolecular, compound-specific, and bulk carbon isotope patterns in C3 and C4 plants: a review and synthesis. *New Phytol.* **161**, 371–385 (2004).
208. Chikaraishi, Y., Kaneko, M. & Ohkouchi, N. Stable hydrogen and carbon isotopic compositions of long-chain (C21–C33) *n*-alkanes and *n*-alkenes in insects. *Geochim. Cosmochim. Acta* **95**, 53–62 (2012).
209. Quinby, B. M., Creighton, J. C. & Flaherty, E. A. Stable isotope ecology in insects: a review. *Ecol. Entomol.* **45**, 1231–1246 (2020).
210. Hood-Nowotny, R. & Knols, B. G. J. Stable isotope methods in biological and ecological studies of arthropods. *Entomol. Exp. Appl.* **124**, 3–16 (2007).
211. Sessions, A. L. Isotope-ratio detection for gas chromatography. *J. Sep. Sci.* **29**, 1946–1961 (2006).

212. Feldhaar, H., Gebauer, G. & Blüthgen, N. Stable isotopes: past and future in exposing secrets of ant nutrition (Hymenoptera: Formicidae). *Myrmecol. News* **13**, 3–13 (2010).
213. Makki, R., Cinnamon, E. & Gould, A. P. The Development and Functions of Oenocytes. *Annu. Rev. Entomol.* **59**, 405–25 (2014).
214. Choi, H. M. T. *et al.* Third-generation *in situ* hybridization chain reaction: multiplexed, quantitative, sensitive, versatile, robust. *Development* **145**, dev165753 (2018).
215. Feyereisen, R. Origin and evolution of the CYP4G subfamily in insects, cytochrome P450 enzymes involved in cuticular hydrocarbon synthesis. *Mol. Phylogenet. Evol.* **143**, 106695 (2020).
216. Balabanidou, V. *et al.* Cytochrome P450 associated with insecticide resistance catalyzes cuticular hydrocarbon production in Anopheles gambiae. *Proc. Natl. Acad. Sci.* **113**, 9268–9273 (2016).
217. Kim, D. H. & and Rossi, J. J. RNAi Mechanisms and Applications. *BioTechniques* **44**, 613–616 (2008).
218. Shan, G. RNA interference as a gene knockdown technique. *Int. J. Biochem. Cell Biol.* **42**, 1243–1251 (2010).
219. Tomoyasu, Y. & Denell, R. E. Larval RNAi in Tribolium (Coleoptera) for analyzing adult development. *Dev. Genes Evol.* **214**, 575–578 (2004).
220. Posnien, N. *et al.* RNAi in the Red Flour Beetle (Tribolium). *Cold Spring Harb. Protoc.* **2009**, pdb.prot5256 (2009).
221. Parker, J., Eldredge, K. T., Thomas, I. M., Coleman, R. & Davis, S. R. Hox-logic of body plan innovations for social symbiosis in rove beetles. 198945 Preprint at https://doi.org/10.1101/198945 (2018).
222. Bray, N. L., Pimentel, H., Melsted, P. & Pachter, L. Near-optimal probabilistic RNA-seq quantification. *Nat. Biotechnol.* **34**, 525–527 (2016).
223. Pimentel, H., Bray, N. L., Puente, S., Melsted, P. & Pachter, L. Differential analysis of RNA-seq incorporating quantification uncertainty. *Nat. Methods* **14**, 687–690 (2017).
224. Blomquist, G. J. & Bagnères, A.-G. *Insect Hydrocarbons: Biology, Biochemistry, and Chemical Ecology*. (Cambridge University Press, 2010).
225. Wicker-Thomas, C. *et al.* Flexible origin of hydrocarbon/pheromone precursors in Drosophila melanogaster. *J. Lipid Res.* **56**, 2094–2101 (2015).
226. Maier, T., Leibundgut, M., Boehringer, D. & Ban, N. Structure and function of eukaryotic fatty acid synthases. *Q. Rev. Biophys.* **43**, 373–422 (2010).
227. Barber, M. C., Price, N. T. & Travers, M. T. Structure and regulation of acetyl-CoA carboxylase genes of metazoa. *Biochim. Biophys. Acta* **1733**, 1–28 (2005).
228. Dennis, M. W. & Kolattukudy, P. E. Alkane biosynthesis by decarbonylation of aldehyde catalyzed by a microsomal preparation from *Botryococcus braunii*. *Arch. Biochem. Biophys.* **287**, 268–275 (1991).

229. Holze, H., Schrader, L. & Buellesbach, J. Advances in deciphering the genetic basis of insect cuticular hydrocarbon biosynthesis and variation. *Heredity* **126**, 219–234 (2021).
230. Gu, P., Welch, W. H., Guo, L., Schegg, K. M. & Blomquist, G. J. Characterization of a Novel Microsomal Fatty Acid Synthetase (FAS) Compared to a Cytosolic FAS in the Housefly, *Musca domestica*. *Comp. Biochem. Physiol. B Biochem. Mol. Biol.* **118**, 447–456 (1997).
231. Chertemps, T. *et al.* A female-biased expressed elongase involved in long-chain hydrocarbon biosynthesis and courtship behavior in *Drosophila melanogaster*. *Proc. Natl. Acad. Sci.* **104**, 4273–4278 (2007).
232. Reed, J. R. *et al.* Unusual mechanism of hydrocarbon formation in the housefly: cytochrome P450 converts aldehyde to the sex pheromone component (Z)-9-tricosene and CO2. *Proc. Natl. Acad. Sci.* **91**, 10000–10004 (1994).
233. Cinnamon, E. *et al.* Drosophila Spidey/Kar Regulates Oenocyte Growth via PI3-Kinase Signaling. *PLOS Genet.* **12**, e1006154 (2016).
234. MacLean, M., Nadeau, J., Gurnea, T., Tittiger, C. & Blomquist, G. J. Mountain pine beetle (*Dendroctonus ponderosae*) CYP4Gs convert long and short chain alcohols and aldehydes to hydrocarbons. *Insect Biochem. Mol. Biol.* **102**, 11–20 (2018).
235. Feyereisen, R. Origin and evolution of the CYP4G subfamily in insects, cytochrome P450 enzymes involved in cuticular hydrocarbon synthesis. *Mol. Phylogenet. Evol.* **143**, 106695 (2020).
236. Mpuru, S., Reed, J. R., Reitz, R. C. & Blomquist, G. J. Mechanism of hydrocarbon biosynthesis from aldehyde in selected insect species: Requirement for O2 and NADPH and carbonyl group released as CO2. *Insect Biochem. Mol. Biol.* **26**, 203–208 (1996).
237. Reed, J. R. *et al.* Unusual mechanism of hydrocarbon formation in the housefly: cytochrome P450 converts aldehyde to the sex pheromone component (Z)-9-tricosene and CO2. *Proc. Natl. Acad. Sci.* **91**, 10000–10004 (1994).
238. Reed, J. R., Quilici, D. R., Blomquist, G. J. & Reitz, R. C. Proposed mechanism for the cytochrome P450-catalyzed conversion of aldehydes to hydrocarbons in the house fly, Musca domestica. *Biochemistry* **34**, 16221–16227 (1995).
239. Qiu, Y. *et al.* An insect-specific P450 oxidative decarbonylase for cuticular hydrocarbon biosynthesis. *Proc. Natl. Acad. Sci.* **109**, 14858–14863 (2012).
240. Masters, B. S. S. & Okita, R. T. The history, properties, and function of NADPH-cytochrome P-450 reductase. *Pharmacol. Ther.* **9**, 227–244 (1980).
241. Dallerac, R. *et al.* A Δ9 desaturase gene with a different substrate specificity is responsible for the cuticular diene hydrocarbon polymorphism in Drosophila melanogaster. *Proc. Natl. Acad. Sci.* **97**, 9449–9454 (2000).
242. Chertemps, T., Duportets, L., Labeur, C., Ueyama, M. & Wicker-Thomas, C. A female-specific desaturase gene responsible for diene hydrocarbon biosynthesis and courtship behaviour in *Drosophila melanogaster*. *Insect Mol. Biol.* **15**, 465–473 (2006).

243. Katoh, K. & Standley, D. M. MAFFT Multiple Sequence Alignment Software Version 7: Improvements in Performance and Usability. *Mol. Biol. Evol.* **30**, 772–780 (2013).
244. Price, M. N., Dehal, P. S. & Arkin, A. P. FastTree 2 – Approximately Maximum-Likelihood Trees for Large Alignments. *PLOS ONE* **5**, e9490 (2010).
245. Mathis, A. *et al.* DeepLabCut: markerless pose estimation of user-defined body parts with deep learning. *Nat. Neurosci.* **21**, 1281–1289 (2018).
246. Nath, T. *et al.* Using DeepLabCut for 3D markerless pose estimation across species and behaviors. *Nat. Protoc.* **14**, 2152–2176 (2019).
247. Pimentel, H., Bray, N. L., Puente, S., Melsted, P. & Pachter, L. Differential analysis of RNA-seq incorporating quantification uncertainty. *Nat. Methods* **14**, 687–690 (2017).
248. Gutierrez, E., Wiggins, D., Fielding, B. & Gould, A. P. Specialized hepatocyte-like cells regulate Drosophila lipid metabolism. *Nature* **445**, 275–280 (2007).
249. Stringer, C., Wang, T., Michaelos, M. & Pachitariu, M. Cellpose: a generalist algorithm for cellular segmentation. *Nat. Methods* **18**, 100–106 (2021).
250. Witte, V., Leingärtner, A., Sabaß, L., Hashim, R. & Foitzik, S. Symbiont microcosm in an ant society and the diversity of interspecific interactions. *Anim. Behav.* **76**, 1477–1486 (2008).
251. MacMillan, H. A., Nørgård, M., MacLean, H. J., Overgaard, J. & Williams, C. J. A. A critical test of *Drosophila* anaesthetics: Isoflurane and sevoflurane are benign alternatives to cold and CO2. *J. Insect Physiol.* **101**, 97–106 (2017).
252. Wilson, E. E., Holway, D. & Nieh, J. C. Cold anaesthesia decreases foraging recruitment in the New World bumblebee, Bombus occidentalis. *J. Apic. Res.* **45**, 169–172 (2006).
253. Bartholomew, N. R., Burdett, J. M., VandenBrooks, J. M., Quinlan, M. C. & Call, G. B. Impaired climbing and flight behaviour in Drosophila melanogaster following carbon dioxide anaesthesia. *Sci. Rep.* **5**, 15298 (2015).
254. Friard, O. & Gamba, M. BORIS: a free, versatile open-source event-logging software for video/audio coding and live observations. *Methods Ecol. Evol.* **7**, 1325–1330 (2016).
255. Moran, N. A., McCutcheon, J. P. & Nakabachi, A. Genomics and Evolution of Heritable Bacterial Symbionts. *Annu. Rev. Genet.* **42**, 165–190 (2008).
256. Krupp, J. J., Nayal, K., Wong, A., Millar, J. G. & Levine, J. D. Desiccation resistance is an adaptive life-history trait dependent upon cuticular hydrocarbons, and influenced by mating status and temperature in *D. melanogaster*. *J. Insect Physiol.* **121**, 103990 (2020).
257. Qiu, Y. *et al.* An insect-specific P450 oxidative decarbonylase for cuticular hydrocarbon biosynthesis. *Proc. Natl. Acad. Sci.* **109**, 14858–14863 (2012).
258. Seevers, C. H. The Systematics, Evolution and Zoogeogrpahy of Staphylinid Beetles Associated with Army Ants (Coleoptera, Staphylinidae). *Fieldiana Zool.* **47**, 137–351 (1965).

259. Kistner, D. H. & Jacobson, H. R. Cladistic Analysis and Taxonomic Revision of the Ecitophilous Tribe Ecitocharini with Studies of Their Behavior and Evolution (Coleoptera, Staphylinidae, Aleocharinae). *Sociobiology* **17**, 333–465 (1990).
260. Shigenobu, S., Watanabe, H., Hattori, M., Sakaki, Y. & Ishikawa, H. Genome sequence of the endocellular bacterial symbiont of aphids Buchnera sp. APS. *Nature* **407**, 81–86 (2000).